

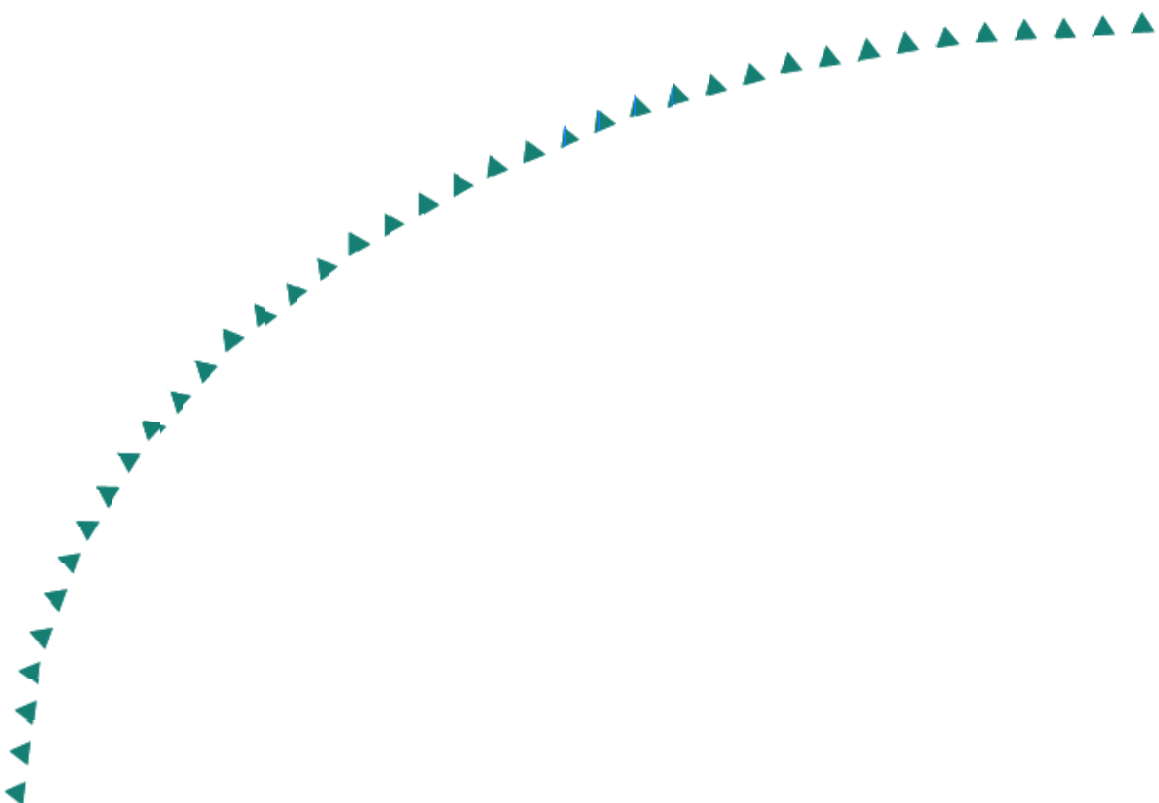
2004-02

Final Report

Repair of Fatigued Steel Bridge Girders with Carbon Fiber Strips



Research



Technical Report Documentation Page

1. Report No. MN/RC – 2004-02	2.	3. Recipients Accession No.	
4. Title and Subtitle REPAIR OF FATIGUED STEEL BRIDGE GIRDERS WITH CARBON FIBER STRIPS		5. Report Date December 2003	
		6.	
7. Author(s) Carol Shield, Jerome Hajjar, Katsuyoshi Nozaka		8. Performing Organization Report No.	
9. Performing Organization Name and Address University of Minnesota Department of Civil Engineering 500 Pillsbury Drive S.E. Minneapolis, MN 55455		10. Project/Task/Work Unit No.	
		11. Contract (C) or Grant (G) No. (c) 74708 (wo) 102	
12. Sponsoring Organization Name and Address Minnesota Department of Transportation Office of Research Services 395 John Ireland Boulevard Mail Stop 330 St. Paul, Minnesota 55155		13. Type of Report and Period Covered Final Report	
		14. Sponsoring Agency Code	
15. Supplementary Notes http://www.lrrb.gen.mn.us/PDF/200402.pdf			
16. Abstract (Limit: 200 words) <p>This report investigates a method of repairing fatigued steel bridge girders using carbon fiber reinforced polymer (CFRP) strips. This type of repair would be used to prevent the propagation of cracks which could lead to failure of the bridge girders. The main advantages of using CFRP is it is lightweight and durable, resulting in ease of handling and maintenance. Therefore, it would not require the closing of traffic on the bridge during rehabilitation. Effective bond length was determined by a series of experimental tests with actual materials, as well as through the use of analytical equations. Finally, tests were conducted on full-scale cracked girders; the application of the CFRP strips to the steel girders resulted in significant strain reduction, except in the case of small cracks where it was difficult to clearly identify the benefits.</p>			
17. Document Analysis/Descriptors Fatigue Cracks Carbon Fiber Reinforced Polymer Strips		18. Availability Statement No restrictions. Document available from: National Technical Information Services, Springfield, Virginia 22161	
19. Security Class (this report) Unclassified	20. Security Class (this page) Unclassified	21. No. of Pages 163	22. Price

Repair of Fatigued Steel Bridge Girders with Carbon Fiber Strips

Final Report

Prepared by

Katsuyoshi Nozaka
Carol K. Shield
Jerome F. Hajjar
Department of Civil Engineering
University of Minnesota

December 2003

Published by

Minnesota Department of Transportation
Office of Research Services
Mail Stop 330
395 John Ireland Boulevard
St. Paul, Minnesota 55155

This report presents the results of research by the authors and does not necessarily represent the views or policies of the Minnesota Department of Transportation. This report does not contain a standard or specified technique. The Minnesota Department of Transportation does not endorse any product.

Acknowledgements

CFRP and adhesive materials were donated by Sika Corp., Fyfe Co., and 3M. Additional help on the project was provided by Paul Bergson, Dr. Robert J. Dexter, Eray Baran, and Yuying Hu all at the University of Minnesota.

Table of Contents

1	Introduction.....	1
2	Literature Review.....	5
2.1	Rehabilitation or Strengthening of Steel Girders.....	5
2.1.1	Studies on Composite Plates Bonded on Steel.....	5
2.1.2	Studies on Steel Plates Bonded on Steel.....	7
2.2	Bond Strength.....	8
2.2.1	Test Specimen for Bond Strength.....	8
2.2.2	Experimental Studies.....	9
2.2.3	Computational Studies.....	10
2.2.4	Analytical Studies.....	11
3	Experimental Tests.....	13
3.1	Materials for Rehabilitation.....	13
3.1.1	Adhesive.....	13
3.1.2	CFRP Strip.....	14
3.2	Effective Bond Length Tests.....	15
3.2.1	Test Setup and Specimen.....	15
3.2.2	Test Matrix.....	17
3.2.3	Instrumentation.....	18
3.3	Preliminary Test on Rehabilitated Girder.....	19
3.3.1	Test Setup and Specimen.....	19
3.3.2	Test Matrix.....	20
3.3.3	Instrumentation.....	20
3.4	Cyclic Fatigue Loading Tests on Rehabilitated Girders.....	21
3.4.1	Test Setup and Specimen.....	21
3.4.2	Test Matrix.....	23
3.4.3	Instrumentation.....	24
4	Results and Discussion.....	25
4.1	Effective Bond Length Tests.....	25
4.1.1	Summary of Test Results.....	25
4.1.1.1	Effective Bond Length.....	25
4.1.1.2	Effect of Multiple Layers of CFRP.....	26
4.1.1.3	Failure Mode.....	27
4.1.1.4	Effect of Cyclic Loading during Curing.....	28
4.1.2	Moment-CFRP Strain Relationship.....	29
4.1.2.1	Computational Model.....	29
4.1.2.2	Effect of Configuration.....	30
4.1.2.3	Effect of Multiple Layers of CFRP.....	32
4.1.3	Strain Distribution in CFRP Strip.....	33
4.1.4	Analytical Estimation of Effective Bond Length.....	35
4.1.4.1	Analytical Solutions for Shear Stress Distributions.....	35
4.1.4.2	Simplified Equations for Effective Bond Length.....	39
4.1.5	Recommendation for Bonded Lengths and Bonded Configuration.....	42
4.2	Preliminary Test on Rehabilitated Girder.....	42
4.2.1	Stiffness Increase of the Girder.....	42
4.2.2	Strain Distribution in Girder.....	43
4.2.3	Strain Distribution in CFRP Strip.....	44
4.3	Cyclic Fatigue Loading Tests on Rehabilitated Girders.....	45
4.3.1	Crack Growth.....	46

4.3.1.1	NR-3: No Bonded CFRP.....	46
4.3.1.2	R-3-1: Bonded CFRP with Shorter Crack Length at Rehabilitation.....	48
4.3.1.3	R-3-2: Bonded CFRP with Longer Crack Length at Rehabilitation.....	49
4.3.1.4	Comparison on Crack Growth.....	49
4.3.1.5	R-3-3: Bonded CFRP without Stop-Holes.....	50
4.3.2	Other Considerations on Application of Bonded CFRP Strips.....	51
4.3.2.1	Influence of Crack on Strain Distributions in Girder.....	51
4.3.2.2	Influence of Crack on Strain Distributions in CFRP Strip.....	51
4.3.2.3	Propagation of Debond.....	53
4.3.2.4	Estimation of Crack Growth.....	53
5	Conclusion.....	55
5.1	Effective Bond Length Tests.....	55
5.2	Static and Cyclic Loading Tests on Large-Scale Girders.....	56
5.3	Concluding Remarks and Recommended Future Work.....	57
	References.....	59
	Tables.....	65
	Figures.....	69
	Appendix A. Design of Specimen and Test Setup for Effective Bond Length Tests	A-1
	Appendix B. Cyclic Loading Test Using Test Setup for Effective Bond Length Tests	B-1
	Appendix C. Cyclic Tests on Rehabilitated W27x94 Girder	C-1
	Appendix D. Recommended Application Procedure	D-1

List of Tables

Table 3.1 Tensile Test Results for Sikadur 330 Adhesive	65
Table 3.2 Tensile Test Results for DP-460NS Adhesive	65
Table 3.3 Tensile Test Results for Carbodur CFRP Strip	65
Table 3.4 Tensile Test Results for Tyfo UC CFRP Strip	65
Table 3.5 Specimen Matrix for Effective Bond Length Test	66
Table 3.6 Specimen Matrix for Cyclic Fatigue Loading Tests	67
Table 4.1 Summary of Effective Bond Length Test	68

List of Figures

Figure 1.1 Typical Moment Distribution in Two Span Continuous Girder	69
Figure 1.2 Crack Initiated from Weld Toe (Circle A in Fig. 1)	69
Figure 1.3 Rehabilitation of Fatigued Tension Flange with Bonded CFRP Strip	70
Figure 2.1 Sketch of Specimen in Ref. 20	70
Figure 2.2 Single and Double Lap Specimens	71
Figure 2.3 Free Body Diagram of Single-Lap Specimen	71
Figure 2.4 Sketch of Spew Fillet	71
Figure 3.1 Experimental Test Setup and Dimensions - Two-77 kip actuators	72
Figure 3.2 Detail of Hole	72
Figure 3.3 Dimensions of Specimens and Holding Devices	73
Figure 3.4 Typical Specimen before being Bolted to W14×68 Girder - Specimen 1-2	74
Figure 3.5 Detail of Bolted Connection between Base Girder and Specimen	74
Figure 3.6 Configurations of Specimen around Slit	75
Figure 3.7 Strain Gauge Instrumentation of Base Girder	76
Figure 3.8 Strain Gauge Instrumentation of CFRP Strips	77
Figure 3.9 Sketch of Test Setup for W27x94 Girder	78
Figure 3.10 Test Setup for Static Test on W27×94	78
Figure 3.11 Sketch of Rehabilitated Fatigued Tension Flange	79
Figure 3.12 Gauge Instrumentation on W27x94 -1	79
Figure 3.13 Gauge Instrumentation on W27x94 -2	80
Figure 3.14 Gauge Instrumentation on CFRP Strip	80
Figure 3.15 Rehabilitated Girder and Instrumented Gauges	81
Figure 3.16 LVDTs for Deflection Measurement	81
Figure 3.17 Experimental Test Setup and Dimensions for Cyclic Test on W27x84	82
Figure 3.18 Detail of Dead Load Application Device (Section A-A)	83
Figure 3.19 Sketch for Calculation of Loss of Dead Load	83
Figure 3.20 Instrumentation for W27x84 (all gauges are shown)	84
Figure 4.1 Post Failure Photograph - Specimen 1-3	85
Figure 4.2 Post Failure Photograph - Specimen 1-5	85
Figure 4.3 Post Failure Photograph - Specimen 1-8	86
Figure 4.4 Post Failure Photograph – Specimen 1-14	86
Figure 4.5 Detail of Splice Plates and Web Plates for Application of Cyclic Loading during Adhesive Curing	87
Figure 4.6 Applied Moment vs. CFRP Strain - Specimen 1-1	88
Figure 4.7 Applied Moment vs. CFRP Strain - Specimen 1-2	88
Figure 4.8 Applied Moment vs. CFRP Strain - Specimen 1-3	89
Figure 4.9 Applied Moment vs. CFRP Strain - Specimen 1-5	89
Figure 4.10 Applied Moment vs. CFRP Strain - Specimen 1-8	90
Figure 4.11 Applied Moment vs. CFRP Strain - Specimen 1-14	90
Figure 4.12 Applied Moment vs. CFRP Strain - Specimen 2-2	91
Figure 4.13 Applied Moment vs. CFRP Strain - Specimen 3-1	91
Figure 4.14 Computational Model of Specimen for Effective Bond Length Test	92
Figure 4.15 Detail of Circle A (Configuration 1)	92
Figure 4.16 Comparison of Strain Gradient (same Strain at Bottom Surface)	93
Figure 4.17 Tensile Strain Distribution in Specimen 1-4	94
Figure 4.18 Tensile Strain Distribution in Specimen 1-8	95
Figure 4.19 Tensile Strain Distribution in Specimen 1-14	95
Figure 4.20 Comparison between FEM and Test Results for Specimen 1-14	96

Figure 4.21 Tensile Strain Distribution in Specimen 2-3.....	96
Figure 4.22 Shear Stress Distribution Based on Measured Strain in Specimen 1-14.....	97
Figure 4.23 Shear Stress Distribution Based on Measured Strain in Specimen 2-3.....	97
Figure 4.24 Dimension of Single-Lap Joint: Elastic Adhesive.....	98
Figure 4.25 Simplified Free Body Diagram for Analytical Model.....	98
Figure 4.26 Dimension of Single-Lap Joint: Elastic-Plastic Adhesive.....	98
Figure 4.27 Shear Stress Distributions for Example Lap Joint.....	99
Figure 4.28 Effective Bond Length for Adhesive Elastic Region.....	99
Figure 4.29 Moment-Deflection Curves with and without CFRP.....	100
Figure 4.30 Sections and Locations of Neutral Axis.....	100
Figure 4.31 Strain Distributions in Cross Section at Center.....	101
Figure 4.32 Strain Distributions in Cross Section at 10 in. from Center.....	101
Figure 4.33 Strain Near Crack Tip with and without CFRP.....	102
Figure 4.34 Tensile Strain Distribution in CFRP.....	102
Figure 4.35 Test Setup for Cyclic Loading Tests on W27x84	103
Figure 4.36 Welded Steel Plates for Initiating Crack.....	103
Figure 4.37 Specimen with Crack and Holes (NR-3).....	104
Figure 4.38 Sketch of Crack Length and Hole Locations (NR-3).....	104
Figure 4.39 Crack Reached Inner Surface of Tension Flange.....	105
Figure 4.40 Crack Tip Growing through Thickness of Flange (NR-3).....	105
Figure 4.41 Crack Growth vs. Number of Cycles (NR-3).....	106
Figure 4.42 Sketch of Crack Length and Hole Locations (R-3-1).....	106
Figure 4.43 Specimen with Crack and Holes (R-3-1).....	107
Figure 4.44 Rehabilitated Specimen with Bonded CFRP Strip.....	107
Figure 4.45 Crack Growth vs. Number of Cycles (R-3-1).....	108
Figure 4.46 South Crack Reached Inner Surface of Tension Flange.....	108
Figure 4.47 Sketch of Crack Length and Hole Locations (R-3-2).....	109
Figure 4.48 Specimen with Crack and Holes (R-3-2).....	109
Figure 4.49 Crack Tip in Web (R-3-2).....	110
Figure 4.50 Crack Growth vs. Number of Cycles (R-3-2).....	110
Figure 4.51 Comparison of Crack Growth vs. Number of Cycles.....	111
Figure 4.52 Comparison of Crack Growth vs. Number of Cycles - Modified.....	111
Figure 4.54 Strain Distribution in Section at Center (NR-3).....	113
Figure 4.55 Strain Distribution in Section 20 in. from Center (NR-3).....	113
Figure 4.56 Strain Distribution in CFRP Strips (R-3-1) – 0 Cycles.....	114
Figure 4.57 Strain Distribution in CFRP Strips (R-3 -1) – After 2 Million Cycles.....	114
Figure 4.58 Change in Tensile Strain at Center o f CFRP Strip (R-3-1).....	115
Figure 4.59 Change in Tensile Strain at Center o f CFRP Strip (R-3-2).....	115
Figure 4.60 Idealized Composite Sections.....	116

Executive Summary

In the construction of older steel bridges, it was common to weld a cover plate onto the outer face of the top flange over the interior pier of a continuous steel I-girder, where the top flange was in tension due to flexure, without extending the steel cover plate into the positive moment region, where the top flange would be in compression due to flexure. However, many girders with these cover plate details have developed fatigue cracks at the weld toe of the cover plate ends after being subjected to cyclic tensile loads, e.g., from traffic flow. Since crack initiation from the weld toe of the cover plate ends was recognized as potentially causing catastrophic failure of the steel girders, it has become important to retrofit the fatigued bridge girders. Several rehabilitation methods have been developed, including two general approaches. In the first approach, peening, arc melting, grinding, and/or hole drilling are directly applied to the weld of the cover plate ends, thus modifying the stress state around the weld or eliminating the crack. These methods are not always successful; for example, several girders that have been rehabilitated by hole drilling alone had cracks reinitiate from the holes. In the second approach, steel plates are bolted to the tension flange over the crack, restoring the flexural capacity and the strength of the section.

All rehabilitation methods listed above, except for hole drilling, require direct access to the topside of the tension flange on which the cover plate is welded. This in turn requires the removal of the concrete deck that covers the top of the tension flange in the negative moment region and partial closing of the traffic on the bridge being rehabilitated, resulting in expensive and time-consuming work that is inconvenient for the public. Although a retrofit procedure in which a steel angle is bolted to the girder web near the top flange has been investigated in recent work in order to avoid having to close traffic during the rehabilitation, the angle member to be bolted to the girder tends to be long in order to develop the full yield strength of the angle, resulting in problems associated with handling a heavy, large angle member and drilling many holes in the web on site. (McKeefry and Shield, 1999) There is a current need to develop a new rehabilitation method that can be used either together with or separately from hole drilling that does not require removal of the concrete deck. The use of Carbon Fiber Reinforced Polymer (CFRP) strips, adhered to the inside face of the girder tension flange, is a proposed method for repairing these cracked bridge girders under investigation in this report.

The main advantages of using CFRP strips are their light weight and durability, resulting in an ease of handling and maintenance. This rehabilitation method would not require access to the top of the tension flange, resulting in no need to close the traffic during the rehabilitation work. In addition, no specific machines for handling are required because of the considerably lower weight of CFRP strips as compared to steel members. Therefore, although the unit price of a CFRP strip may be higher than that of steel, the cost of workers and machines will be reduced, generally resulting in a decrease in the total rehabilitation cost.

Composite materials have been extensively used in the aerospace, automobile, and mechanical industries, where light weight and durability are critical issues in the applications of composite materials. In structural engineering applications, composite materials have gained popularity in the last several decades mainly for the rehabilitation and strengthening of concrete columns and beams because of their durability and high strength compared with concrete. A series of experimental tests on the stiffness and strength of steel girders strengthened using composite materials has been conducted by Gillespie et al. (1996a, 1996b, 1997), and Edberg et al. (1996) at the University of Delaware. In this research, Gillespie found that among various reinforcing geometries and schemes, reinforcement using pultruded strips resulted in the greatest increases in stiffness and strength. Rehabilitation of two severely corroded steel girders using pultruded CFRP strips yielded girders with 97% of their original (uncorroded) stiffness, and an ultimate capacity that was 113% of the original section strength, indicating the efficiency of the rehabilitation method. In a companion study to investigate the effect of the CFRP retrofit on crack growth, Gillespie showed that the CFRP retrofit could not eliminate crack growth, but could substantially slow crack growth rate. Sen et al. (1996) conducted a study on strengthened steel girders with a concrete slab to investigate the possibility of extending the service life of the steel girders. Although the stiffness of the girder was not increased significantly by the strengthening, the strength of the rehabilitated girder increased more than 200%. In addition, thicker composite laminates with the steel girder that had a lower yield strength tended to have a larger gain on the strength. However, it should be noted that, in several specimens, the composite laminates were mechanically bolted to the tension flange as well as bonded at the ends of the laminate to avoid debonding failure of the laminates.

As shown above, a possibility of use of bonded CFRP strips for strengthening and rehabilitation has been investigated. However, there have been only a few studies on the

rehabilitation of fatigued steel girders with bonded CFRP strips. In addition, little guidance can be found in the literature on the bond mechanism between CFRP and steel. To use CFRP strips for the rehabilitation of fatigued steel flanges, it is necessary to develop a design philosophy, including an appropriate bond length and application procedure. The bond length that engages the maximum possible strength in the CFRP strip and the adhesive is defined in this work as the effective bond length. The effective bond length was determined experimentally and compared to the results of FEM analysis and a simplified analytical procedure developed. Cracked steel girders were rehabilitated with CFRP strips in the lab to determine the effect of the CFRP strip on crack propagation.

CFRP strips from two manufacturers were tested; both were unidirectional carbon fiber reinforced composites with an epoxy matrix. The adhesives used in this project were two-part, room-temperature-cure epoxy adhesives. A total of 27 specimens were tested to study the effective bond length of CFRP strips in this application. These consisted of twenty-three one-layer specimens, three two-layer specimens and one three-layer specimen. The main variables in these tests were the CFRP and adhesive material, the crack and bond configuration, and the bond length.

It was thought that the existence of sharp corners in the adhesive layer affected the strength of the specimen because the stress concentrations at the corners could initiate failures in the adhesive layer (resulting in either adhesive or cohesive failures). Therefore, several different geometries of bond area and plate separation (defined as configurations) were created to modify, and specifically to relieve, the stress concentration in the adhesive.

There was no specimen that failed only due to tensile failure in the CFRP strips; all specimens finally failed by some amount of debonding. A combination of the Tyfo UC CFRP strip and the DP-460 NS adhesive achieved the highest strain in the CFRP strip. The reason for this seemed to be the ductility of the adhesive relative to the other adhesives tested. Because of the stress concentration at the edges of the adhesive layer, the adhesive yielded quickly as the CFRP strip was loaded; thus, a large ductility in the adhesive was required to achieve a high strain in the CFRP strip.

Tensile strain distributions along the outer surface of the CFRP strip were measured for several specimens to determine directly the effective bond length. The specimen fabricated with Tyfo UC CFRP strip and DP-460NS adhesive had a non-zero tensile strain region that increased

gradually from approximately 4 in. long to approximately 7 in. long as the load in the strip increased. This increase in the non-zero tensile strain region did not occur in the specimen fabricated with CarboDur CFRP strip and Sikadur 330 adhesive, where this non-zero tensile strain region was approximately 6 in. long. A reason for this increase in the non-zero tensile strain region in the specimen with the DP-460NS adhesive seems to be due to the propagation of yielding in the adhesive layer. The interface in the yielded region was able to transfer the load because a constant shear stress was retained, coupled with the adhesive having adequate ductility. Thus, based upon the measured tensile strain distribution, the effective bond length for a specimen with a Tyfo UC CFRP strip and the DP-460 NS adhesive was determined to be 7 in.

In addition to the experimental tests, a finite element analysis and analytical study were conducted to investigate if the effective bond length of the CFRP strip may be estimated without the use of experimental tests, i.e., through the use of computational analysis or with a closed-form equation. A model of the effective bond length test specimen was analyzed in two-dimensions using a commercial finite element program, ABAQUS. Each mesh consisted of approximately 20,000 nodes and 20,000 elements. The analyses were geometrically nonlinear and materially linear except for the adhesive, for which an elastic-perfectly plastic stress-strain curve was specified. All materials, steel, adhesive, and CFRP strip, were modeled as isotropic materials. A closed form solution that contained some simplifying approximations was also obtained as

$$L = \frac{5}{\beta} + \frac{1}{\beta} \left[\sqrt{2 \left(\frac{\gamma_{ult}}{\gamma_y} - 1 \right) + 1} - 1 \right]$$

where $\beta = \sqrt{\frac{G_a}{t_a} \left(\frac{1}{E_2 t_2} \right)}$, G_a , t_a , γ_{ult} , γ_y are the shear modulus, thickness, ultimate

shearing strain, and yield shearing strain of the adhesive and E_2 and t_2 are the Young's modulus and thickness of the CFRP strip. The effective bond length may be identified using these models if the tensile strain distribution in the CFRP strip at failure is known. A comparison of the tensile stresses in the CFRP strip using the experimental, closed form analytical and finite element analysis are shown in Figure E-1. It is evident from this figure, that all three methods yield close approximations, and thus it is possible to estimate the strain distribution in the CFRP strip without experimental tests. Extrapolation of this result indicates that the closed form solution should provide a reasonable estimate for the required bonded length.

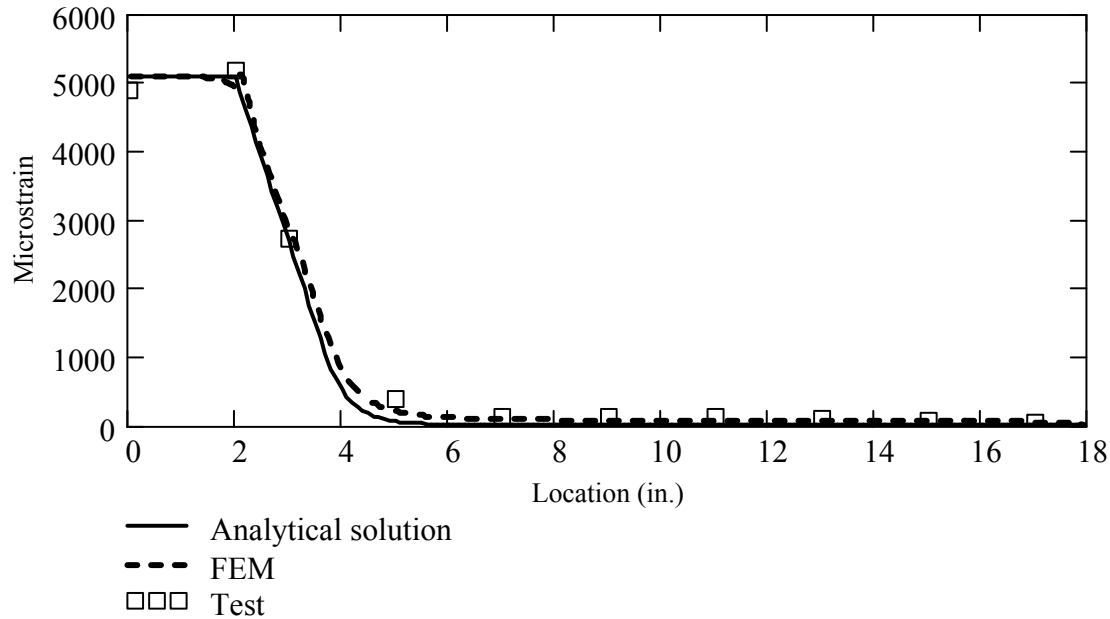


Figure E-1 Comparison of Computational, Analytical, and Experimental Test Results

The recommendations for bonded length for a single CFRP strip (arrived at through a series of experimental tests and analysis) are 8 in., plus a 2 in. unbonded region, on either side of the flange crack. Among the materials tested, 3M DP-460 NS adhesive and Fyfe Tyfo UC CFRP strips resulted in the highest strain in the CFRP strips at failure and are recommended for further research. The adhesive yielded soon after the specimen was loaded, and large ductility within the adhesive was required to redistribute the stresses successfully within the adhesive layer during increased loading.

Five tests were conducted on full-scale cracked girders to ascertain the effectiveness of the proposed retrofit. A static test on a W27×94 rehabilitated girder with bonded CFRP strips showed significant strain reduction near the crack tip when the crack tip was located in the web plate. However, in the subsequent cyclic loading tests on W27×84 rehabilitated girders with **small** cracks in the tension flange, the effect of bonded CFRP strips on the crack growth was not clearly identified. It appeared that the CFRP strip did little to help slow the growth of small cracks. It is suggested that pretensioning the CFRP strips may increase the effect these strips had on girders with small cracks. The CFRP strips, bonded to the steel using an adhesive with large ductility, did not show any signs of debonding failure after two million cycles under 5 ksi nominal stress range.

1 Introduction

In the construction of older steel bridges, it was common to weld a cover plate onto the tension flange over the pier of a continuous steel girder without extending the steel cover plate into the positive moment region. The cover plate was required to increase the flexural capacity of the section, and based on design calculations, the required length of the cover plate was usually shorter than the length from the pier to the inflection point at which the bending moment under dead load in the girder became zero, as shown in Figure 1.1. It was not necessary to extend the cover plates into the positive moment region based on the design considerations in force at the time of construction. However, many cover plate details have developed fatigue cracks at the weld toe of the cover plate ends after being subjected to cyclic tensile loads, e.g., from traffic flow [1, 2]. A typical girder with cover plate terminations is shown in Figure 1.2. After crack initiation from the weld toe of the cover plate ends was recognized as potentially causing catastrophic failure of the steel girders, design specifications were changed to require extension of the cover plates into the positive moment region of the girder so that stress reversals in the weld toe were reduced substantially, thus preventing fatigue cracking.

Because many old bridges currently in service were built without extending the cover plate into the positive moment region of the girders, it has become important to retrofit the fatigued bridge girders in order to avoid a catastrophic failure caused by crack propagation. Several studies on rehabilitation methods have been conducted, resulting in two general approaches. In the first approach, peening, arc melting, grinding, and hole drilling are directly applied to the weld of the cover plate ends, modifying the stress state around the weld or eliminating the crack [1, 2]. In the second approach, steel plates are bolted to the tension flange over the crack, restoring the flexural capacity and the strength of the section [3, 4]. As can be easily understood, the first approach is effective on cracks that have not severed the tension flange, while bolting of steel plates is applicable even after the crack has propagated through the thickness of the tension flange. Nonetheless, all rehabilitation methods listed above, except for hole drilling, require direct access to the topside of the tension flange on which the cover plate is welded. This in turn requires the removal of the concrete deck that covers the top of the tension flange in the negative moment region. In addition, the removal of the concrete deck requires

partial closing of the traffic on the bridge being rehabilitated, resulting in expensive and time-consuming work that is inconvenient for the public. For the case of hole drilling rehabilitation, several cases in which cracks had re-initiated from the holes have been reported [5], and hole drilling may affect the net section strength due, supporting a necessity to develop a new rehabilitation method, which can be used either together with or separately from hole drilling.

One approach, a bolted steel angle retrofit [6], avoids having to close the traffic during rehabilitation. In this retrofit scheme, steel angle members were bolted to both sides of the web plate of the fatigued girder. The results indicated that the crack was arrested in the web, and did not grow after nearly 2,000,000 cycles. Although the results were encouraging for the use of bolted steel angle members for rehabilitation, the angle member to be bolted to the girder tends to be long in order to develop the full yield strength of the angle member (specifically, to ensure full yielding across the outstanding leg of the angle that is parallel to the tension flange of the girder). The size of the angle member was designed so that the full yield force of the legs of the angle members was close to the yield force of the original tension flange. However, this retrofit had the problems associated with handling a heavy, large angle member and drilling many holes in the web on the rehabilitation site, resulting in costly rehabilitation work. In addition, the existences of diaphragms that are attached to the girder prevent using long angle members in such situations. Thus, it is required to find a new rehabilitation method that is easy to apply and does not require the closing of traffic on the bridges being rehabilitated. In the current study, the possibility of using Carbon Fiber Reinforced Polymer (CFRP) strips will be investigated.

The main advantages of using CFRP strips are their light weight and durability, resulting in an ease of handling and maintenance. Composite materials have been extensively used in the aerospace, automobile, and mechanical industries, where light weight and durability are critical issues in the applications of composite materials. In civil engineering applications, composite materials have gained popularity in the last several decades mainly for the rehabilitation and strengthening of concrete columns and beams because of their durability and high strength compared with concrete [e.g., 7 - 17]. In the current study, CFRP strips will be bonded on the inner surface of the fatigued tension flange over a crack as shown in Figure 1.3. Therefore, this rehabilitation method does not require access to the top of the tension flange, resulting in no need to close the traffic during rehabilitation work. In addition, no specific machines for handling are required because of the considerably lower weight of CFRP strips compared to steel. Based on

the above advantages, although the unit price of a CFRP strip may be higher than that of steel, the cost of workers and machines will be reduced, generally resulting in a decrease in the total rehabilitation cost. The report will first present development of a test setup and specimen to investigate the effective bond length of the bonded CFRP strip with adhesive onto the steel flange, and the experimental tests will then be presented. Results from cyclic loading fatigue tests on rehabilitated girders with bonded CFRP strip will be presented to investigate the fatigue resistance of bonded CFRP strips as well as the effects of rehabilitation on the crack growth.

Chapter 2 presents reviews of previous research that have been done on the rehabilitation of steel girders; in addition, studies on the bond strength with basic single-lap and double-lap test specimens are discussed. Details of the test setup, specimens, and experimental procedures for each test are discussed in Chapter 3. Effective bond length tests were conducted to determine the effective bond length for the materials used in this project. In order to further investigate the stress reduction at the crack tip, which in turn results in an increase of the fatigue life of the girder, cyclic loading tests on rehabilitated girders were conducted. The results of the experimental tests as well as corroborating numerical analyses are presented in Chapter 4. Chapter 5 concludes this report including discussions on the proposed future research subjects.

2 Literature Review

One method of rehabilitation or strengthening of civil engineering structures is bonding a CFRP strip or a steel plate to the surface of the steel or concrete structure. In past work, it has been recognized that the bond strength is significantly controlled by the surface conditions of the substrates to be bonded together. Therefore, it is important to categorize studies based on the substrates discussed in those studies. This work focuses on the rehabilitation of steel girders, and the following will discuss studies related to rehabilitation or strengthening of steel girders, including literature on the determination of bond strength in order to gain a better understanding of the bond strength of the adhesive and to list available testing methods to determine the bond strength.

2.1 Rehabilitation or Strengthening of Steel Girders

2.1.1 Studies on Composite Plates Bonded on Steel

This section will discuss studies on the use of composite materials with steel girders. As stated earlier, the use of composite materials in civil engineering is relatively new, especially with steel girders; little research has been done on this subject. In addition, research to date has focused mainly on the strengthening of steel girders with composite materials bonded on the outer surface of the tension flange without a crack [18-22]. Although the existence of a crack in the flange, as is the case of the current study, could cause a significant difference in the bond strength between the steel and composite materials, it is important to review these existing studies in order to gain a better understanding of the strength and behavior of the bonding between the steel and composite materials.

Gillespie et al. [18-20] and Edberg et al. [21] conducted a series of experimental tests on the stiffness and strength of steel girders strengthened using composite materials. In the first phase, five strengthening schemes were examined: 1) composite-plated, 2) sandwich-reinforced, 3) composite-wrapped, 4) channel pultrusion-reinforced and 5) strip pultrusion-reinforced. After the application of the strengthening scheme, each specimen was loaded monotonically and

cyclically with four-point bending. First, the specimens were loaded up to 20 kip and back to 1 kip; this was repeated five times and constituted the service load testing (stiffness tests). The specimens were then loaded monotonically to failure for the strength test. The stiffness tests indicated increases in stiffness of 11-30% on all strengthening schemes. The authors indicated that the increase in stiffness was predictable using finite element analyses; it is important to be able to predict the increase in stiffness of the girder for design purposes. The results of the strength tests showed that several specimens failed due to debonding of the composite reinforcement at one end. It was suggested by the authors that debonding of the composite materials could have been avoided by reducing the thickness of the composite materials toward the ends. Ultimate loads observed in the experiments suggested that strengthening Schemes 3 and 5 were the most efficient. Based on these test results and geometry of the strengthening schemes, Scheme 5, which would have the least effect on the clearance under bridges, was selected for further research.

In the second phase, the rehabilitation of corroded steel girders, using strengthening Scheme 5 as discussed above, was investigated. Two full-scale specimens were removed from service; each girder was 240 in. long, and was loaded monotonically under three-point bending. Pultruded unidirectional carbon/vinyl ester strips were bonded to the interior and exterior of the tension flange using two-part epoxy adhesive. The stiffness observed on the rehabilitated full-scale specimen was 97% of the original (not corroded) girder stiffness. In addition, despite the occurrence of local flange buckling in the compression flange, the ultimate load capacity was 113% of that of the original section, indicating the efficiency of the rehabilitation method.

Separately from the studies on strengthening of girders, notched steel plates rehabilitated with composite strips were tested under cyclic loading. The specimen was a flange plate cut from new A709 grade 36 girders, and pultruded unidirectional carbon/vinyl ester strips were bonded on one side of the plate over the notch as shown in Figure 2.1. The specimen was tested under cyclic loading with two stress ranges. The results for the rehabilitated specimen had a slope of 2.13×10^{-5} on a linear plot of crack length vs. loading cycle, while the unrehabilitated specimen results had an almost infinite slope. This test result indicated that the crack growth cannot be eliminated, but can be decreased by the use of bonded composite strips.

Sen et al. [22] conducted a study on strengthened steel girders with a concrete slab to investigate the possibility of extending the service life of the steel girders. The stiffness and

strength of the specimen were compared before and after rehabilitation with CFRP laminates that were bonded to the outer surface of the tension flange. Two types of steel girders with different yield strengths and two thicknesses (2 and 5 mm) for the CFRP laminate were examined. Although the stiffness of the girder was not increased significantly, the strength of the rehabilitated girder increased more than 200%. In addition, thicker composite laminates with the steel girder that had a lower yield strength tended to have a larger gain on the strength. However, it should be noted that, in several specimens, the composite laminates were mechanically bolted to the tension flange as well as bonded at the ends of the laminate to avoid debonding failure of the laminates.

2.1.2 Studies on Steel Plates Bonded on Steel

Bonding between steel and steel seems to have a long history of application. Indeed, steel-to-steel bonding has been used as a mechanical joint instead of bolted joints because of its simplicity, light weight, and short lap length compared to bolted joints. However, like composite-to-steel bonding, steel-to-steel bonding has not been widely used in the field of civil engineering. A few studies have been found in this category, and are briefly discussed below.

Albrecht et al. [23] conducted fatigue tests of adhesively bonded and end-bolted cover plates with four load ranges. The specimen, fabricated using W14×30 steel girders on which two cover plates were bonded to each side of the tension flange symmetrically about the centerline of the girder, were loaded under four-point bending. The stress range was varied from 21 ksi to 30 ksi, and the failure mode and fatigue life were investigated. The first four specimens out of 36 showed a debonding failure at the end of the cover plate (near the loading point). Thus, in the next specimen, the end of the cover plates that was near the loading point was clamped by high strength bolts. However, the end of the steel cover plates near the support debonded. Thus, the steel cover plates were bolted at both ends in all subsequent tests. The bonded specimen with both ends bolted had a crack initiation at the bolt-hole in the tension flange. However, the results indicated that the bonded and end bolted steel cover plates had significantly longer fatigue life (fatigue category B) than conventionally welded cover plates (fatigue category E or E').

The above study did not use the bonded steel plates for rehabilitation, but rather as cover plates; thus, there was no crack in the tension flange when the cover plates were bonded. In contrast, Adunutula [24] conducted a numerical study in which a cracked steel plate was

retrofitted by a bonded steel plate. He conducted a series of finite element analyses on a cracked steel plate (base plate) retrofitted by a bonded plate (cover plate) in order to investigate the effects of bonded plates on crack propagation in the base plates. The cover plate was bonded to a center cracked base plate or to a single edge notched base plate. The stress intensity factors at the crack tip with and without the cover plate were calculated and compared. After retrofitting, the stress intensity factors decreased by a factor of 1.3 and 2.2 for the center cracked base plate and the edge cracked base plate, respectively. The stress intensity factor at the crack tip was not significantly affected by changing the width of cover plates while keeping the width of the base plate fixed. It should be noted that because the failure criterion of the adhesive material was not implemented in the analysis, the analyses ignored any possibility of the debonding of the cover plate, possibly resulting in a decrease in the efficiency of the retrofit.

2.2 Bond Strength

This section will discuss existing testing methods for determining bond strength and related studies. Because adhesives have been used for mechanical joints [25] and for rehabilitation of skins of airplanes [26], there are several testing methods to determine bond strength in these fields.

2.2.1 Test Specimen for Bond Strength

Testing methods of interest use specimen called single-lap and double-lap specimens, which are illustrated in Figure 2.2. These testing methods are primarily used to measure the shear strength of an adhesive as indicated in the American Society for Testing Materials (ASTM) standards: D1002 for single-lap joints [27], and D3528 for double-lap joints [28]. A single-lap shear specimen consists of two adherends bonded together with an adhesive. Tensile loads are applied at both ends of the adherends. Because there is a misalignment of the neutral axes in both adherends, the joint will bend, causing peeling stress due to a relative displacement of the two adherends in the vertical direction as shown in Figure 2.3. Based on the thicknesses of the adherends and the adhesive, and their material properties, this peeling stress may become significant and cause failure. The shear stress distribution is non-uniform, having high stress concentrations at the edges. Therefore, the test result of the single-lap shear specimen does not indicate the pure shear strength of the adhesive, but the strength under a combined stress state of

shear and peeling stress at the high stress location, as stated in the ASTM standard (ASTM D 4896). On the other hand, the double-lap shear specimen does not have a misalignment in the specimen as a whole. However, there is still a misalignment of the neutral axis internally; i.e., the applied load will shift from the inner adherend to the outer adherend (or vice versa). Thus, the outer adherend will act like one of the adherends in the single-lap specimen; i.e., a free body diagram of the outer adherend is the same as the upper adherend in Figure 2.3, and peeling stresses will be induced in the adhesive. Therefore, the measured strength of the adhesive is not the pure shear strength of the adhesive.

Although single-lap and double-lap specimens do not give the exact shear strength of the adhesive, these specimens are useful for some applications. Because single-lap or double-lap joints are used in the application of mechanical joints [25], the strength of those joints can be defined by single-lap or double-lap specimens as long as the sizes of adherends closely approximates those in the field application. In other words, the stress distributions in the adhesive layer need to be similar between application and test specimen. The bond strength defined by single-lap specimen is also useful in the application of skin patching because of the similarity of the geometry at an overlap region; i.e., a part of the overlap region can be assumed as a group of single-lap joints [26]. Therefore, much research has been conducted on predicting the bond strength of lap joint specimens, including numerical and experimental studies; a few of these will be discussed in the following sections.

2.2.2 Experimental Studies

One interesting study has been reported by Ikegami et al. [29]; they conducted a round robin of experimental tests on several joint types, including butt, single-lap, and double-lap, at several institutions. The results indicated that the strengths of single-lap joints made by each institution (there were a total 11 institutions) varied up to 40%, although the adherends, adhesive, and dimensions of the joints were the same for all specimens. They also fabricated joints at one institution and distributed them to three institutions for testing to see whether the fabrication process at each institution affected the results. The variation of the joint strength was decreased, clearly indicating the importance of a consistent fabrication process of joints.

Sugibayashi et al. [30], Kyogoku et al. [31-33], and Ono et al. [34] conducted a series of experiments on single-lap specimens with various adherend materials and thicknesses with an

epoxy adhesive. They found lap lengths that yielded the maximum strength of the joints for each combination of adherends and thicknesses, indicating difficulty in concluding one optimum bond length for all possible combinations of materials. In addition, they conducted experiments with tapered lap joints, and observed an approximately 100% increase in the joint strength; this was due to a decrease in the stiffness of the adherends at the ends of the overlap region, resulting in less peel stress at the edges of the adhesive layer. Furthermore, they predicted the joint strength using a proposed failure criterion based on stresses obtained by finite element analysis. Although the predictions seemed to reasonably represent a trend of the joint strength, it should be noted that stresses obtained by finite element analysis vary depending on the meshes used for the analysis models due to the singularity at corners in the adhesive layer, affecting the accuracy of the predictions.

2.2.3 Computational Studies

Dorn et al. [35] and Harris et al. [36] also conducted finite element analyses and predicted the joint strengths obtained by experimental tests. In both studies, the specimen had spew fillets (see Figure 2.4) at the ends of the adhesive layers to represent a realistic joint geometry; it has been recognized that the existence of spew fillets decreases the maximum stress at the edges of the adhesive layer, and increases the joint strength. Harris et al. predicted the strength of single-lap joints with aluminum adherends and four types of adhesives using both stress and strain criteria. Failure of the specimen occurred mainly in the adhesive layer. The results indicated that the strengths of joints with two out of four adhesives were closely predicted by the stress criterion while the other two were predicted by the strain criterion. It seems that the joint strength was controlled by the stress criterion if the joint was made with a brittle adhesive and by the strain criterion if the joint was made with a ductile adhesive. On the other hand, experimental tests conducted by Dorn et al. resulted in the failure in one of the adherends, ABS plastic, instead of failure in the adhesive; the other adherend was steel or aluminum alloy. Thus, the authors used a strain criterion in the ABS plastic to predict the strength of the joints. For both studies, it seems difficult to predict the joint strength prior to the experiment because a location of failure in the joints needed to be known prior to the application of these failure criteria.

2.2.4 Analytical Studies

Before finite element analysis was widely available to researchers, stress distributions in the adhesive layer in bonded joints (especially single-lap joints) were analytically investigated. Solving for exact stress distributions in the adhesive layer in closed form is not possible. Therefore, researchers have made various assumptions and simplifications to obtain closed form solutions. It has been usual to consider only shear and peeling stresses in the adhesive layer because of its thickness, as shown in Figure 2.3. However, two differential equations derived from Figure 2.3 include both shear and peeling stresses in each equation, making it difficult to solve in closed form.

Volkersen [37] derived a simple solution considering only shear stress in the adhesive layer and tensile load in the adherends. Goland and Reissner [38] included bending moment of the adherends in order to include the effect of the eccentricity of the load path on the stress distributions. In their analysis, an overlap portion of the single lap joint was modeled as one beam to solve for edge loads, shear and moment, in the overlap region. On the other hand, Hart-Smith [39] treated the two adherends separately, having bending effects of the adherends considered. In addition, he solved problems for single-lap and double-lap joints with linear elastic and elastic-plastic adhesives [40, 41]. Other researchers have followed these studies and improved the solutions for shear and peeling stress distributions in the adhesive layer [42-46].

Although there are many solutions for the shear stress distribution in the adhesive layer for the single-lap joint, comparison of the maximum shear stress revealed that the differences between several assumptions, including consideration of the strain gradient through the thickness of the adhesive layer and shear deformation of the adherends, was not significant [47]. In addition, the solutions based on analytical solutions were not exact if the stress singularity at the edges of the adhesive layer was considered. Therefore, in order to use these analytical solutions for design purposes for bonded joints, calibrations of the analytical solutions seem necessary. Hence, it is reasonable to use an analytical solution with the simplest assumptions, resulting in simple solutions, for design purposes. The simplest analytical model considers only shear stress in the adhesive layer and tensile load in the adherends; derivations of these solutions for the materials used in this work will be discussed later in Chapter 4.

3 Experimental Tests

3.1 Materials for Rehabilitation

In this section, the properties of the materials used in this project will be presented. A total of five adhesives and two CFRP strips were tested. The adhesive plays the most important role in the rehabilitation with bonded CFRP strips since the adhesive has to transfer the load from the steel flanges to the CFRP strip and the adhesive is usually the weakest link in bonded systems. If the adhesive fails prematurely, including adhesive and cohesive failures, the high strength of the CFRP strip cannot be utilized efficiently. In addition, the effectiveness of the rehabilitation depends on the stiffness and the strength of the CFRP strip. CFRP strips with high stiffness are able to increase the moment of inertia of the section being rehabilitated, reducing the stress at a crack tip. Use of a strip having high strength can increase the moment capacity of the section. Furthermore, adhesive strength could vary depending on the materials to be bonded, indicating the importance of obtaining the right combination of adhesive and CFRP strip.

3.1.1 Adhesive

The adhesives utilized in this project were two-part, room-temperature-cure epoxy adhesives. The adhesives were applied without any primers. Since the application of adhesives for the rehabilitation of steel girders will be conducted under the bridge, it was required that the application process be simple in order to minimize the repair and application errors. Two-part epoxy adhesives satisfy these requirements. Furthermore, a viscous adhesive was needed to allow for overhead application.

The first adhesive tested in this project was Sikadur 330, a product of Sika Corp. The mechanical properties of the bulk adhesive as reported by the manufacturer are 4.35 ksi (30 MPa) and 1.5% for tensile strength and elongation at rupture (testing methods are not specified), respectively. Tensile coupon tests were conducted following ASTM D 638 [48] on this adhesive to verify the material properties indicated by the manufacturer. It should be noted, however, that the shape of specimen was out of tolerance. Averages of five specimens resulted in 670 ksi, 6.0

ksi, and 0.9% for elastic modulus, tensile strength, and elongation at rupture, respectively, as shown in Table 3.1. The curing and working time (pot life) are seven days and 30 minutes, respectively. The second adhesive was Sikadur 30, also a product of Sika Corp. The difference between Sikadur 30 and Sikadur 330 is that Sikadur 30 contains fine sand to make the adhesive more viscous. The tensile strength and elongation at rupture specified in the data sheet are 3.6 ksi and 1% (ASTM D 638), respectively. The curing and working time (pot life) are seven days and 70 minutes, respectively. The third adhesive used was Polystrate EPOXY PLUS 25, a product of Devcon. The shear strength of this epoxy is 2.5 ksi as reported by the manufacture for single lap tests on cold rolled steel (ASTM D 1002 [27]). Twenty-four hours and 25 minutes are curing time and working time, respectively. The fourth adhesive was DP-460NS, a product of 3M. Single lap shear strength with cold rolled steel (ASTM D 1002) specified in the data sheet is 3.6 ksi. Averages of five tensile tests on this adhesive resulted in 364 ksi, 5.1 ksi, and 2.1% for elastic modulus, tensile strength, and elongation at rupture, respectively, as shown in Table 3.2. The tensile coupon was shaped as that for metals specified in ASTM E8 [49] instead; however, loading rate was set according with ASTM D 638. The curing and working time (pot life) are twenty-four hours and 60 minutes, respectively. The last adhesive tested was Tyfo TC adhesive, a product of Fyfe Co.; tensile strength and elongation at rupture are 6.8 ksi and 3.3% (ASTM D 638), respectively as specified in the data sheet. The curing and working time (pot life) are three days and 1 to 2 hours, respectively.

3.1.2 CFRP Strip

Two CFRP strips were tested; both were unidirectional carbon fiber reinforced polymer with epoxy matrix. It has been recognized that direct contact between carbon and steel causes corrosion on steel surfaces [50], and this could be a cause of premature failure of adhesion in the rehabilitation of steel flanges as well as the loss of a part of the cross section. However, as manufactured, fibers in both strips were covered by a matrix, which consisted of epoxy resin; thus, direct contact between carbon fiber and steel should not occur with these CFRP strips. Therefore, corrosion of steel surfaces will not be discussed further in this report.

The first CFRP strip was CarboDur, a product of Sika Corp. The thickness and width of the strip were 0.05 in. and 4 in., respectively. The tensile strength, tensile modulus, and elongation at rupture (all in the fiber direction) specified in the data sheet were 406 ksi, 23 900

ksi and 1.9 % (ASTM D 3039 [51]), respectively. Averages of five tensile tests conducted for this project (based on the test procedures specified in ASTM 3039) resulted in 380 ksi, 22 700 ksi and 1.7%, for tensile strength, modulus of elasticity, and elongation of rupture, respectively, as shown in Table 3.3. The second CFRP strip was Tyfo UC composite laminate, a product of Fyfe Co. The thickness and width of the strip were 0.075 in. and 4 in., respectively. The tensile strength, tensile modulus, and elongation at rupture were specified as 405 ksi, 22 500 ksi and 1.8 % (ASTM D 3039), respectively, in the data sheet. The strips were also tested for this project (ASTM D 3039), and averages of three specimens were 290 ksi, 16 500 ksi, and 1.8% for the tensile strength, tensile modulus, and elongation at rupture, respectively, as shown in Table 3.4.

3.2 Effective Bond Length Tests

This section will explain the details of the effective bond length tests, including geometries of the test setup and the specimens, the test matrix, and instrumentation for the experiments. The effective bond length is defined as the shortest bond length that engages the largest possible strength of the CFRP strip. Failures of bonded joints include adherend, adhesion, and cohesion failures. Because the strength of bonded joints cannot exceed the strength of the adherends, the main objective of the effective bond length tests was to determine if a bond length existed that would utilize the full strength of the adherend.

3.2.1 Test Setup and Specimen

The general layout of the test setup and specimen with dimensions are shown in Figure 3.1 to Figure 3.3. The girder was a W14×68 Grade 50 steel ($d = 14.04$ in.; $b_f = 10.035$ in.; $t_w = 0.415$ in.; $t_f = 0.720$ in.) and was 170 in. in length. A large hole and a slit, 0.5 in. in width, were created at the center of the girder (Figure 3.2); the slit represented a crack in the tension flange in the field applications although the width of the crack was exaggerated. The specimen was loaded in tension by placing it on the tension side of the girder that was loaded in flexure. The hole and slit were created in order to separate the compression force in the top flange from the tensile force in the CFRP strip. If the tension flange in the girder had been left in place, i.e., without the slit, the tension flange and a part of the web would have yielded before reaching the rupture strain of the CFRP strip, making it impossible to reuse the girder for multiple tests. The

size of the girder, mainly the size of the compression flange, was calculated so that the top flange would not yield or fail by local buckling when two layers of CFRP applied to the bottom flange reached their rupture strength in tension.

The specimen consisted of between one and three CFRP strips bonded onto two steel plates, depending on the specimen as shown in Figure 3.3. The two steel plates were made of Grade 50 steel; a picture of typical specimen is shown in Figure 3.4. The difference between Specimen Type A and Specimen Type B is the gap between the steel plates and the length of the plates. Specimen Type B were made longer in length so that two layers of CFRP could be tested because multiple layers of strips would require more bolts to keep the plates from slipping with respect to the bottom flange. By bonding the CFRP strip on the steel plates instead of bonding directly on to the tension flange of the girder, it was possible to re-use the steel plates by removing the CFRP strip and adhesive left on the steel plates after each test. The specimen was bolted to the underside of the tension flange of the base girder as can be seen in Figure 3.5. Initially, the bolted connection was designed for the bearing strength of bolts against the failure load of the CFRP strip. However, the bolts were pretensioned to achieve the slip critical condition after several experiments because slip between the steel plates and the flange was observed during the tests. The number of bolts was also sufficient for design as a slip critical connection.

The girder with specimen was loaded under four-point bending with displacement control. Loading was applied using either one or two MTS 77 kip actuators, one 220 kip actuator or one 600 kip actuator, depending on the availability of these actuators. For loading set-up, the girder was loaded with 80 in. of distance between loading points in order to create a constant moment region. The total span of the girder was 160 in. for all tests except for the set-up with one 600 kip actuator; in which case, the span was 120 in. by placing the supports 20 in. inside from the position illustrated in Figure 3.1. In the case of a two-actuator setup, two 77 kip actuators were directly connected to the girder as shown in Figure 3.1, and one actuator was controlled as a slave of the other actuator using load feedback. For the one-actuator setup, a spreader beam was connected to the actuator to achieve the four-point loading condition. Round bars with 2 in. diameter were placed at all loading points on the girder and at supports except for the two-actuator loading case.

The specimens were fabricated as follows. Steel surfaces were first abraded (grit #40 for initial abrasion and #100-150 for finish) and wiped with acetone to remove any contamination on the steel surfaces, and the CFRP surface was wiped with acetone. The steel plates were then connected with lift bars (Figure 3.3) and a spacer was inserted for Specimen Type A to secure the plates. Before application of the adhesive, aluminum flat bars were placed and fixed on the steel plates in order to position the CFRP strip at the center of the plates along these aluminum bars. The adhesive was mixed and applied onto the surfaces. The CFRP strip was placed on the steel plates with lightly applied pressure; mixing time and method varied for each adhesive as specified by the manufacturer. The aluminum flat bars that were placed prior to application of the CFRP strip were removed immediately and the adhesive was cured at room temperature. Several specimens with 3M DP-460 NS adhesive were cured in an oven to reduce the curing time, and these specimens were cure for 30 min at 200°F.

This test setup and specimen were designed so that results of the effective bond length tests can be applicable to the field application of CFRP strips. In other words, the strength determined through the experiments was representative of the strength of the rehabilitation. Detail discussions on the validity of the test setup can be found in Appendix A.

3.2.2 Test Matrix

A total of 27 specimens were tested, as shown in Table 3.5. These consisted of twenty-three one-layer specimens, three two-layer specimens and one three-layer specimen. The first number in the name of specimen indicates the number of layers. The main variables in these tests were CFRP and adhesive material, crack and bond configuration, and bond length. The bond thickness was changed according to the application procedure specified by the manufacturer and is listed in Table 3.5. Selected combinations of variables were tested on several specimens in order to investigate consistency of the results as indicated in the note column in the tables.

It was thought that the existence of sharp corners in the adhesive layer affected the strength of the specimen because the stress concentrations at corners could initiate failures in the adhesive layer (adhesion or cohesion). Therefore, several different geometries of bond area and plate separation (defined as configurations) were created to modify (relieve) the stress concentration in the adhesive. Figures, which illustrate these different configurations, are shown

in Figure 3.6. Configurations 1 through 3 had a 0.5 in. slit between steel plates (Type A specimen). In Configuration 1, adhesive was left on the CFRP strip, creating 90-degree corners between the adhesive and the steel plates. In Configuration 2, the slit between steel plates was filled with adhesive to eliminate those corners. In Configuration 3, the adhesive was removed from the CFRP in the slit between the plates in order to create 90-degree corners between the adhesive and the CFRP strip. In Configurations 4 and 5, the slit was closed by extending the steel plates by 0.25 in. from both sides. Configuration 5 was a slight modification of Configuration 3 and had 90-degree corners on both sides of the adhesive layer. A main difference between Configurations 3 and 5 was that Configuration 5 was created without a gap between the steel plates; thus, the edge of the adhesive did not line up with the edge of the steel, better simulating the field application. In Figure 3.6, Configuration 5 is illustrated with Specimen Type B (no gap between plates); however, this configuration was also possible with Specimen Type A (0.5 in. gap between plates) considering that the existence of a gap does not affect the stress concentration in the adhesive layer. Several specimens with Configuration 5 were actually tested using Specimen Type A as listed in Table 3.5.

3.2.3 Instrumentation

The girder and specimens were instrumented with Tokyo Sokki Kenkyujo, FLA-3-11-3LT strain gauges as illustrated in Figure 3.7 and Figure 3.8. The small black rectangles in the figures indicate the gauge locations. The base girder was instrumented with a total of 11 gauges located at the center of the span (section B-B) and at sections 30 in. apart from the center (section A-A). Gauges at the center were to monitor the strain distribution in the compression flange for comparison with strain measured on the CFRP strip. Gauges located 30 in. from the center were placed to calculate the moment in the girder, and compared to the applied moment to ensure constant moment existed between the loading points.

At least one strain gauge was placed on the CFRP strip for each specimen in order to see the maximum strain at the failure of the specimen. This information was used to determine how much of the strength of the CFRP strip was achieved. For selected specimen, CFRP strips were heavily instrumented with strain gauges to investigate tensile strain distributions along the length of the CFRP strips; these results also indicated the adequacy of the bond length. In addition, tensile strain distributions were compared to those from finite element analyses to see the

validity of the analyses. These heavily instrumented specimens were 1-4, one of 1-8, 1-14, and 2-3. Gauging schemes for these specimens are illustrated in Figure 3.8. It should be noted that Figure 3.8 shows only one half of the specimen and gauges were instrumented symmetrically with respect to the centerline except for specimen 1-8 and 2-3, which had gauges only on one half of the CFRP strip. In addition to the gauges shown in Figure 3.8, one strain gauge was attached to the CFRP strip in the slit for several specimens with Configuration 3 as shown in Figure 3.6 in order to check the strain gradient through the thickness of the CFRP strip.

3.3 Preliminary Test on Rehabilitated Girder

Preliminary static loading tests were conducted with a large-scale fatigued steel girder to investigate the effect of rehabilitation with bonded CFRP strips. The results of experimental tests were used to justify the effect of the rehabilitation before planning cyclic loading tests on full-scale girders. It was not certain that a thin layer of CFRP (0.05 in.) could affect the crack growth because of the relatively small increase in moment of inertia after the rehabilitation.

3.3.1 Test Setup and Specimen

The girder tested in this experiment was a W27x94 rolled steel section with a length of 180 in.; the girder was used for another project on the study of fatigued steel flange rehabilitation with bolted angle members [6]. Figure 3.9 and Figure 3.10 are a sketch and a picture, respectively, of the test setup; the test setup was identical with that for the effective bond length tests with two actuators. The girder was loaded monotonically under four-point loading; one actuator was under displacement control as the master and the other one was controlled as the slave using load feedback. The girder already had a crack at its center, and it was arrested at one bolt hole in the web plate. Therefore, in order to conduct further tests on this girder, the crack was re-initiated from the bolt hole into the web plate; the final length of the crack before the experimental tests was about 4 in. from the bottom of the girder as shown in Figure 3.12.

Materials used for rehabilitation of the girder were CarboDur CFRP strip and Sikadur 330 adhesive. Although, a combination of Fyfe UC and DP-460NS adhesive was found to give a better result in the effective bond length test, products of Sika were used here because Fyfe UC and DP-460NS had not been tested at the time of this static test. One layer of strip was applied on both sides of the web plate, i.e., one CFRP strip on one side of a free edge portion of the

tension flange. A sketch of the rehabilitation is shown in Figure 3.11; the CFRP strips were bonded with 8 in. of bond length and a 4 in. unbonded region in the center, representing Configuration 5 in the effective bond length tests. Adhesive was applied after surface treatment of steel flanges, including abrasion of the surface of the tension flange with sand paper and wiping with acetone.

3.3.2 Test Matrix

Two tests were conducted; 1) up to 31 kips of load per actuator without rehabilitation, 2) up to 31 kips of load per actuator with rehabilitation. Maximum applied load of 31 kips was determined based on the nominal stress of 5 ksi in the original (uncracked) section.

3.3.3 Instrumentation

Measured data in these tests included strains in the girder and CFRP strip, deflections at the center of the girder, and load and stroke of the actuators. Strain gauges used through these tests were the same as for the effective bond length tests, Tokyo Sokki Kenkyujyo, FLA-3-11-3LT gauges. Deflections were measured with a standard size Linear Variable Differential Transformers (LVDT), a product of Columbia Research Laboratories, with a linear range of ± 0.5 in.

Strain gauges were placed at 2 sections on the W27x94 girder as shown in Figure 3.12 and Figure 3.13, at the center and at 10 in. from the center. In addition, one strain gauge was placed just above, about 0.25 in., the crack tip. The section 10 in. from the center was in the same section with the end of the CFRP strip; thus, results from this section could indicate how much force was recovered in the tension flange through the rehabilitation. Although CFRP strip was bonded to the flange on either side of the web, only one of the strips was instrumented as shown in Figure 3.14; these gauges were used to measure the strain distribution in the CFRP strip and to compare with that obtained in the effective bond length tests. Figure 3.15 shows a picture of rehabilitated girder after instrumentation. Note that because the crack had not grown straight in the web plate, the location of the gauge near the crack tip was not actually in the same section with the gauges at the center section as can be seen in the picture. In addition to the strain gauges, two LVDTs were placed at the center of the girder on both sides of the crack as shown in Figure 3.16; and the deflection of the girder was recorded during the experiments.

3.4 Cyclic Fatigue Loading Tests on Rehabilitated Girders

This section presents details of the test setup, specimen, and instrumentation for the cyclic fatigue loading tests on rehabilitated girders. The objective of this series of tests was to determine the effect of the rehabilitation on the crack growth having the cross section size and a crack length comparable with that in the field. Because the hole drilling rehabilitation method has been widely used in the practice, this rehabilitation scheme was combined with the bonded CFRP strips when the specimen was rehabilitated during the experiments. Crack growth was monitored before and after rehabilitation, and results were compared to examine the decrease in the crack growth.

3.4.1 Test Setup and Specimen

The general layout of the test setup and specimen with dimensions are shown in Figure 3.17 and Figure 3.18. The girder was a W27×84 and was 336 in. in length. The specimen was loaded under four-point bending with 320 in. of total span. The length between the support and actuator, and the distance between actuators were 120 in. and 80 in., respectively as shown in Figure 3.17. The two actuators were MTS 77 kip actuators, and both were under load control with a synchronized command signal (sine wave); cyclic loading between 1 to 2 Hz was applied, depending on the load range, during the experiments. The load range will be discussed in the next subsection.

The specimens, W27×84 girders, were donated by the Minnesota Department of Transportation (Mn/DOT) and the size of the specimen was determined so that the size of the girder reasonably represented girders in service, as well as being based on the availability of girders from Mn/DOT. Materials used for the rehabilitation were Fyfe Tyfo UC CFRP strip and 3M DP-460 NS adhesive and surface preparation and application procedures were the same as those discussed in Sections 3.2 and 3.3.

Threaded rods, box tube sections, and a floor beam (W14×211) were parts of a dead-load holding device. In order to simulate the field conditions, a dead load (10 ksi nominal stress at the top and bottom flanges in the constant moment region) needed to be maintained during the application of the rehabilitation, and throughout the cyclic fatigue loading tests. In particular, a device was required so that the dead load was kept on the girder in case the hydraulics was

accidentally shut off during the cyclic loading. This device was designed to hold the dead load by restraining the deflection of the girder; i.e., the device kept the girder at the deflection that corresponded to approximately 10 ksi nominal stresses at the top and bottom flanges in the constant moment region. Because the load to be carried by the device was not significantly large, the main issue of designing the device was stiffness, i.e., total elongation of the device. The total elongation of the device was assumed to be equal to the elongation of the threaded rod because of its significance among the contribution from all parts.

The device was installed so that the box tube on top of the girder did not contact the girder while the girder was under cyclic loading. First, the box tube was placed on the girder and secured in position by nuts while the dead load was applied by the actuators. Then, during the cyclic loading, the minimum load was set to a value slightly larger than that corresponding to the dead load in order to avoid repeated contact between the girder flange and the box tube sections. Because the threaded rods extend once the actuators are off and the girder tries to go back to its original position, some loss of the dead load was expected. The load in the threaded rods after release of the dead load by the actuator can be calculated as follows. First, the loss of dead load reduces the deflection of the girder. The deflection of the girder, in turn, can be linearly related with the load at the location of the box tube (point B in Figure 3.19). Therefore, the force at point B after the loss can be expressed as follows.

$$P_{b_after_loss} = \frac{\Delta_{b_dead} - \Delta_{b_elongation}}{\Delta_{b_dead}} \cdot P_b(\Delta_{b_dead}) \quad (1)$$

On the other hand, the elongation of the threaded rods can be calculated as,

$$\Delta_{b_elongation} = \frac{P_{b_after_loss} \cdot L_{rod}}{2 \cdot E \cdot A_{rod}} \quad (2)$$

Then, substituting Equation (2) into Equation (1) yields,

$$P_{b_after_loss} = \frac{\Delta_{b_dead}}{\frac{L_{rod}}{2 \cdot E \cdot A_{rod}} + \frac{\Delta_{b_dead}}{P_b(\Delta_{b_dead})}} \quad (3)$$

In the above equations, Δ_{b_dead} is the deflection of the girder at the location of the box tube due to the application of dead load by the actuators; $P_b(\Delta_{b_dead})$ is the required load at the location of the box tube section to maintain the deflection, Δ_{b_dead} ; $\Delta_{b_elongation}$ is the elongation of the threaded rod; $P_{b_after_loss}$ is the load at the location of the box tube after the elongation of the

threaded rods take place; L_{rod} is the initial length of threaded rod; E is the elastic modulus of threaded rod; A_{rod} is the area of the threaded rod.

The loss of dead load can then be obtained by comparing $P_{b_after_loss}$ with the load at the location of the box tube corresponding to 10 ksi nominal stress at the top and bottom flanges in the constant moment region, P_{b_dead} . Based on the above equations, the loss of dead load was calculated to be less than 5% (with $L_{rod} = 53$ in. and 1" diameter threaded rod); thus, the device was thought to be adequate for the purpose.

3.4.2 Test Matrix

A total of four specimens were tested and a description of the test specimen is shown in Table 3.6. The main parameters being studied were application of bonded CFRP strips and the time of application of the rehabilitation. Three of the specimens were first repaired by hole drilling to represent a rehabilitation scheme being used in practice. All specimens were cyclically loaded from 17.8 kip to 23.2 kip per actuator, corresponding to 3 ksi nominal stress range at the top and bottom flanges. This stress range was selected because it is representative of the largest stress range measured in these types of bridges around the Minneapolis/St. Paul metropolitan area [6].

Two of the specimens with 3 ksi nominal stress range (NR-3, R-3-1) were rehabilitated after the crack length became approximately 2 in., both with drilled holes and one without and one with a bonded CFRP strip in order to confirm the effect of the bonded CFRP strips on the crack growth. The specimen having a 3 ksi nominal stress range (R-3-2) was rehabilitated with a bonded CFRP strip after the crack reached the inner surface of the tension flange; the crack length at the time of rehabilitation for this specimen was assumed to be longer than 2 in. in specimens NR-3 and R-3-1. The last specimen was rehabilitated only with the bonded CFRP strips to investigate the direct influence of bonded CFRP strips on the crack growth, and the stress range was increased to 6.5 ksi.

Because a crack needed to be initiated and grown to a certain length before the experiments were actually started as listed above, two steel plates butted up to each other were welded to the bottom of the tension flange, and the girder was loaded with higher load compared to that during the experiments, approximately a 10 ksi nominal stress range. Loading was

continued until the crack became a desired length, and the two steel plates were removed before the girder was rehabilitated.

3.4.3 Instrumentation

Figure 3.20 shows the typical instrumentation of the specimen; a black rectangle indicates a gauge in the figure. Two sections in the girder were instrumented with three and four gauges: at the center and 20 in. from the center, respectively. These gauges were placed in order to check whether an appropriate load was applied to the girder and to monitor any changes in applied moment that occurred as the crack grew.

In the figure, all possible gauges are shown. Some of the specimens were instrumented with fewer gauges. Specimen NR-3 was not rehabilitated with bonded CFRP strips; thus, this specimen did not have any gauges on the strips as shown in the figure. Specimen R-3-1 had all the gauges shown, while Specimen R-3-2 and R-3-3 did not have gauges on the strips except for two gauges at the center of the strips. Gauges on the CFRP strips were placed to measure strain distributions in the strips and to check how the strain changed under cyclic loading. In addition, these gauges on the strips were thought to be able to detect debonding under cyclic loading.

4 Results and Discussion

4.1 Effective Bond Length Tests

In this section, test results of the effective bond length tests are presented. First, a summary of test results is discussed to show how the adhesive and CFRP strip were selected for further study and how the effective bond length was determined by the experiments. Applied moment vs. CFRP strain curves for selected specimens are then presented along with the results of finite element analyses to discuss the behavior of the specimens and the correlation between the experiments and analyses. The final results presented in this section are tensile strain distributions in the CFRP strips measured during the experiments and those obtained by the analyses.

4.1.1 Summary of Test Results

A summary of the results of the effective bond length tests is listed in Table 4.1, which includes for each specimen the maximum applied moment, the tensile strain in the CFRP strip measured on the outer surface of the CFRP strip at its center at failure, and the failure modes of the specimens (D stands for a debonding failure and F for a partial tensile failure in the CFRP strip). As discussed in Section 3.2, the main objective of the effective bond length test was to determine the effective bond length for the materials used in this project. The effective bond length is defined as the shortest bond length that would achieve the highest possible strain in the CFRP strip at failure. A bond length longer than the effective bond length will not increase the maximum strain in the CFRP strip further.

4.1.1.1 Effective Bond Length

As can be seen in Table 4.1, a combination of a Tyfo UC strip and DP-460 NS adhesive achieved the highest strain in the CFRP strip, more than 13,000 microstrain. It should be noted that several tests were terminated before the failure of the specimen. These tests were terminated to avoid large inelastic deformation in the test girder. By comparing the results of Specimens 1-6 to 1-16, except for Specimen 1-10, with the same configuration (Configuration 5), two

combinations, the Tyfo UC composite and the DP-460 NS adhesive, and the Tyfo UC composite and the Fyfe TC adhesive, resulted in the highest strains in the strips. The reason for this seemed to be the ductility of adhesive; e.g., the rupture strain of the DP-460 NS is approximately 2.1%. Because of the stress concentration at the edges of the adhesive layer, the adhesive yielded quickly as the CFRP strip was loaded; thus, a large ductility was required to achieve a high strain in the CFRP strip. A reason for selecting the adhesive DP-460NS for further experiments in this project was the ease of application of the DP-460NS, which comes in a cartridge with a mixing nozzle. On the other hand, the Fyfe TC adhesive, which can be mixed in a large amount at once, would be suitable for application over a large area. A comparison between Specimens 1-13 and 1-14 indicates no improvement in the results due to an increase in the bond length. Thus, the effective bond length seems to be 8 in. or less for one layer of strip.

4.1.1.2 Effect of Multiple Layers of CFRP

As can be seen in the results with multiple layers of strips, increasing the number of layers improved the maximum moment at failure; however, the strain at failure was not increased compared with a single layer-specimen having the same materials. For specimens with the Sikadur 330 adhesive, a two-layer specimen achieved approximately twice the maximum moment at failure as did the single-layer specimen (Specimen 1-3 vs. 2-1 and Specimen 1-5 vs. 2-2). However, the three-layer specimen (Specimen 3-1) showed only a slight increase over the two-layer specimen, i.e., approximately 2.2 times the maximum moment of the single-layer specimen. On the other hand, the maximum moment at failure of the two-layer specimen with the DP-460NS adhesive was approximately 1.7 times that of the single-layer specimen (Specimen 1-14 vs. Specimen 2-3). This is a reasonable increase considering the slight decrease in the strain in the strip at failure; the strain in the strip for the two-layer specimen was approximately 77% of that in the single-layer specimen.

Although the maximum moment at failure seems to be linearly related to the number of layers, i.e., the total cross sectional area of the CFRP strips, between the single and two-layer specimens, less increase in the maximum moment for the three-layer specimen raises a doubt regarding the possibility of having a constant strain distribution through the thickness of the CFRP strip. This result indicated that a strain gradient exists through the thickness of the CFRP strip. The existence of the strain gradient through the thickness was confirmed by placing strain gauges on both surfaces of the strip, as discussed in the Section 4.1.2.3.

4.1.1.3 Failure Mode

The last column in Table 4.1 indicates the failure mode for each specimen. In Table 4.1, D stands for a debonding failure and F for a partial tensile failure in the CFRP strip. Figure 4.1 shows a typical debonding failure, with several fibers being left on the adhesive surface. Figure 4.2, Figure 4.3, and Figure 4.4 illustrate typical combined strip fracture/debonding failures. There was no specimen that failed only due to tensile failure in the CFRP strips, and all specimens finally failed by some amount of debonding. The specimens with the Sikadur 330 adhesive and Configurations 1, 2, and 4 failed mainly by the CFRP debonding from the adhesive. No failure in the CFRP strip was observed in these specimens. As the configuration was changed to 3 and 5, a partial tensile failure in the CFRP strips was observed; however, it was not possible to determine which failure, strip fractures or debonding, occurred first by observations during the experiments. The failure in the CFRP strip, i.e., the amount of broken fibers, was further increased by using the more ductile adhesive, DP-460NS, as shown in Figure 4.4. This trend of increasing broken fibers can be explained by the increase in the maximum strain measured. However, the maximum strains measured on the bottom surfaces were not as high as the rupture strain of the CFRP strips; thus, it was suspected that a strain concentration existed in the CFRP strip near the corner of the adhesive layer, e.g., around circle A in Figure 3.6.

Although all specimens finally failed by debonding, the difference in the maximum moment and the CFRP strain at failure suggests that the initiation of the debonding failure occurred in different ways and at different times for each configuration and adhesive. In the specimens with a brittle adhesive (Sikadur 330) and Configurations 1, 2, and 4, a crack initiated in the adhesive layer at the location of the stress concentration (e.g., circles B and C in Figure 3.6). This crack propagated toward the CFRP-adhesive interface and caused the final debonding failure. On the other hand, the specimen with the ductile adhesive (DP-460NS) was able to sustain more load before the crack initiated in the adhesive layer, resulting in a higher strain in the CFRP strip. These specimens with the ductile adhesive were able to achieve the rupture strain locally in the CFRP strip but not at the location where the strain in the CFRP strip was measured using a strain gauge during the experiments.

4.1.1.4 Effect of Cyclic Loading during Curing

In order to investigate the effect of vibration from traffic on curing and final strength development of the adhesive, vibration was simulated with an actuator using the same test setup as the effective bond length tests. Specimen 1-15 was bolted to the girder as soon as the CFRP strip was applied to the steel plates (prior to set time), and the girder was cyclically loaded to simulate vibration from traffic. The cyclic loading was started approximately one hour after application of the CFRP strip because of the time to attach the specimen to the girder. A crack opening in the fatigued tension flange due to vibration from the traffic was simulated as an opening displacement of the gap between the two steel plates of the specimen. Assuming an approximate 0.5 ksi stress range in the tension flange due to traffic in the field, a gap opening at the peak of each cycle corresponding to a 1 in. LVDT gage length was determined to be 17×10^{-6} in.; the girder was then loaded in displacement control at 0.25 Hz of frequency to produce the determined gap opening. The gap opening was measured by an LVDT with a linear range of ± 0.1 in.

Because the stiffness of the girder was small before the adhesive cured, i.e., there was effectively no bottom flange or web at the center section, steel plates having a dimension of $11'' \times 11'' \times 1/4''$ were welded onto the web plate to cover the hole in the web, and the tension flange was connected with splice plates as illustrated in Figure 4.5. The splice plates bolted onto the inner side of the flange were 2'' wide and 0.5'' thick and bolted through four bolts on each side. The splice plates bolted onto the outer side of the flange, i.e., onto the steel plates to which the CFRP strips were attached, were 2'' wide and 0.5'' thick and bolted through one bolt on each side. After 24 hours of cyclic loading, these welded plates and splice plates were removed; the specimen was then tested to failure.

Although the target peak gap opening was 17×10^{-6} in., a measured peak gap opening under the cyclic loading was approximately 25×10^{-6} in. due to the difficulty of precisely controlling the gap opening with the displacement control of the actuator. As can be seen in Table 4.1, however, the vibration did not degrade the strength of the adhesive (Specimen 1-15). Thus, it can be concluded that vibration from typical automobile traffic should not affect the adhesive bond strength. In addition, considering the fact that the gap opening measured during the cyclic loading was larger than that intended, corresponding to the 0.5 ksi stress range, and the fact that the number of trucks which will pass the bridge during the curing time of the adhesive

will not be significant, it is reasonable to conclude that vibration from truck traffic should not affect the adhesive bond strength significantly. Therefore, there is no need to close the bridge to traffic during the application of the CFRP strips and while the adhesive cures.

4.1.2 Moment-CFRP Strain Relationship

Applied moment vs. CFRP strain ($M-\varepsilon$) curves for several specimens are shown in Figure 4.6 to Figure 4.13 together with computational results; a typical computational model is presented in the first section. The strain on the upper surface (in the gap) and the bottom surface of the CFRP strip were measured, both results are shown in the same figure (see Figure 3.6 for the gauge locations). Tensile strain in the CFRP strips from the computational results was taken from an outermost element at the center of the CFRP strip.

4.1.2.1 Computational Model

A specimen model was analyzed in two-dimensions using a commercial program, ABAQUS, which utilizes the finite element method (FEM); a typical computational model is shown in Figure 4.14. The computational model was one half of the girder shown in Figure 3.1 due to symmetry. All elements were modeled with 4-node isoparametric elements with 4 integration points. The meshes consisted of approximately 22 000 nodes and 22 000 elements. Analyses were geometrically nonlinear and materially linear except for the adhesive for which an elastic-perfectly plastic stress-strain curve was specified based on the tensile test results conducted for this research. All materials, steel, adhesive and CFRP strip, were modeled as isotropic materials (see Section 3.1 for details of material properties). Boundary conditions representing symmetry, i.e., displacements in horizontal direction equal zero, were introduced at the center. The vertical displacement was restrained at the lower right edge of the model, representing a simple support. During the analysis, a point load at a node 40 in. from the support (Figure 4.14) was incrementally increased up to 10 kips. Although the analysis was conducted using a two-dimensional model, the actual widths of all materials were used by assuming a plane-strain condition. For simplicity, the bolted connection between the steel plate and the girder was assumed perfect; thus, there was no slip or separation between the steel plate and the base girder in the analyses.

A detail of one of the computational models around the center is shown in Figure 4.15; the adhesive layer and the CFRP strip were divided into five and three elements, respectively, in this model. The adhesive layer of the Sikadur 330 adhesive (thickness of 0.06 in.) was divided into five elements as shown in Figure 4.15, while for other models the adhesive layer of the DP-460NS (thickness of 0.02 in.) was divided into three elements through the thickness. Both CFRP strips, CarboDur and Tyfo UC, were divided into three elements. Two elements through the thickness of the adhesive layer were used by Dorn [35] and other researchers for the analysis of bonded joints; thus, three elements through the thickness were thought to be sufficient. By using three or five elements depending on the thickness, the minimum size of elements in the adhesive layer was approximately 0.01”×0.01” for both adhesives. The geometry around the slit was modified to represent the five configurations shown in Figure 3.6.

4.1.2.2 Effect of Configuration

Test results of the specimens with Configurations 1 to 5 are shown in Figure 4.6 to Figure 4.11 together with computational results. It should be noted that Specimen 1-14 in Figure 4.11 was analyzed with two values of Young’s modulus for the Tyfo UC CFRP strip due to a large difference between data obtained from the tensile test for this research and that specified by the manufacturer. Because the correlation with the test results is better for the Young’s modulus obtained for this research, the Young’s modulus of the strip seems to be smaller than that specified by the manufacturer. The rest of the figures indicating the computational results of strain in the Tyfo UC CFRP are based on the data obtained for this research, $E=16\ 500$ ksi. On the other hand, Young’s modulus for the CarboDur CFRP strip obtained by the tensile tests conducted for this research was close to that specified by the manufacturer; the value specified by manufacturer ($E=23\ 900$ ksi) was used for all analyses.

Test results of Specimens 1-2 and 1-3 (Configurations 2 and 4, respectively) shown in Figure 4.7 and Figure 4.8 initially compared well with the computational results, but deviated from the computational results as the applied moment increased and exhibited nonlinear behavior. On the other hand, test results of Specimens 1-5, 1-8, and 1-14 (Configurations 3, 5, and 5, respectively) shown in Figure 4.9, Figure 4.10, and Figure 4.11 are approximately linear and compared well with the computational results up to failure. One possible reason for the discrepancies between the computational and test results for Specimens 1-1, 1-2, and 1-3 is the fact that the ductility of the adhesive controlled the failure of the specimen itself although any

failure criteria, including that for the adhesive and the CFRP strips, were not implemented in the analyses. Because of the low strength and ductility of the adhesive in these specimens (Siakdur 330) combined with the high stress concentration at the corners in the adhesive layer, the adhesive likely had a tension or shear failure even at a low applied moment. Cracks then vertically initiated from the corners at the gap (e.g., circles B and C in Figure 3.6) toward the CFRP strip, and a part of the tensile load carried by the adhesive was moved into the CFRP strip, resulting in nonlinear behavior of the M - ε curves.

In addition to the nonlinear behavior of the M - ε curves, the applied moment and the strain suddenly decreased at several points in time due to initial debonding for Specimens 1-1, 1-2, and 1-3 as can be seen in Figure 4.6 and Figure 4.8. After the first decrease in moment and strain, the M - ε curves became linear. To compare the slopes of the M - ε curves after initial debonding (which simulates Configuration 3), the computational results of Specimen 1-5 (Configuration 3) are plotted together with the results of Specimens 1-1, 1-2, and 1-3 in Figure 4.6 to Figure 4.8. As can be seen from these figures, the slopes of the M - ε curves of Specimens 1-1, 1-2, and 1-3 approached that of Specimen 1-5, i.e., Configuration 3, after decreases in moment and CFRP strain due to the debonding failure. Therefore, it seemed that Configurations 1, 2, and 4 eventually behave similar with Configuration 3 because the debonding failure occurred early in the loading.

Although the test results of Specimen 1-5 (Configuration 3) were approximately linear and compared well with the computational results, an initial debonding failure was observed, as shown in Figure 4.9. It was assumed that making an unbonded region near the gap or slit longer than that in Configuration 3 (0.5 in.) would eliminate the initial debonding early in the loading. In Configuration 3, the unbonded region was the same length as the gap between two steel plates, while the unbonded region was increased to 4 in. in Configuration 5 (see Figure 3.6 for details of configurations). The assumption was confirmed by the fact that the M - ε curve of Specimen 1-8 (Configuration 5) was approximately linear up to the final failure without any debonding and compared well with the computational results, as shown in Figure 4.10. Because Specimens 1-8 and 1-14 (both Configuration 5) did not experience a decrease in the moment during the experiments, it seems that the failure of the specimen occurred when the ductility of the adhesive was exhausted.

It should be noted that the above discussion was made mainly on Specimens 1-1, 1-2, 1-3, 1-5, and 1-8, which had the Sikadur 330 adhesive and the Carbodur CFRP strip, while Specimen 1-14 had the DP-460NS adhesive and the Tyfo UC CFRP strip. Although the DP-460NS adhesive has more ductility compared with the Sikadur 330 adhesive, it was thought that the effect of configuration on the strength of the specimen would be similar to these with the Sikadur 330 adhesive. Therefore, it was decided to use Configuration 5 for the specimens in all further tests.

4.1.2.3 Effect of Multiple Layers of CFRP

Figure 4.9, Figure 4.12, and Figure 4.13 show the results of Specimens 1-5, 2-2, and 3-1 (all Configuration 3); all specimens were made with the Carbodur CFRP strip and the Sikadur 330 adhesive. These results indicate a significant difference between tensile strains on the top and the bottom surfaces of the CFRP strips. In addition, the CFRP strip at the center, where the strain was measured, had an opposite curvature to that of the girder, i.e., a larger strain on the top surface. This opposite curvature in the CFRP strip is also confirmed by computational results as shown in Figure 4.9, in which the computational results of the CFRP strain on both the bottom and the top surfaces are plotted.

In Figure 4.16, average strains of both surfaces of the CFRP strips in Specimens 1-5, 2-2, and 3-1 are plotted together. As can be seen in the figure, in the linear region of the curves, the applied moment at the same average strain linearly increased as the number of layers, indicating the effectiveness of increasing the number of layers of CFRP strips. Therefore, it may be possible to further increase the total load in the CFRP strips, i.e., applied moment, at the same average strain. On the other hand, the maximum moment observed during the experiments was not linearly related with the number of layers of the specimen. The debonding failure that occurred in Specimen 3-1 was the reason for the lower than expected increase in the maximum moment over that of Specimen 2-1. Because it is difficult to conclude that the failure observed in Specimen 3-1 will occur in all specimens with three layers of strips based on one test, additional specimens with multiple layers of strips need to be tested to confirm the failure observed in this research.

4.1.3 Strain Distribution in CFRP Strip

Tensile strain distributions in the CFRP strip were measured for several specimens to determine directly the effective bond length as shown in Figure 4.17 to Figure 4.21. For the analytical estimation of the effective bond length, the effective bond length was defined as the sum of two parts: 1) bond length where the adhesive has yielded and 2) bond length required to transfer approximately 99% of the total load in the strip at the center into the steel plate when the adhesive is elastic for its entire bond length. Because regions where the adhesive was elastic were hard to determine in the measured strain distributions in the CFRP strips, the effective bond lengths were determined as the distance from the edge of the adhesive layer to the location where strain in CFRP strain became reasonably low for strain distribution just prior to failure. Because increase in the tensile strain in the CFRP strip would be small at a location where shear stress is small, i.e., no-load transfer is taking place, compared with locations where the shear stress is large or yielded, the location where the tensile strain was roughly constant during the experiment was selected as one end of the effective bond length. In addition, shear stress distributions calculated with the measured tensile strain distributions in the CFRP strips as discussed later in this section were considered to determine the effective bond length.

For Specimens 1-4 and 1-14, strain gauges were distributed over the entire length of the strips, while gauges were placed only on one half of the strip for Specimens 1-8 and 2-3; the locations of strain gauges on CFRP strips are illustrated in Figure 3.8. Plots were made for several load levels (expressed by the nominal moment level in the beam) to see how the strain distribution changed.

Because the strain decreased twice as the adhesive debonded in Specimen 1-4, the data were divided into three plots as shown in Figure 4.17. Specimen 1-4 consisted of Sikadur 330 adhesive and a CarboDur CFRP strip with Configuration 4. As can be seen in the figure (Figure 4.17-a), the tensile strain increased rapidly towards the center with an effective bond length of approximately 10 in., and the strain distribution was symmetric with respect to the center of the strip before the first debonding occurred. After the first failure, the strain decreased, and the strain distribution shifted to the left. A constant strain region clearly indicated no shear stress existed between the CFRP strip and the adhesive in the debonded region. As the load increased, the CFRP strip debonded again and the strain distribution became symmetric with respect to the

center, having approximately 14 in. of debonded length in the center. Specimen 1-8 was fabricated with the same materials as those for Specimen 1-4, with Configuration 5. As can be seen in Figure 4.18, the effective bond length is approximately 5 in. for this specimen. Configuration 5 had 4 in. of unbonded region at the center of the CFRP strip; thus, the CFRP strip was not bonded for the first 2 in. of the horizontal axis. Unlike Specimen 1-4, Specimen 1-8 did not show any debond failure up to the final failure.

Specimen 1-14 had a Tyfo UC CFRP strip and DP-460NS adhesive with Configuration 5, and strain gauges were placed along the entire length of the CFRP strip (see Figure 3.8); the results of the strain distribution in the strip is shown in Figure 4.19. As can be seen in the figure, the non-zero tensile strain region increased gradually from 4 in. long to 7 in. long as the load increased, i.e., between 2 to 6 in. and between 2 to 9 in. in the horizontal axis, which was not observed in the other two specimens. A reason for this increase in the non-zero tensile strain region seems to be a propagation of yielding in the adhesive layer. Unlike the adhesive-CFRP interface in the debonded region, the interface in the yielded region was able to transfer the load because of a constant yield shear stress and adequate ductility in the adhesive. The measured effective bond length of 7 in. supports the conclusion made in Section 4.1.1 that assumed the effective bond length is 8 in. or less. In addition, the tensile strain distributions of Specimen 1-14 are compared with computational results at two load levels as shown in Figure 4.20. The experimental and computational results compare well as can be seen in the figure. The analysis indicated that a part of the adhesive layer had already yielded at $M = 200$ kip-in., indicating the importance of ductility of the adhesive for a longer effective bond length, i.e., for a higher load and strain in the CFRP strip.

The strain distribution for the specimen with two layers of strips, Specimen 2-3 made with Tyfo UC CFRP strip and DP-460 NS adhesive, is shown in Figure 4.21. As can be seen in the figure, an increase in the number of layers clearly requires a longer bond length corresponding to the higher load to be transferred from the CFRP strips into the steel plates. Unlike the strain distribution for Specimen 1-14, there is not much region with near-zero strain, making it difficult to determine whether the bonded length was sufficient. However, the failure surface of the specimen indicated that failure was due to an adhesive failure at the high stress concentration region. Therefore, it was concluded that the effective bond length for two layers is 16 in.

In order to see the progression of the yield region in the adhesive layer, estimated shear stress distributions in the adhesive layer for Specimens 1-14 and 2-3 were obtained based on the measured strain in the CFRP strips. Considering force equilibrium in the adhesive layer (shear) and CFRP strip (tensile), the shear stress in the adhesive layer was calculated as follows.

$$\tau\left(\frac{x_{i+1} + x_i}{2}\right) = \frac{(\varepsilon_{i+1} - \varepsilon_i) \cdot E_c \cdot t_c}{|x_{i+1} - x_i|} \quad (4)$$

where, ε_i is the tensile strain measured at location x_i , E_c is the elastic modulus of the CFRP strip, t_c is the thickness of the CFRP strip, and x_i is the distance measured from the edge of the adhesive layer near the crack to the location of strain gauge i . The shear stress distributions for Specimens 1-14 and 2-3 are shown in Figure 4.22 and Figure 4.23, respectively. Because the tensile strain in the CFRP strip measured on the outer surface is different from the one at the surface bonded to the adhesive due to the strain gradient through the thickness, the shear stress calculated above is approximate. However, the shear stress distributions should be able to capture the yielding of the adhesive. The two shear stress distributions clearly indicate the progression of the yielded region, and it can be seen that the adhesive yielded at approximately 2.5 ksi of shear stress, slightly less than the estimated value, 2.9 ksi, which was derived from the tensile strength of the adhesive, 5.1 ksi (see Section 3.1), i.e., $5.1/\sqrt{3} = 2.94$ ksi.

4.1.4 Analytical Estimation of Effective Bond Length

As discussed in Chapter 2, it is useful to derive a simple analytical solution of the effective bond length for design purposes. Thus, in this section, the derivation of a simple analytical solution will be presented.

4.1.4.1 Analytical Solutions for Shear Stress Distributions

An analytical model considered here is the single-lap joint as shown in Figure 4.24. A tensile force per unit width, T , is applied at both ends of the adherends as shown in the figure. E_1 , E_2 , and G_a are the elastic modulus of Materials 1 and 2, and shear modulus of the adhesive,

respectively; t_1 , t_2 , and t_a are thicknesses of Materials 1 and 2, and the adhesive, respectively. In addition, τ_y and γ_y are shear yield stress and ultimate shear strain, respectively. The assumptions made throughout the analysis include: (1) both adherends remain elastic, (2) shear deformation of both adherends are ignored, (3) shear strain in the adhesive layer is assumed constant through the thickness, (4) failure of the joint occurs when the maximum shear strain in the adhesive layer reaches the ultimate shear strain, and (5) peeling stress can be ignored.

Making use of the above assumptions, a free body diagram of the single-lap joint can be simplified as shown in Figure 4.25. Based on the analysis by Tsai et al. in [44] and ignoring shear deformation of the adherends, a differential equation for shear strain can be derived for the free body diagram from force equilibrium in the horizontal direction.

$$\frac{d}{dx}T_1 = -\tau \quad \frac{d}{dx}T_2 = \tau \quad (5)$$

Then, using Assumption (3), shear strain in the adhesive layer can be written as,

$$\gamma = \frac{1}{t_a}(u_2 - u_1) \quad (6)$$

where, u_1 and u_2 are horizontal displacements of Materials 1 and 2, respectively. Differentiating Equation (6) once and using the relationship between displacements and strain yields,

$$\frac{d}{dx}\gamma = \frac{1}{t_a}\left(\frac{T_2}{E_2t_2} - \frac{T_1}{E_1t_1}\right) \quad (7)$$

Differentiating Equation (7) once and substituting Equation (5) into Equation (7) yields,

$$\frac{d^2}{dx^2}\gamma = \frac{1}{t_a}\left(\frac{1}{E_2t_2} + \frac{1}{E_1t_1}\right)\tau \quad (8)$$

Two cases must be considered: 1) adhesive remains elastic and 2) adhesive become plastic. In the first case, the shear strain can be expressed in terms of the shear stress as

$$\tau = G_a\gamma$$

However, in the second case, the differential equation needs to be solved separately for the elastic and plastic parts once the adhesive starts yielding. For the case where the adhesive is elastic for all regions, the differential equation can be rewritten as

$$\frac{d^2}{dx^2}\tau - \beta^2\tau = 0 \quad -c \leq x \leq c \quad (10)$$

Where, $\beta = \sqrt{\frac{G_a}{t_a} \left(\frac{1}{E_1 t_1} + \frac{1}{E_2 t_2} \right)}$ which has the general solution

$$\tau(x) = A \sinh(\beta x) + B \cosh(\beta x) \quad -c \leq x \leq c \quad (11)$$

The boundary conditions, $T_1 = 0$ @ $x = -c$ and $T_2 = 0$ at $x = c$ together with $T = T_1 + T_2$ and Equations (7) and (9), yield,

$$\frac{d}{dx} \tau = \frac{G_a}{t_a} \left(\frac{T}{E_2 t_2} \right) \quad @ x = c \quad (a)$$

and (12)

$$\frac{d}{dx} \tau = \frac{G_a}{t_a} \left(\frac{-T}{E_1 t_1} \right) \quad @ x = -c \quad (b)$$

The two constants, A and B, can be obtained as

$$A = \frac{\beta c \tau_{ave}}{\cosh(\beta c)} \left(\frac{1 - \frac{E_2 t_2}{E_1 t_1}}{1 + \frac{E_2 t_2}{E_1 t_1}} \right) \quad B = \frac{\beta c \tau_{ave}}{\sinh(\beta c)} \quad \text{where} \quad \tau_{ave} = \frac{T}{2c} \quad (13)$$

However, if the adhesive has already yielded, two differential equations are required, one for the elastic part and one for the plastic part, in terms of shear strain.

$$\gamma = \begin{cases} \gamma_e(x') & -c' \leq x' \leq c' \\ \gamma_p(\xi) & 0 \leq \xi \leq L_{pl} \end{cases} \quad (14)$$

For simplicity, two different coordinates are introduced as shown in Figure 4.26; a part expressed with x' indicates the elastic part and a part expressed with ξ indicates the plastic part. A length L_{pl} indicates the region where the adhesive has yielded. The two governing differential equations are from Equation (8),

$$\text{Elastic part: } \frac{d^2}{dx'^2} \gamma_e = \beta^2 \gamma_e \quad -c' \leq x' \leq c' \quad (15)$$

$$\text{Plastic part: } \frac{d^2}{d\xi^2} \gamma_p = \frac{\beta^2}{G_a} \tau_y \quad 0 \leq \xi \leq L_{pl} \quad (16)$$

The general solution for elastic part is that given in Equation (11),

$$\gamma_e(x') = C_1 \sinh(\beta x') + C_2 \cosh(\beta x') \quad -c' \leq x' \leq c' \quad (17)$$

The general solution for Equation (16) is,

$$\gamma_p(\xi) = \frac{\beta^2}{2G_a} \tau_y \xi^2 + D_1 \xi + D_2 \quad 0 \leq \xi \leq L_{pl} \quad (18)$$

These two differential equations can be solved using boundary conditions, including 1) T_1 and $T_2 = 0$ at $x=c$ ($\xi = L_{pl}$) and $-c$ ($x' = -c'$), respectively, 2) T_1 and T_2 are continuous at $x'=c'$, and 3) $\gamma = \gamma_y$ at $\xi=0$ ($x' = -c'$). From the first boundary condition with first derivatives of Equations (17) and (18), and Equation (7),

$$\frac{d}{d\xi} \gamma_p(L_{pl}) = \frac{\beta^2}{G_a} \tau_y L_{pl} + D_1 = \frac{T}{t_a E_2 t_2} \quad (19)$$

and

$$\frac{d}{dx'} \gamma_e(-c') = C_1 \cosh(-\beta c') \beta + C_2 \sinh(-\beta c') \beta = \frac{-T}{t_a E_1 t_1} \quad (20)$$

The second boundary condition indicates first derivatives of Equations (17) and (18) are equal at $x'=c'$; i.e., $\frac{d}{dx'} \gamma_e(c') = \frac{d}{d\xi} \gamma_p(0)$. This yields,

$$C_1 \cosh(\beta c') \beta + C_2 \sinh(\beta c') \beta = D_1 \quad (21)$$

The third boundary condition can be rewritten by substituting $\gamma = \gamma_y$ at $\xi=0$ ($x' = -c'$) into Equations (17) and (18) as:

$$C_1 \sinh(\beta c') + C_2 \cosh(\beta c') = \gamma_y \quad (22)$$

and

$$D_2 = \gamma_y \quad (23)$$

Then, solutions are given by

$$\gamma_e(x') = C_1 \sinh(\beta x') + C_2 \cosh(\beta x') \quad -c' \leq x' \leq c' \quad (24)$$

$$\gamma_p(\xi) = \frac{\beta^2}{2G_a} \tau_y \xi^2 + \left(\frac{T}{t_a E_2 t_2} - \frac{\beta^2}{G_a} \tau_y L_{pl} \right) \xi + \gamma_y \quad 0 \leq \xi \leq L_{pl} \quad (25)$$

where

$$\begin{aligned}
C_1 &= \frac{1}{2\beta \cosh(\beta c')} \left[\frac{T}{t_a} \left(\frac{1}{E_2 t_2} - \frac{1}{E_1 t_1} \right) - \frac{\beta^2}{G_a} \tau_y L_{pl} \right] \\
C_2 &= \frac{1}{2\beta \sinh(\beta c')} \left[\frac{T}{t_a} \left(\frac{1}{E_2 t_2} + \frac{1}{E_1 t_1} \right) - \frac{\beta^2}{G_a} \tau_y L_{pl} \right] \\
\text{and} \quad c' &= \frac{2c - L_{pl}}{2}
\end{aligned} \tag{26}$$

Once the shear strain distribution is derived, the shear stress distribution can be obtained by multiplying the elastic part, i.e., $-c' < x' < c'$, by the shear modulus, and $\tau = \tau_y$ for the plastic region, i.e., $0 < \xi < L_{pl}$. Because it has been assumed that the adhesive has yielded only at one end, the above equation is valid until the shear stress at $x' = -c'$ reaches the yield stress. In expressions for coefficients, an unknown value L_{pl} was left in place; L_{pl} can be expressed in terms of applied tensile load T using Equation (22) using the assumption that $\tanh(\beta c') = 1$ because $\beta c'$ is likely larger than 2, as follows,

$$L_{pl} = \frac{T - \gamma_y \beta t_a E_2 t_2}{\gamma_y \beta^2 t_a E_2 t_2} \tag{27}$$

As an example, the shear stress distribution is shown in Figure 4.27 together with a computational result using the following material properties: $E_1 = 29\,000$ ksi, $t_1 = 1.0$ in. for steel, $E_2 = 16\,500$ ksi, $t_2 = 0.075$ in. for CFRP (Fyfe UC), and $G_a = 130$ ksi, $t_a = 0.02$ in. for adhesive (DP-460NS). The total bond length is 18 in., i.e., $c = 9$ in., and yield shear stress is 2.9 ksi, based on the tensile strength determined by tensile tests conducted for this research. The tensile load in the adherends was selected so that the tensile strain in the CFRP strip is approximately 5000 microstrain. In the figure, the horizontal axis of the analytical solutions are shifted so that $x = c$ is at the edge of the adhesive layer in the computational result. The two distributions are reasonably compared; however, the computational result has a longer non-zero stress region. One reason for this is that the stiffness of the tension flange would be larger than $E_1 \times t_1$ as discussed in the next section.

4.1.4.2 Simplified Equations for Effective Bond Length

In the last section, analytical solutions of the shear strain and stress distributions were derived. From these expressions, it is possible to determine the effective bond length. Before the effective bond length was determined, further simplifications were made in the analytical

equation obtained in the last section. In the derivation of the analytical solution, a steel flange was represented by one of the adherends as shown in Figure 4.24 even though the steel flange is connected to a web plate. The existence of the web plate will increase the stiffness of the steel flange, i.e., (E_1t_1) . In addition, for a given CFRP strip, the parameter β would not vary significantly with the thickness of steel flange of rolled sections; e.g., $\beta = 2.388$ to 2.324 for $t_1 = 0.5$ in. to 1.5 in. although the parameter β plays an important role in determining the shape of the stress distribution. Therefore, in the following discussions, (E_1t_1) is assumed large compared to

(E_2t_2) , and is thus assumed to be equal $\sqrt{\frac{G_a}{t_a} \left(\frac{1}{E_2t_2} \right)}$. It should be noted that assuming large

(E_1t_1) will give conservative estimates of the effective bond length because the stiffer the adherends, the longer the effective bond length will be.

Expressions for the shear strain and stress in the adhesive for a given bond length where the adhesive has already yielded were determined in the last section. The effective bond length can be obtained by analyzing the shear stress distribution for a given tensile load correlated with the failure of the specimen. For this purpose, a bond length for non-zero shear stress in the adhesive layer needs to be determined including parts where the adhesive remains elastic and is yielded. A part of the bond length which remains elastic is defined as the bond length in which 99% of a part of the total load carried by the elastic region is transferred through the adhesive layer. A length where the adhesive remains elastic calculated with the above assumption is plotted against $1/\beta$ in Figure 4.28 for several combinations of E_2 and t_2 : $E_2 = 10\,000, 20\,000,$ and $30,000$ ksi and $t_2 = 0.05, 0.1, 0.15,$ and 0.2 in. As can be seen in the figure, the relationship between the bond length for the elastic part and $1/\beta$ seems linear; therefore, the bond length for the region where adhesive remains elastic, L_{el} , can be expressed in a simple equation as follows.

$$L_{el}(\beta) = \frac{5}{\beta} \quad (28)$$

The plot for this equation is also shown in Figure 4.28; as can be seen in the figure, Equation (28) is a conservative estimate. On the other hand, assuming that the shear strain at $\xi=L_{pl}$ is $\chi(L_{pl})$, it is possible to express a part of the bond length, where $\tau = \tau_y, L_{pl}$, as a function of $\chi(L_{pl})$ by substituting L_{pl} and T , which is obtained from Equation (27) in Equation (25), and solving for L_{pl} .

$$L_{pl} = \frac{1}{\beta} \left[[2(\gamma_o - 1) + 1]^{0.5} - 1 \right] \quad \text{where} \quad \gamma_o = \frac{\gamma(L_{pl})}{\gamma_y} \quad (29)$$

Then, a total effective bond length is the summation of L_{el} and L_{pl} corresponding to the maximum tensile load.

$$L_{eff} = L_{el}(\beta) + L_{pl}(\beta, \gamma_o) \quad (30)$$

where,

$$L_{el}(\beta) = \frac{5}{\beta} \quad L_{pl} = \frac{1}{\beta} \left[[2(\gamma_o - 1) + 1]^{0.5} - 1 \right] \quad \text{while} \quad L_{pl} \leq \frac{1}{\beta} \left[\frac{E_1 t_1}{E_2 t_2} - 1 \right]$$

$$\gamma_o = \frac{\gamma(L_{pl})}{\gamma_y} \quad \text{and} \quad \beta = \sqrt{\frac{G_a}{t_a} \left(\frac{1}{E_2 t_2} \right)}$$

In the above equation, Equation (30), the limit of L_{pl} is needed to satisfy the assumption that the adhesive has yielded only at one end. The proposed equation for the effective bond length requires the ultimate shear strain of the adhesive; however, the ultimate shear strain of the adhesive used in the experiment (DP-460NS) was not available at the time of this report. Because some experimental results were available, it was possible to calculate the required ultimate shear strain and L_{pl} in order to achieve the tensile strain, i.e., tensile load, in the CFRP strip observed during the experiment. For example, the tensile strain at failure for Specimen 1-14 was about 12 000 microstrain, i.e., $T = 0.075 \times 12\,000 \times 10^{-6} \times 16\,500 = 14.85$ kips/in. Substituting T into Equation (27) gives $L_{pl} = 4.52$ in.; substituting L_{pl} into Equation (29), and solving for γ_o yields $\gamma_o = 65$, i.e., an ultimate shear strain at the edge of the adhesive layer is 1.47. Then, an effective bond length becomes $2.18 + 4.52 = 6.7$ in. compared with the measured effective bond length of Specimen 1-14 of 7 in.

A simple analytical solution was proposed for the estimation of the effective bond length in this section. For further validation of the proposed equation, it is required to conduct effective bond length tests and to know the ultimate shear strain for several adhesives to compare the proposed equation and the experimental results. However, further validation of the proposed equation will not be conducted in this study.

4.1.5 Recommendation for Bonded Lengths and Bonded Configuration

The measured strain profiles for the Fyfe Tyfo UC Strip used with the 3M 460NS adhesive indicate that 7 inches of bonded length past the debonded zone is sufficient to develop the maximum achievable strength of the joint. However, a 7 inch bonded length was not tested. Therefore, an 8 minimum inch bonded length is recommended for single layer applications. In addition, a 4 inch debond length roughly centered over the crack, or the likely location of crack breakthrough is recommended to lessen the severity of the stress concentration. Thus the total length of a one-layer CFRP strip applied for retrofit should be a minimum of 20 inches long (two 8 inch long bonded regions on either side of a 4 inch long debonded region). The tensile strain distributions along the CFRP strip for Specimen 2-3 (Figure 4.12) clearly indicate that the effective bond extends about twice as long for the two layer specimen as for the one layer specimen 1-14 (Figure 4.20) even though both specimen had a bonded length of 16 inches. This strain distribution also indicates that additional length beyond the 16 inches would likely not be effective, therefore a total strip length of at least 36 inches (two 16 inch long bonded regions on either side of 4 inch long debonded region) is recommended when applying a two layer CFRP strip retrofit.

4.2 Preliminary Test on Rehabilitated Girder

This section presents the results of static tests on a rehabilitated girder. As outlined in Section 3.3, a W27×94 rolled beam with a 4" deep crack at its center was statically loaded with and without rehabilitation. Sikadur 330 adhesive and Carbodur CFRP strips were used for rehabilitation of the girder in this section. The stiffness increase due to the rehabilitation will be discussed based on the deflection of the girder. Strain distributions at two sections will be compared before and after the rehabilitation to determine strain (stress) reduction near the crack. The strain distribution in the CFRP strip will be compared to that obtained in the effective bond length test to verify the effective bond length determined in the last section. The purpose of these tests was to conduct a preliminary assessment of the effectiveness of the rehabilitation scheme with bonded CFRP on a large-scale girder, based on the results of the effective bond length tests.

4.2.1 Stiffness Increase of the Girder

The stiffness of the girder before and after the rehabilitation is compared by moment vs. deflection curves as shown in Figure 4.29. As expected, there was no significant increase in the

stiffness. To corroborate these results, the moment of inertia of the uncracked, cracked, and rehabilitated cross sections were computed. A 7% increase in the moment of inertia was calculated based on the cracked steel cross section (without the tension flange and a part of the web). The cracked section consists of the compression flange and a part of the web, from the top of the web to 4 in. from the bottom of the section (corresponding to the location of the crack tip). Sketches of the cracked sections without and with CFRP strips are illustrated as b and c in Figure 4.30, respectively, together with the uncracked section, Figure 4.30-a. In the calculations for the cracked sections, it was assumed that an initially plane cross section remained plane after deformation, and that there was no slip between the CFRP strip and the tension flange.

What should be noted in Figure 4.29 is that the stiffness increase seems to become notable as the applied moment increases. The possible reason for this is a nonlinear relationship between load and crack opening. The web near the crack tip yielded at a low load level and the effective area of the web, i.e., the elastic region, decreased, resulting in an increase in the crack opening at the tension flange. The increase in the crack opening increases the strain in the CFRP strip to satisfy compatibility, resulting in a larger stiffness increase than can be calculated based on simple beam theory, which assumes that an initially plane cross section remains so after deformation. In addition, in order to achieve an increase in the stiffness of the girder, a stiffness increase due to bonded CFRP must be greater than the loss of stiffness due to the decrease in the effective area of the web.

4.2.2 Strain Distribution in Girder

Strain distributions in the girder before and after the rehabilitation are shown in Figure 4.31 and Figure 4.32 for the cross section at the center of the girder and for the cross section 10 in. from the center, respectively. The vertical axis is the location through the depth of the girder, and the horizontal axis indicates strain. In the figures, the theoretical strain distributions based on the uncracked girder and the section without the tension flange, the cracked section (see Figure 4.30), are plotted in addition to the test results. It should be noted that the strain near the crack tip is not shown in the figure because the crack tip was not located in the same cross section as that in Figure 4.31. The strains near the crack tip (about 0.25 in. from the crack tip) before and after the rehabilitation are shown in Figure 4.33, indicating the strain concentration at the crack tip.

At both sections, the strain 19 and 26 in. from the bottom of the section were not decreased significantly, while a 40% decrease in strain was measured 9 in. from the bottom. In addition, the strain near the crack tip, which was well beyond the yield strain of steel before the rehabilitation, was reduced about 60% after the rehabilitation at the load level corresponding to nominal stress of 5 ksi. It should be noted, however, a reduction of strain is less than 60% at a lower load level. This indicates that the rehabilitation was more effective near the crack tip at larger load. These decreases in strain were estimated to be approximately 10% based on simple beam theory, which assumes that an initially plane cross section remains planar. As discussed in the last subsection, this higher effectiveness of the rehabilitation was believed to be due to the nonlinear relationship between the load and crack opening. Thus, under the same applied moment, the CFRP strips were loaded more than expected by simple beam theory as the load increased, indicating that the CFRP strips were acting more effectively and were able to reduce the strain near the crack tip more than expected.

The 60% reduction in strain near the crack tip was surprisingly large. However, the crack length, 4 in. from the bottom of the section, was far more severe than the case where the rehabilitation would be applied in practice. As discussed above, the crack opening and the effectiveness of the rehabilitation seem to relate to each other. Thus, the decrease in strain at the crack tip would have been smaller if the crack length was shorter. Furthermore, it is uncertain whether any reduction in strain can be achieved if the crack tip is in the tension flange. Therefore, additional experimental tests on fatigued girders, having a crack that represents a realistic crack to be rehabilitated, were conducted. Through the additional experimental tests, the fatigue life of rehabilitated girders was investigated in addition to strain reduction. The results of these experimental tests will be presented in the Section 4.3.

4.2.3 Strain Distribution in CFRP Strip

The tensile strain distribution in the CFRP strip in the cracked W27x94 girder is shown in Figure 4.34, along with the results of Specimen 1-8 of the effective bond length tests. Because the relationships between applied moment and strain in the strip are different in the two tests, plots are made at three load levels at which strains at the center of the strip are close. For example, the applied moments of the highest strain level in the figure are 1120 and 160 kip-in. for the static test on the W27x94 girder and Specimen 1-8, respectively.

The two results seem to have similar effective bond lengths, as can be seen in the figure, although the strain near 5 in. is slightly higher in the static test on the W27x94 girder as compared to that in Specimen 1-8. This difference probably resulted from the larger tensile strain on the outer surface of the tension flange in the W27x94 girder. As can be seen in Figure 4.32, the strain at the inner surface of the tension flange in the cross section 10 in. from the center, which was the opposite surface from the one where the end of the CFRP strip was located, was 100 microstrain after the rehabilitation. On the other hand, the strain in the steel plate at the end of the CFRP strip for Specimen 1-8 was approximately 36 microstrain. The strain in Specimen 1-8 was calculated assuming that a composite section of girder, specifically a W14x68 with the steel plate attached, is effective at the end of the strip, and using the equation, $\epsilon = M/(S_x \times E_s) = 160/(155 \times 29\,000) = 36 \times 10^{-6}$, where S_x is the elastic section modulus of the composite section. As discussed in Appendix A, the magnitude of the shear stress at the end of the strip increases as tensile strain in the adherend (steel plate) increases. In addition, integrating the shear stress along the length of the strip approximately gives the tensile load in the strip. Thus, the larger shear stress at the end of the strip (10 in. in Figure 4.34) results in a larger tensile load, i.e., tensile strain in the strip, near 5 in. in Figure 4.34. This observation explains the fact that the tensile strain measured 5 in. along the strip in this test was slightly larger than that measured in Specimen 1-8, considering the difference in the tensile strain in the adherends (the steel plates). Note that the shear stress distributions in the adhesive layer near the center, i.e., around 2 to 3 in. in the figure, are likely to be similar in both results because the tensile strain in the adherends (the CFRP strips) are close each other.

4.3 Cyclic Fatigue Loading Tests on Rehabilitated Girders

In this section, results of cyclic fatigue loading tests on rehabilitated girders with bonded CFRP strips are presented. As pointed out in the last section, the main purpose of this test was to determine whether the bonded CFRP strips affect, i.e., slow or stop, crack growth in the girder having a crack length representative of field conditions. Crack growth in each specimen is presented separately, then together to compare those results to identify the effects of the rehabilitation. In addition, other factors to be considered for the application of bonded CFRP strips are pointed out and discussed.

4.3.1 Crack Growth

4.3.1.1 NR-3: No Bonded CFRP

Pictures of the test setup, specimen, and steel plates welded onto the bottom of the tension flange to initiate a crack are shown in Figure 4.35 and Figure 4.36. In order to initiate the crack, the girder was loaded with a nominal stress range of 10 ksi at 1.0 Hz. After 2,978,000 cycles, the cyclic loading was stopped because the crack length had become approximately 2 in. The steel plates were then removed and 1" diameter holes were drilled at the crack tip as shown in Figure 4.37. As can be seen in the figure, however, the holes did not include the crack tip due to misalignment of the drill bit. The holes were located so that the perimeter of the holes intersects the crack tip; i.e., the center of the hole was $\frac{1}{2}$ " from the crack tip. A sketch of the locations of the holes and crack lengths is shown in Figure 4.38. In addition, the crack was observed on the inner surface of the tension flange, north side, at this time, indicating the crack had already propagated through the thickness of the tension flange (0.64"); a picture of the crack on the inner surface is shown in Figure 4.39.

After the holes were drilled, cyclic loading with a stress range of 3 ksi superimposed on a static dead load of 10 ksi was continued to grow the crack further. The frequency for cyclic loading was increased to 2 Hz at this time. As cyclic loading continued, both crack tips grew toward the edges of holes. Once the crack reached the edges of holes, the crack started growing toward the inner surface of the tension flange; a picture of the crack tip on the south side 1,000,000 cycles after the holes were drilled is shown in the Figure 4.40. The crack tip was located approximately $\frac{6}{16}$ " from the bottom of the tension flange.

Considering the fact that in the literature it has been indicated that cracks re-initiate from the drilled holes in the field [52] and that the stress level measured in the negative moment region of the steel girders in service was less than 3 ksi (approximately 1.5 ksi) [54], this experimental result was not expected. In addition, the number of cycles causing approximately 3 ksi of nominal stress in the tension flange in the negative moment region was estimated to be 100,000 cycles for 10 years based on reports available in the University of Minnesota, Department of Civil Engineering [53, 54]; this is far fewer than the number of cycles the specimen was subjected to.

A crack arresting method consisting of drilling holes has been reported by Fisher et al. [2]; it was reported that if the radius of the hole satisfies Equation (31), the crack would not re-initiate from the hole.

$$\frac{\Delta K}{\sqrt{\rho}} < 4\sqrt{\sigma_y} \quad (31)$$

where, ΔK is the range of the stress intensity factor at the crack tip, ρ is the radius of the hole, and σ_y is yield strength of steel in ksi. The range of the stress intensity factor at the crack tip in the specimen was calculated to be 3.4 by assuming the crack is an elliptical shape in the solid steel [55] with the longer radius equal to 1" and the shorter radius equal to 0.5", and a nominal stress range of 3 ksi. Substituting this into Equation (31) together with the radius of the hole, 0.5", and yield strength of the steel, 50 ksi, yields,

$$\frac{3.4}{\sqrt{0.5}} = 4.8 < 4\sqrt{50} = 28.3 \quad (32)$$

Therefore, this analysis indicates that the crack will never re-initiate, supporting the result of specimen NR-3. Because the crack did not re-initiate, cyclic loading on this specimen was continued in order to investigate how fast the crack grows into the web because the crack length was relatively short after 1 million cycles.

Approximately 2,442,000 cycles after the holes were drilled, both crack tips reached the inner surface of the tension flange. The crack tip reached into the web just above the K-region after 2,718,000 cycles. The crack growth vs. the number of cycles is plotted in Figure 4.41; the crack growth in the vertical axis indicates the distance between the crack tip and the bottom of the tension flange. The horizontal axis is the number of cycles since the rehabilitation by drilling holes. As can be seen in the figure, the crack growth rates were not equal for the two crack tips; the south crack grew faster than the north crack. What should be noted in the figure is that the crack growth of the south crack became slower as the crack grew toward the inner surface of the flange. One possible reason for this is that the north crack started to grow faster as the south crack growth became slower, indicating that the stress concentration at the south crack tip was reduced due to the north crack tip.

4.3.1.2 R-3-1: Bonded CFRP with Shorter Crack Length at Rehabilitation

As it done for Specimen NR-3, two steel plates were welded under the bottom flange to initiate a crack in the tension flange and the girder was loaded with a nominal stress range of 15 ksi at 1 Hz. The nominal stress range was increased as compared to Specimen NR-3 in order to reduce the number of cycles to grow the crack. The crack became approximately 2" after 1,049,000 cycles; holes were then drilled at crack tips. A sketch showing the crack length and locations of holes, and a picture of the specimen, are shown in Figure 4.42 and Figure 4.43, respectively. As can be seen in the figures, one of holes missed the crack tip again, while the other hole intersected the crack.

As indicated in Section 3.4, this specimen (R-3-1) was rehabilitated with bonded CFRP strips to the inner surface of the tension flange in addition to the holes, as shown in Figure 4.44. The dead load holding device was installed before the CFRP strips were bonded to keep the dead (10 ksi nominal stress) in the girder in case hydraulics is turned off. The estimated loss of the dead load was less than 0.5 ksi, as indicated in Section 3.3; a measured loss of dead load, however, was approximately 2 ksi., i.e., stresses at the top and the bottom flange decreased 2 ksi (from 10 to 8 ksi) after turning off the hydraulics. In order to avoid any compression stresses in the CFRP strips during the experiment, it was decided that the CFRP strips should be bonded with the hydraulics being turned off. This in turn increased the tensile strain in the CFRP strips while the girder was under cyclic loading with a nominal stress range of 3 ksi, compared when the CFRP strips were bonded while the hydraulics was on, keeping 10 ksi nominal stresses in the girder. Because an increase in the tensile strain was estimated to be small, approximately 100 microstrain, and the peak tensile strain in the CFRP strips was estimated to be less than 20% of the maximum strain observed during the effective bond length test, it was concluded that the increase in the tensile strain should not greatly affect the fatigue life of the adhesive [25, 56].

After the application of the CFRP strips, the girder was loaded with a nominal stress range of 3 ksi at 2 Hz; crack growth was then monitored during the experiment. A plot of the crack length vs. the number of cycles is shown in Figure 4.45. Because the crack tip on the south side was already at 0.1875" from the bottom of the tension flange when the holes were drilled, the south crack starts from 0.1875" in the figure. On the other hand, the north crack did not grow at all during the experiment; and the cyclic loading was terminated at 2 million cycles. During

the cyclic loading, the south crack reached the inner surface of the tension flange, and had grown to approximately 0.25" as shown in Figure 4.46.

4.3.1.3 R-3-2: Bonded CFRP with Longer Crack Length at Rehabilitation

A crack was initiated at the center of the girder by applying cyclic loading with a nominal stress range of 15 ksi at 1Hz. For this specimen, cyclic loading was continued until the crack length became more than 2" and propagated through the thickness of the tension flange. After 2,145,000 cycles, the crack tips were at 1.875" and 0.875" from the center of the tension flange; holes were then drilled as shown in Figure 4.47 and Figure 4.48. During the experiment, it was noticed that the flanges were not parallel to each other and that torsion was induced in the specimen. This seemed to be a reason for the large difference of the crack lengths. At the time the holes were drilled, the crack had already grown into the web and the crack tip was near the edge of the K-region as shown in Figure 4.49. After holes were drilled, the crack at the south side was observed along the hole with the crack tip at 0.3125" from the bottom of the tension flange. It was thought that the crack was long enough and would not be missed during the field inspections, indicating an extreme case for the rehabilitation.

CFRP strips were then bonded to the inner surface of the tension flange as was done for Specimen R-3-1, and cyclic loading was continued with a nominal stress range of 3 ksi (from 10 to 13 ksi) at 2 Hz. After 176,000 cycles, both cracks had reached the top surface of the tension flange as shown in Figure 4.50, and the crack continued growing into the web. After 1 million cycles, the crack tip had grown 0.1875" from the edge of the K-region, about 1.5625" from the bottom of the girder, and the experiment was terminated.

4.3.1.4 Comparison on Crack Growth

In this section, the crack growths of three specimens discussed above are compared. Plots for the crack growth vs. the number of cycles of the south crack for each specimen are drawn together in Figure 4.51. Because the crack lengths at the beginning of the experiments, i.e., the height of crack tips measured from the bottom of the tension flange, were different in each specimen, the plots were shifted horizontally toward the left so that the crack lengths for all specimens were 0.3125" at 0 cycles in the plot as shown in Figure 4.52. Although this comparison still ignores the effect of the location of the hole in each specimen, it seems that this is the best way to compare the results. Distances from the center of the tension flange to the

edge of the hole in each specimen (and the distances between the two holes) are 0.8750” (2.4375”), 1.1250” (2.1875”) and 1.8750” (2.7500”) for Specimens NR-3, R-3-1, and R-3-2, respectively.

As it can be seen in the figure, the crack growth was not arrested by the bonded CFRP, and the crack growth becomes faster as the total distance between holes becomes larger. Thus, the effect of the rehabilitation on the crack growth seems insignificant. However, one of the cracks (north side) in Specimen R-3-1 did not grow at all during the experiment while both cracks grew toward the holes in Specimen NR-3, indicating a possible benefit from bonding CFRP strips. In addition, because of the longer crack length in Specimen R-3-2, the crack lengths observed on the top and bottom surfaces of the tension flange were approximately the same as the crack on the top surface, as can be seen in Figure 4.48 and Figure 4.49. Thus it was reasonable that the crack in Specimen R-3-2 propagated through the thickness of the flange faster than the other specimens in which the lengths of the cracks were short or no crack on the top surface of the tension flange was observed. Therefore, it can be concluded that the crack growth will be reduced if the girder is rehabilitated before the crack reaches the top surface of the tension flange. To further verify this conclusion, additional specimens need to be tested to repeat the experiments.

It should be noted that the motivation of this project was to slow or arrest cracks reinitiating from the holes drilled in the tension flanges which have been reported on several bridges although the crack did not reinitiate from the holes in any of specimens reported above. This suggests increasing the stress range or modifying the specimen, i.e., cracks could be intentionally initiated from the holes, to simulate the field condition for further investigations.

4.3.1.5 R-3-3: Bonded CFRP without Stop-Holes

Because the results of the three specimens rehabilitated with holes and bonded CFRP strips indicated that holes alone were possible to stop the crack growth, an additional experiment on a specimen that was rehabilitated only with bonded CFRP strips was conducted. As was done for other specimens, two steel plates were welded under the bottom flange to initiate a crack in the tension flange and the girder was loaded with a nominal stress range of 15 ksi at 1 Hz. Once the crack became approximately 2.9” long, the stress range was increased to 6.5 ksi to record the crack growth without rehabilitation. The stress range was increased compared to the other specimens to increase the crack growth rate. After approximately 2.4 million cycles, the crack

became 3.7” long and the specimen was rehabilitated with bonded CFRP strips. While the CFRP strips were bonded to the inner surface of the tension flange, dead load was introduced in the girder as was done for Specimens R-3-1 and R-3-2.

After the application of the CFRP strips, the girder was loaded with a nominal stress range of 6.5 ksi, and crack growth was recorded to compare with that before rehabilitation. A plot of the crack length vs. the number of cycles is shown in Figure 4.53; in the figure the number of cycles after the stress range was increased to 6.5 ksi is indicated. As can be seen in the figure, it seems that the crack was about to grow exponentially at the time of rehabilitation. After rehabilitation, the crack length did not increase for approximately three-hundred thousand cycles; then the crack started growing exponentially. To illustrate the effect of the rehabilitation, a plot of the crack length data shifted to the left by 300,000 cycles is superimposed on the recorded data (solid diamonds are shifted data, crosses are recorded data). Because it appears the crack growth without rehabilitation was faster than that with rehabilitation, it seems that the bonded CFRP strips were able to slightly reduce the crack growth.

4.3.2 Other Considerations on Application of Bonded CFRP Strips

4.3.2.1 Influence of Crack on Strain Distributions in Girder

In order to see any changes corresponding to the loss of cross section due to crack growth, strains in two sections of the W27x84, Specimen NR-3, are plotted in Figure 4.54 and Figure 4.55; Figure 4.54 is at the center of the girder and Figure 4.55 is 20 in. from the center. The vertical and horizontal axes indicate the location of strain gauges measured from the bottom of the section and strain in microstrain, respectively. The plots are showing the strain due to the load corresponding to 10 ksi nominal stress in the uncracked section. As can be seen in the figures, there was no change in the strain at all locations measured due to the small crack size in the girder. This result indicates that there is no need for checking the stress increase in the section except near the crack tip if the crack length is approximately 2” in width and 1” in height.

4.3.2.2 Influence of Crack on Strain Distributions in CFRP Strip

As indicated in Section 3.4, strain gauges were instrumented on a half-length of the CFRP strip to see if any changes were caused by the crack growth. Tensile strain distributions due to the load corresponding to 3 ksi nominal stress (i.e., data were measured during a loading

from 10 ksi to 13 ksi nominal stress, taking offsets at 10 ksi nominal stress) in the uncracked section are shown in Figure 4.56 and Figure 4.57. Figure 4.56 is the strain distribution at the beginning of the cyclic loading, i.e., just after bonding the CFRP strips, while data in Figure 4.57 were taken after 2 million cycles. The vertical and horizontal axes indicate tensile strain and locations measured from the center of the CFRP strips, respectively. It should be noted that, because there were 4" unbonded regions in the CFRP strips, 0 to 2" in the figures were not bonded. Each figure has two strain distributions measured on two CFRP strips, i.e., each side of the web.

Based on the crack growth during the cyclic loading in this specimen (see the last section for the crack growth), no significant change in the strain distribution was expected. The shape of the distribution, however, is slightly different near the end (from 6 in. to 10 in.) between the two plots; the strains at the center of the CFRP strips were close. There was no clear reason for this difference. In addition to the strain distribution in the CFRP strips, the strains at the center of CFRP strips were plotted against the number of cycles after bonding the CFRP strips for Specimen R-3-1 as shown in Figure 4.58. There was no significant change in the strain that makes it possible to conclude an effect of the crack growth in the strain. On the other hand, the same plot was made for Specimen R-3-2 and is shown in Figure 4.59, indicating a slight increase in strain after 1 million cycles when the crack tip was about 1.5625" from the bottom of the girder. Therefore, it seems that, under the loading corresponding to 3 ksi nominal stress range and with the crack length considered in this specimen, there will be no effect of the cyclic loading on the strain in the CFRP strip until the crack will grow further into the web.

To see if measured strains at the center of the CFRP strips can be estimated by calculation, the composite sections consisting of a cracked steel section and the CFRP strips were analyzed; idealized sections were shown in Figure 4.60. Assuming plane sections remain plane, strains at the top surface of the tension flange under a load corresponding to 3 ksi nominal stress were obtained as 120 and 140 microstrain for Specimens R-3-1 and R-3-2, respectively; these compared well with the measured strains. This indicates stresses can be estimated by calculating the moment of inertia for composite sections, and also the reduction of the stress can be estimated. Therefore, it seems possible to estimate the reduction of stress intensity based on the stress reduction if the crack length is relatively small compared to the width of the tension flange.

4.3.2.3 Propagation of Debond

During the cyclic loading tests after the CFRP strips were bonded in Specimens R-3-1 and R-3-2, no debonding was observed. As indicated in Appendices B and C, cyclic loading tests on the Sikadur 330 adhesive and the Carbodur CFRP strips resulted in debonding failures. The main reason for the differences on the cyclic tests in the Appendices and ones on W27x84 girders was the maximum load in the CFRP strips during the cyclic loading compared to the maximum static strength, i.e., the maximum load in the CFRP strip measured during the effective bond length tests. It has been reported that if the cyclic loading applied on bonded joints is less than 20~30% of the strength based on static tests, there would be no fatigue failure in the joints, including debonding failure [25, 56]. The maximum strain observed during the effective bond length tests were approximately 12 000 and 5000 microstrain for a combination of Tyfo UC strip and DP-460 NS adhesive, and Carbodur strip and Sikadur 330 adhesive, respectively. Thus, the maximum strain during the cyclic loading was less than 2%, e.g., $170/12\ 000 = 0.014$ for specimen R-3-1. It should be noted that the maximum strain in the CFRP strip measured in specimen R-3-1 includes the strain due to the loss of dead load as discussed in section 3.4. On the other hand, the maximum strain during the cyclic loading was approximately 70%, e.g., $3500/5000 = 0.70$, for specimen C-H in Appendix B. Therefore, the materials proposed in this report, Tyfo UC strip and DP-460NS adhesive, will not have debonding problems under the load corresponding to 3 ksi nominal stress range in the uncracked section.

4.3.2.4 Estimation of Crack Growth

As indicated in Section 4.3.2.2, it seems that the strain (stress) in the section can be calculated using the moment of inertia of the composite section consisting of the steel girder and one layer of strip; it is then possible to estimate the reduction of the stress intensity factor. A nominal stress in the tension flange is usually used for the calculation of stress intensity factor; the reduction of the stress intensity factor is the same as the stress reduction because stress and stress intensity factor are linearly related. By considering the well known equation, $\sigma = M/S_x$ (where σ is stress, M is applied moment, and S_x is elastic section modulus), the reduction of the stress intensity factor can be calculated as follows:

$$\Delta K = \frac{S_{x_steel}}{S_{x_composite}}, \quad (33)$$

where, ΔK is the reduction of the stress intensity factor (the range of the stress intensity factor for the original girder divided by that for the rehabilitated girder), $\Delta S_{x_composite}$ is the elastic section modulus for the composite section consisting of an original, uncracked steel section and one layer of strip bonded each side of tension flange, and ΔS_{x_steel} is the elastic section modulus for the original, uncracked steel section. Because the crack growth is known to be linearly related to the third power of the stress intensity factor, $\frac{da}{dN} = 3.6 \times 10^{-10} \times K^3$ (where, K is the stress intensity factor in ksi \sqrt{in} , and da/dN is the crack growth rate in inches per cycle), an increase in the number of cycles for the crack to grow a certain length, i.e., the remaining fatigue life, can be estimated as follows:

$$\Delta N = \left(\frac{1}{\Delta K} \right)^3 \quad (34)$$

where ΔN is the percentage increase in the fatigue life (i.e., the fatigue life in cycles of the rehabilitated girder divided by the fatigue life of the original girder). In the case for the girder discussed in this report, a W27 \times 84, and one layer of CFRP strip, ΔK is 0.97 and ΔN is 1.1; the increase in the fatigue life is not significant as observed through the cyclic loading tests.

It should be noted that the estimation of crack growth discussed above is applicable with one layer of strips bonded on the tension flange. If more than one layer of strips is bonded, the elastic section modulus for the composite section may be overestimated because the outer layer of strips would not be stressed as expected based on the linear distribution of strain through the cross section.

5 Conclusion

In order to investigate the possibility of a rehabilitation method with bonded CFRP strips, experimental tests and computational studies have been conducted. Because little research has been conducted on the use of CFRP strips for rehabilitation of steel members, it was required to design a new test setup and specimen to determine the effective bond length of a CFRP strip bonded onto a steel flange. Once the effective bond length was determined, fatigued steel girders were rehabilitated with bonded CFRP strips in order to investigate the effect of the rehabilitation method on crack growth. In this chapter, major findings from this research will be presented. A recommended rehabilitation procedure is proposed in Appendix B.

5.1 Effective Bond Length Tests

The purpose of the effective bond length tests was to determine the shortest bond length that engages the largest possible strength of the CFRP strip. In order to design the test setup and specimen, a series of finite element analyses were conducted on both a prototype girder and possible specimens; then, the shear stress distributions for all models were compared. This ensured that the experimental results would be applicable to the geometry found in the field applications. Experimental tests on several types of strips and adhesives revealed the effective bond length for selected combinations of CFRP strip and adhesive. In addition, a simple analytical solution was derived to estimate the effective bond length using the given ultimate shear strain of the adhesive.

The major findings from the effective bond length tests are

- Due to the significant influence of the shape and geometry of the test specimen on the shear stress distribution in the adhesive layer, a new specimen was designed for the effective bond length tests to ensure that the results from the experiments were applicable to CFRP strips bonded to steel flanges.
- The ductility of the adhesive is the most significant factor to determine the failure and strength of the bonded joint/strip combination.
- Because the ductility of the adhesive governed the effective bond length, it was not possible to fully utilize the strength of the CFRP strips.

- The failure mode of a one-layer specimen bonded with a ductile adhesive with a bond length equal to or greater than the effective bond length was a combination of debonding and ruptures of the fibers.
- For the combination of the Fyfe Tyfo UC CFRP strip and the 3M DP-460NS adhesive, the effective bond lengths were 8 in. and 16 in. for one-layer and two-layer applications, respectively.
- The minimum total strip lengths are recommended as 20 in. and 36 in. for one-layer and two-layer applications, respectively. When accesses allows, these lengths should be increased by 20% to be conservative.
- Additional specimens with more than two layers of strips need to be tested in order to confirm the effectiveness of increasing layer on the increase in the total load in CFRP strips.
- Finite element analysis was able to reproduce the experimentally observed tensile strain distribution in CFRP strip, and thus the shear stress distribution in the adhesive layer.
- An experimental simulation of the vibration from traffic on the bridge during adhesive curing resulted in no loss of bond strength, indicating that the bridge need not be closed to traffic when applying the retrofit.
- A proposed simple analytical solution can be used as a design equation for the effective bond length once the ultimate shear strain of the adhesive is obtained.

5.2 Static and Cyclic Loading Tests on Large-Scale Girders

Static and cyclic fatigue loading tests were conducted on large-scale girders to determine the effectiveness of the rehabilitation scheme on girder with an extremely large crack (into the web plate) and three girders with small cracks (2 in. in length on the outer surface of the tension flange) were tested.

Major findings are

- In the girder with the relatively large crack, i.e., the crack tip was in the web plate and the tension flange was completely severed, bonded CFRP strips reduced the measured strain near the crack tip approximately 60%, which was more than expected based on an assumed linear strain distribution through cross section.

- Drilling holes seems sufficient to arrest small cracks under a 3 ksi nominal stress range in the girders tested cyclically, i.e., it will be necessary to increase the stress range in future research to reinitiate crack from the holes.
- Given the dimensions and material properties of the CFRP strips tested in this project, the effect of bonded CFRP strips on crack growth appears to be small and is difficult to determine under a 3 ksi nominal stress range when the crack was small in the tension flange.
- Fyfe Tyfo UC CFRP strips and 3M DP-460NS adhesive, bonded CFRP strips showed no signs of debond after more than 2 million cycles under 3 ksi nominal stress range, indicating sufficient fatigue life for field applications.

5.3 Concluding Remarks and Recommended Future Work

Due to the cyclic loading caused by traffic on bridges, cracks initiate from weld toes at cover plate ends that were terminated in the negative moment region. These cracks have attracted the attention of engineers because of the possibility of catastrophic failure of the bridges, and several rehabilitation methods for these cracks have been proposed in the literature. In this report, a new rehabilitation scheme using CFRP strips has been investigated. The CFRP strip is bonded to the inner surface of the tension flange over the crack to make an alternate path for the stress in the tension flange. Because the strips are lightweight and their application does not require access to the outer surface of the tension flange, on which concrete slabs usually exist, it is possible to reduce the total costs for rehabilitation work. In addition, several cases in which cracks have reinitiated from holes drilled to arrest the cracks have been reported; motivating this study.

Through the effective bond length tests, a new test specimen and test setup were designed and the minimum bond length which engages the largest strain in the CFRP strip was determined for several different combinations of strip and adhesive. An analytical equation for predicting the effective bond length was also presented for possible use as a design equation. Cyclic and static tests on large scale girders have indicated some possibility for the reduction of the crack growth with the proposed rehabilitation method although in this research it was difficult to clearly identify the benefit from the bonded CFRP strips on girders with small cracks cycled under a 3 ksi nominal stress range. Therefore, there are several recommendations for

future studies on the use of bonded CFRP strips for rehabilitation of the fatigued girders as follows:

- Additional specimens with multiple layers need to be tested for effective bond length tests in order to confirm the linear increase in the maximum moment.
- Because new adhesive and CFRP strips are still being developed, it is necessary to search for new adhesives and CFRP strips that can increase the bond strength measured in the effective bond length tests.
- Because cracks did not reinitiate from drilled holes, it might be necessary to further investigate causes for reinitiation, or to increase the stress range for future cyclic tests.
- It will be necessary to conduct effective bond length tests and cyclic loading tests under (or after) exposure to the severe environment, including high humidity and temperature cycling. A project which is currently being conducted by another researcher at the University of Minnesota [57] deals with this issue using the same adhesive, 3M DP-460NS, tested in this project.
- Pretensioning CFRP strips will introduce compression stresses in the flange. If a crack exists in the tension flange, introducing compression stress at the crack tip will reduce the crack growth [58]. In addition, if pretensioned CFRP strips are bonded to the tension flange before the crack initiates, the compression stresses due to pretension can reduce the tensile stress range due to live loads to be under the threshold, and the crack will not grow into the tension flange although the crack may initiate at the weld tow.

References

1. Fisher, J. W., Hausammann, H., Sullivan, M. D., and Pense, A. W. (1979). "Detection and Repair of Fatigued Damage in Welded Highway Bridges," Report No. 206, National Cooperative Highway Research Program (NCHRP), Washington, D.C.
2. Fisher, J. W., Barthelemy, B. M., Mertz, D. R., and Edinger, J. A. (1980). "Fatigue Behavior of Full-Scale Welded Bridge Attachments," Report No. 227, National Cooperative Highway Research Program (NCHRP), Washington, D.C.
3. Sahli, A. H., Albrecht, P., and Vannoy, D. W. (1984). "Fatigue Strength of Retrofitted Cover Plates," *Journal of Structural Engineering*, ASCE, Vol. 110, No. 6, June, pp. 1374-1388.
4. Hassan, A., F., Bowman, M., D. (1996). "Fatigue Crack Repair of Steel Beams with Tapered Cover Plate Details," *Journal of Structural Engineering*, ASCE, Vol. 122, No. 11, November, pp. 1337-1346.
5. Andrea, M. D., Grondin, G. Y., and Kulak, G. L. (2001). "Behavior and Rehabilitation of Distortion-Induced Fatigue Cracks in Bridge Girders," Structural Engineering Report No. 240, Department of Civil and Environmental Engineering, University of Alberta, Edmonton, Alberta, Canada.
6. McKeefry, J. A. and Shield, C. K. (1999). "Acoustic Emission Monitoring of Fatigue Cracks in Steel Bridge Girders," Report No. MN/RC-1999-36, Minnesota Department of Transportation, St. Paul, Minnesota.
7. Meier, U., and Kaiser, H. P. (1991). "Strengthening of Structures with CFRP Laminates," *Advanced Composites Materials in Civil Engineering Structures*, Iyer, S. L. Ed., ASCE Specialty Conference, Las Vegas, pp. 224-232.
8. Sharif, A., Al-Sulaimani, G. J., Basunbul, I. A., Baluch, M. H., and Ghaleb, B. N. (1994). "Strengthening of Initially Loaded Reinforced Concrete Beams Using FRP Plates," *American Concrete Institute Structural Journal*, Vol. 91, No. 2, March-April, pp. 160-168.
9. Chajes, M. J., Mertz, D. R., Thomson, T. A., Jr., and Farschman, C. A. (1994). "Durability of Composite Material Reinforcement," *Infrastructure: New Materials and Methods of Repair*, Proceedings of the Materials Engineering Conference, No.804, October, ASCE, New York, New York, pp. 598-605.
10. Finch, W. W., Jr., Chajes, M. J., Mertz, D. R., Kaliakin, V. N., and Faqiri, A. (1994). "Bridge Rehabilitation Using Composite Materials," *Infrastructure: New Materials and Methods of Repair*, Proceedings of the Materials Engineering Conference, No. 804, October, ASCE, New York, New York, pp. 1140-1147.

11. Chajes, M. J., Januszka, T. F., Mertz, D. R., Thomson, T. A., Jr., and Finch, W. W., Jr. (1995). "Shear Strengthening of Reinforced Concrete Beams Using Externally Applied Composite Fabrics," *American Concrete Institute Structural Journal*, Vol. 92, No. 3, May-June, pp. 295-303.
12. Muszynski, L. C., and Sierakowski R. L. (1996). "Fatigue Strength of Externally Reinforced Concrete Beams," *Materials for the New Millennium*, Proceedings of the Materials Engineering Conference, Vol. 1, ASCE, New York, New York, pp. 649-657.
13. Tedesco, J. W., Stallings, M. J. M., El-Mihilmy, M., and McCauley, M. W. (1996). "Rehabilitation of a Concrete Bridge Using FRP Laminates," *Materials for the New Millennium*, Proceedings of the Materials Engineering Conference, Vol. 1, ASCE, New York, New York, pp. 631-637.
14. Arduini, M., and Nanni, A. (1997). "Behavior of Precracked RC Beams Strengthened with Carbon FRP Sheets," *Journal of Composites for Construction*, Vol. 1, No. 2, May, pp. 63-70.
15. Arduini, M., and Nanni, A. (1997). "Parametric Study of Beams with Externally Bonded FRP Reinforcement," *American Concrete Institute Structural Journal*, Vol. 94, No. 5, pp. 493-501.
16. Juvandes, L., Figueiras, J. A., and Marques, A. T. (1998). "Performance of Concrete Beams Strengthened With CFRP Laminates," *Fiber Composite in Infrastructure*, Proceedings of the Second International Conference on Composite in Infrastructure, ICCI, Tucson, Arizona, Vol.1, pp. 126-137.
17. Garden, H. N., Quantrill, R. J., Hollaway, L. C., Thorne, A. M., and Parke G. A. R. (1998). "An Experimental Study of the Anchorage Length of Carbon Fibre Composite Plates Used to Strengthen Reinforced Concrete Beams," *Construction and Building Materials*, Vol. 12, No. 4, pp. 203-219.
18. Gillespie, J. W., Jr., Mertz, D. R., Edberg, W. M., Ammar, N., Kasai, K., and Hodgson, I. C. (1996a). "Rehabilitation of Steel Bridge Girders Through Application of Composite Materials," *Technology Transfer in a Global Community*, International SAMPE Technical Conference, Vol. 28, SAMPE, Covina, California, pp. 1249-1257.
19. Gillespie, J. W., Jr., Mertz, D. R., Kasai, K., Edberg, W. M., Demitz, J. R., and Hodgson, I. (1996b). "Rehabilitation of Steel Bridge Girders: Large Scale Testing," Proceedings of the American Society for Composites, Technomic Publishing Co. Inc., Lancaster, Pennsylvania, pp. 231-240.
20. Gillespie, J. W., Jr., Mertz, D. R., Edberg, William M., and Ammar, N. (1997). "Steel Girder Rehabilitation Through Adhesive Bonding of Composite Materials," Processing Annual Technical Conference - ANTEC, Vol. 1, Society of Plastics Engineers, Brookfield, Connecticut, pp. 1171-1175.

21. Edberg, W. M., Mertz, D. R., and Gillespie, J. W., Jr. (1996). "Rehabilitation of Steel Beams Using Composite Materials," *Materials for the New Millennium*, Proceedings of the Materials Engineering Conference, Vol. 1, ASCE, New York, New York, pp. 502-508.
22. Sen, R., Liby, L., Mullins, G., and Spillett, K. (1996). "Strengthening Steel Composite Beams with CFRP Laminates," *Materials for the New Millennium*, Proceedings of the Materials Engineering Conference, Vol. 2, ASCE, New York, New York, pp. 1601-1607.
23. Albrecht, P. (1987). "Fatigue Strength of Adhesively Bonded Cover Plates," *Journal of Structural Engineering*, ASCE, Vol. 113, No. 6, June, pp. 1236-1250.
24. Adunutula, R. V. (1997). "Adhesively Bonded Plates for Repair or Prevention of Fatigue Distress on Steel." M.S. Thesis, Department of Civil Engineering, Case Western Reserve University, Cleveland, Ohio.
25. Adams, R. D. and Wake, W. C. (1984). "Structural Adhesive Joints in Engineering," Elsevier Applied Science Publishers, New York, New York.
26. Baker, A. A. and Jones, R. (1987). "Bonded Repair of Aircraft Structures," Martinus Nijhoff Publishers, Dordrecht, Netherlands.
27. ASTM (1994). "D 1002: Standard Testing Method for Apparent Shear Strength of Single-Lap-Joint Adhesively Bonded Metal Specimens by Tension Loading (Metal-to-Metal)," American Society for Testing and Materials, Philadelphia, Pennsylvania.
28. ASTM (1996). "D 3528: Standard Test Method for Strength Properties of Double Lap Shear Adhesive Joints by Tension Loading," American Society for Testing and Materials, Philadelphia, Pennsylvania.
29. Ikegami, K., Fujii, T., Kawagoe, H., Kyogoku, H., Motoie, K., Nohno, K., Sugibayashi, T., and Yoshida, F. (1996). "Benchmark Tests on Adhesive Strength in Butt, Single and Double Lap Joints and Double-Cantilever Beams," *International Journal of Adhesion & Adhesives*, Vol. 16, pp. 219-226.
30. Sugibayashi, T., and Ikegami, K. (1984). "Strength and Deformation of Single Lap Joint," *Nippon Kikai Gakkai Ronbunshu*, C Hen, Vol. 50, No. 449, January, pp. 17-27.
31. Kyogoku, H., Sugibayashi, T., and Ikegami, K. (1985). "Strength Evaluation of Asymmetric Single Lap Joints: (1st Report, Effects of the Difference of the Adherend Thickness)," *Nippon Kikai Gakkai Ronbunshu*, A Hen, Vol. 51, No. 465, May, pp. 1461-1466.
32. Kyogoku, H., Sugibayashi, T., and Ikegami, K. (1986). "Strength Evaluation of Asymmetric Single Lap Joints: (2nd Report, Effects of the Taper of Adherends)," *Nippon Kikai Gakkai Ronbunshu*, A Hen, Vol. 52, No. 473, January, pp. 195-200.
33. Kyogoku, H., Sugibayashi, T., and Ikegami, K. (1986). "Strength Evaluation of Asymmetric Single Lap Joints: (3rd Report, Effects of the Mechanical Properties of Adherends)," *Nippon Kikai Gakkai Ronbunshu*, A Hen, Vol. 52, No. 476, April, pp. 1050-1057.

34. Ono, T., Matsuo, K., Sugibayashi, T., and Ikegami, K. (1988). "Tensile Strength of the Single Lap Joint between GFRP and Metals," *Nippon Kikai Gakkai Ronbunshu, A Hen*, Vol. 54, No.500, April, pp. 729-736.
35. Dorn, L. and Liu, W. (1992). "The Stress State and Failure Properties of Adhesive-Bonded Plastic/Metal Joint," *International Journal of Adhesion and Adhesives*, Vol. 13, No. 1, pp. 21-31.
36. Harris, J. A. and Adams, R. D. (1984). "Strength Prediction of Bonded Single Lap Joints by Non-Linear Finite Element Method," *International Journal of Adhesion and Adhesives*, Vol. 4, No. 2, pp. 65-78.
37. Volkersen, O. (1938). "Die Niekraftverteilung in Zugbeanspruchten mit Konstanten Laschenquerschriften," *Luftfahrtforschung*, Vol. 15, pp. 41-47.
38. Goland, M. and Reissner, E. (1944). "The Stresses in Cemented Joints," *Journal of Applied Mechanics*, Vol. 11, pp. A17-A27.
39. Hart-Smith, L. J. (1973). "Adhesive Bonded Single-Lap Joints," Contract Report, NASA CR-112236, Douglas Aircraft Company, McDonnell Douglas Corporation, NASA Langley Research Center, Hampton, Virginia.
40. Hart-Smith, L. J. (1973). "Adhesive Bonded Double-Lap Joints," Contract Report, NASA CR-112235, Douglas Aircraft Company, McDonnell Douglas Corporation, NASA Langley Research Center, Hampton, Virginia.
41. Hart-Smith, L. J. (1978). "Adhesive Bond Stresses and Strains at Discontinuities and Cracks in Bonded Structures," *Journal of Engineering Materials and Technology*, Transactions of the American Society of Mechanical Engineering, Vol. 100, pp. 16-24.
42. Tsai, M. Y. and Morton, J. (1994). "An Evaluation of Analytical and Numerical Solutions to the Single-Lap Joint," *International Journal of Solids and Structures*, Vol. 31, No. 18, pp. 2537-2563.
43. Oplinger, D. W. (1994). "Effects of Adherend Deflections in Single Lap Joints," *International Journal of Solids and Structures*, Vol. 31, No. 18, pp. 2565-2587.
44. Tsai, M. Y., Oplinger, D. W., and Morton, J. (1998). "Improved Theoretical Solutions for Adhesive Lap Joints," *International Journal of Solids and Structures*, Vol. 35, No. 12, pp. 1163-1185.
45. Wu, Z. J. and Wardenier, J. (1997). "Stress Expressions of Single-Lap Adhesive Joints of Dissimilar Adherends," *Composite Structures*, Vol. 38, No. 1-4, pp. 273-280.
46. Cheng, S., Chen, D., and Shi, Y. (1991). "Analysis of Adhesive-Bonded Joints with Nonidentical Adherends," *Journal of Engineering Mechanics*, ASCE, Vol. 117, No. 3, March, pp. 605-623.

47. Carpenter, W. C. (1991). "A Comparison of Numerous Lap Joint Theories for Adhesively Bonded Joints," *Journal of Adhesion*, Vol. 35, pp. 55-73.
48. ASTM (1997). "D 638: Standard Testing Method for Tensile Properties of Plastics," American Society for Testing and Materials, Philadelphia, Pennsylvania.
49. ASTM (2000). "E 8: Standard Testing Method for Tension Testing of Metallic Materials," American Society for Testing and Materials, Philadelphia, Pennsylvania.
50. Nanni, A., Boothby, T., Cetin, K. M., Shaw, B. A., and Bakis, C. (1997). "Environmental Degradation of Repaired Concrete Structure," Non-Metallic (FRP) Reinforcement for Concrete Structures, *Proceedings of the Third International Symposium*, Vol. 2, pp. 155-162.
51. ASTM (1995). "D 3039: Standard Testing Method for Tensile Properties of Polymer Matrix Composite Materials," American Society for Testing and Materials, Philadelphia, Pennsylvania.
52. Hurst, K. F. (2001). "Combining Conventional Techniques and FRP Materials to Repair Fatigued Damage in Metal Bridge Structures," *Proceedings of the Fifth National Workshop on Bridge Research in Progress*, Minneapolis, Minnesota, pp. 267-269.
53. Jajich D. and Schultz, A. E. (2000). "Distortion-Induced Fatigue in Multi-Girder Steel Bridges," Report No. MN/RC-2000-16, Minnesota Department of Transportation, St Paul, Minnesota.
54. Corwin, E. "Effects of Increasing Truck Weight on Steel Bridges," M.S. thesis, Department of Civil Engineering, University of Minnesota, Minneapolis, Minnesota.
55. Tada, H., Paris, P. C., and Irwin, G. R. (1985). "The Stress Analysis of Cracks Handbook," 2nd Ed., Paris Productions, Inc., St. Louis, Missouri.
56. Crocombe, A. D. and Richardson, G. (1998). "Assessing Stress State and Mean Load Effects on the Fatigue Response of Adhesively Bonded Joints," *International Journal of Adhesion and Adhesives*, Vol. 19, pp. 19-27.
57. Hu, Y. "Use of Adhesive to Retrofit Out-of-Plane Distortion Induced Fatigue Cracks in Multi-Girder Bridges," Department of Civil Engineering, University of Minnesota, Minneapolis, Minnesota.
58. Bassetti, A., Nussbaumer A., and Hirt A. (2000). "Fatigue Life Extension of Riveted Bridge Members Using Prestressed Carbon Fibre Composites," *Steel Structures of the 2000's*, ECCS, Istanbul, Turkey, pp. 375-380.

Tables

Table 3.1 Tensile Test Results for Sikadur 330 Adhesive

	1	2	3	4	5	Average
Elastic Modulus (ksi)	679	-	639	-	686	668
Tensile Strength (ksi)	6.2	5.8	6.3	-	5.8	6.0
Elongation at Rupture (%)	0.95	0.88	1.01	-	0.87	0.93

Table 3.2 Tensile Test Results for DP-460NS Adhesive

	1	2	3	4	5	Average
Elastic Modulus (ksi)	-	347	381	368	361	360
Tensile Strength (ksi)	-	5.1	5.1	5.0	5.1	5.1
Elongation at Rupture (%)	-	2.27	1.73	-	2.35	2.12

Table 3.3 Tensile Test Results for Carbodur CFRP Strip

	1	2	3	4	5	Average
Elastic Modulus (ksi)	23 100	22 700	21 800	22 700	23 100	22 680
Tensile Strength (ksi)	411	350	372	401	373	381
Elongation at Rupture (%)	-	-	1.78	1.75	1.69	1.74

Table 3.4 Tensile Test Results for Tyfo UC CFRP Strip

	1	2	3	Average
Elastic Modulus (ksi)	17 000	15 800	16 700	16 500
Tensile Strength (ksi)	306	283	293	294
Elongation at Rupture (%)	1.80	1.79	1.75	1.78

“-“ in tables indicates error during data recording

Table 3.5 Specimen Matrix for Effective Bond Length Test

Specimen	CFRP	Adhesive	Config.	Bond Length	Bond Thickness	Type	Note
1-1	CarboDur	Sikadur 330	1	15 in.	0.06 in.	A	
1-2			2	15 in.	0.06 in.	A	
1-3			4	15 in.	0.06 in.	B	
1-4				26 in.	0.06 in.	B	
1-5			3	15 in.	0.06 in.	A	2 specimens
1-6			5	15 in.	0.05 in.	B	
1-7				8 in.	0.05 in.	A	3 specimens
1-8					B	3 specimens	
1-9				0.02 in.	B		
1-10		Sikadur 30	4	15 in.	0.06 in.	B	
1-11		DP-460NS	5	8 in.	0.02 in.	B	3 specimens (two are heat cured)
1-12		Epoxy Plus 25	5	8 in.	0.02 in.	A	
1-13	Tyfo UC	DP-460NS	5	8 in.	0.02 in.	B	
1-14				16 in.	0.02 in.	A	
1-15				8 in.	0.02 in.	A	Disturbed cure
1-16		Fyfe TC	5	8 in.	0.05 in.	B	
2-1	CarboDur	Sikadur 330	4	15 in.	0.06 in.	B	
2-2			3	15 in.	0.06 in.	A	Retested with pretensioned bolts
2-3	Tyfo UC	DP-460NS	5	16 in.	0.02 in.	A	
3-1	CarboDur	Sikadur 330	3	15 in.	0.06 in.	A	

Table 3.6 Specimen Matrix for Cyclic Fatigue Loading Tests

Specimen	Bond Length (in.)	Minimum Stress (ksi)	Stress Range (ksi)	Minimum Load (kips)	Maximum Load (kips)	Load Range (kips)	Time of Application	Rehabilitation Method
NR-3	-	10.0	3.0	17.8	23.2	5.4	CL2 ¹	HD ³
R-3-1	8	10.0	3.0	17.8	23.2	5.4	CL2	HD&CFRP ⁴
R-3-2	8	10.0	3.0	17.8	23.2	5.4	TFT ²	HD & CFRP
R-3-3	8	10.0	6.5	17.8	30.5	11.7	CL2.9	CFPR

¹ CLX: crack length of X inches on the bottom of the bottom flange

² TFT: cracked through the flange thickness

³ HD: Hole drilling

⁴ CFRP: Application of CFRP Strip

Table 4.1 Summary of Effective Bond Length Test

Specimen	CFRP	Adhesive	Config.	Bond Length	Moment (kips-in.)	Strain at failure ($\mu\epsilon$)	Failure Mode	
1-1	CarboDur	Sikadur 330	1	15 in.	320	4,000	D	
1-2			2	15 in.	320	3,000	D	
1-3			4	15 in.	360	4,000	D	
1-4				26 in.	360	4,000	D	
1-5a			3	15 in.	500	5,000	D	
1-5b					520	6,000	D	
1-6			5	15 in.	440	5,800	D, F	
1-7a					660	8,800	D, F	
1-7b					680	8,900	D, F	
1-7c					400	5,000	D, F	
1-8a					700	10,000	D, F	
1-8b					640	7,700	D, F	
1-8c					500	6,300	D, F	
1-9					360	4,800	D	
1-10			Sikadur 30	4	15 in.	320	2,500	D
1-11a			DP-460NS	5	8 in.	670	9,700	D, F
1-11b	660	9,500*				D, F		
1-11c	740	8,800*				D, F		
1-12	Epoxy Plus 25	5	8 in.	640	9,300	D		
1-13	Tyfo UC	DP-460NS	5	8 in.	880	13,000+	N.A.	
1-14				16 in.	960	12,000	D, F	
1-15				8 in.	1000	14,000	D, F	
1-16		Fyfe TC	5	8 in.	840	12,000+	N.A.	
2-1	CarboDur	Sikadur 330	4	15 in.	720	3,500	D	
2-2 (retested)			3	15 in.	920	4,500+	N.A.	
						1080	5,500	D
2-3	Tyfo UC	DP-460NS	5	16 in.	1650	10,000	D	
3-1	CarboDur	Sikadur 330	3	15 in.	1160	4,000	D	

N.A.: Not Applicable; *: Heat Cured; +: Test was terminated prior to failure

D: Debonding failure; F: Rupture of several fibers

Figures

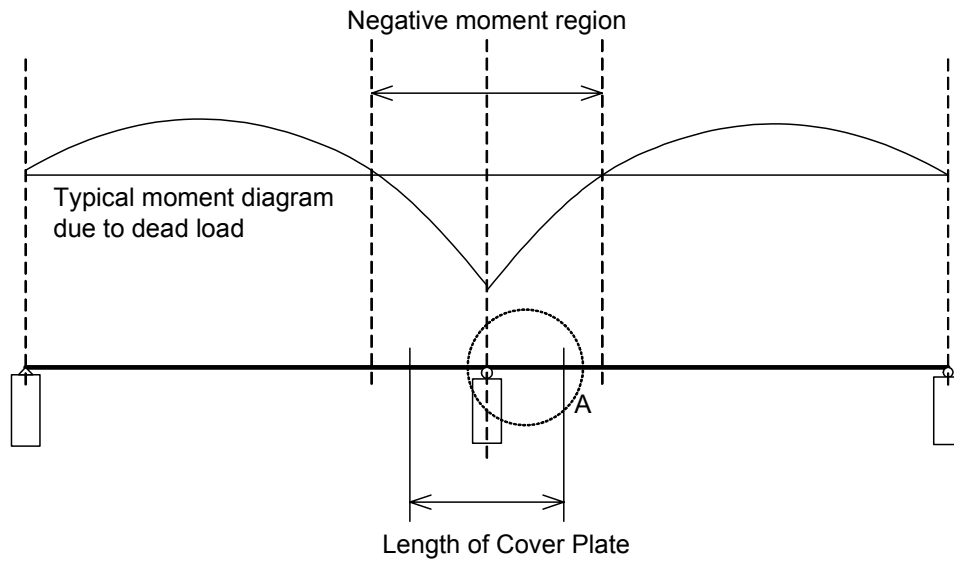


Figure 1.1 Typical Moment Distribution in Two Span Continuous Girder

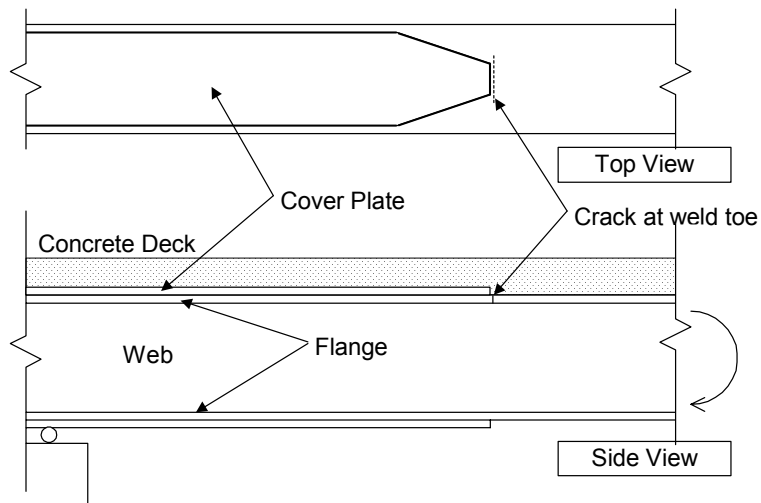


Figure 1.2 Crack Initiated from Weld Toe (Circle A in Fig. 1)

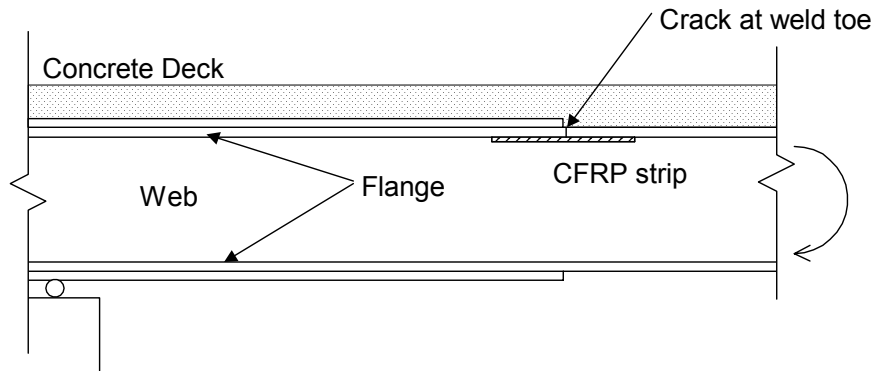


Figure 1.3 Rehabilitation of Fatigued Tension Flange with Bonded CFRP Strip

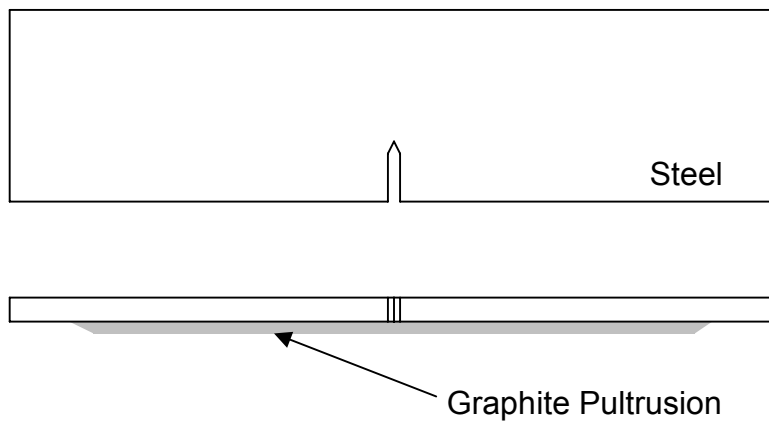


Figure 2.1 Sketch of Specimen in Ref. 20

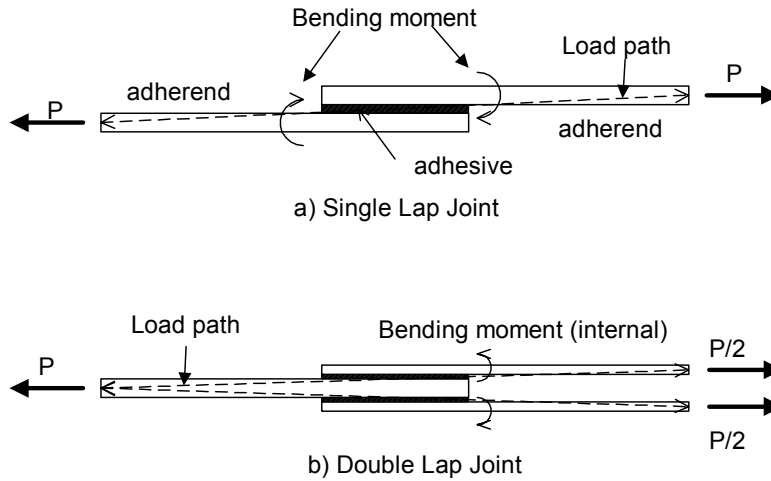


Figure 2.2 Single and Double Lap Specimens

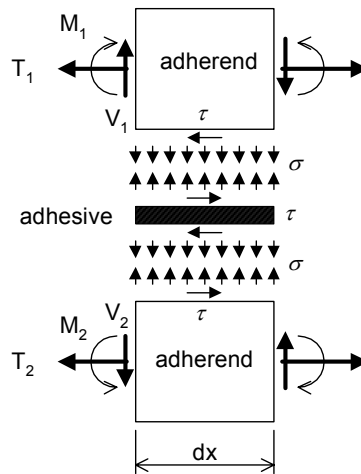


Figure 2.3 Free Body Diagram of Single-Lap Specimen

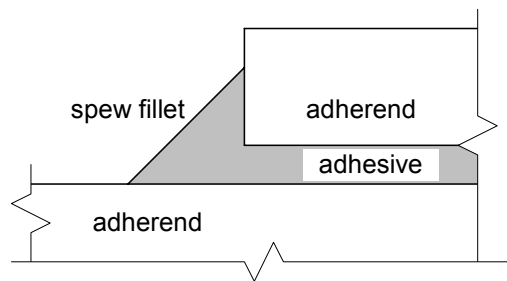


Figure 2.4 Sketch of Spew Fillet

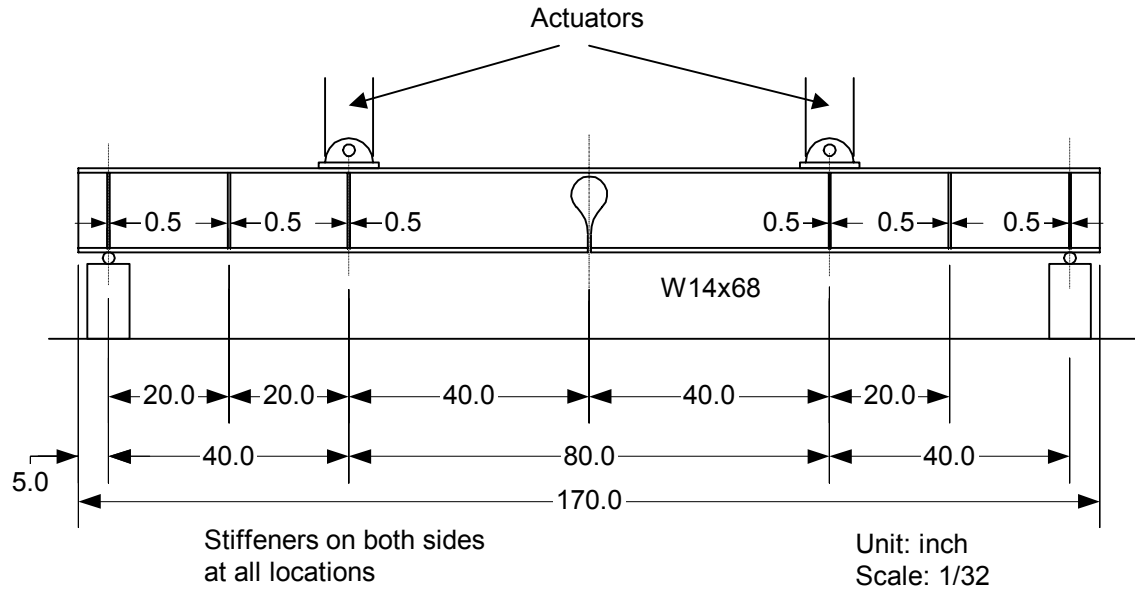


Figure 3.1 Experimental Test Setup and Dimensions - Two-77 kip actuators

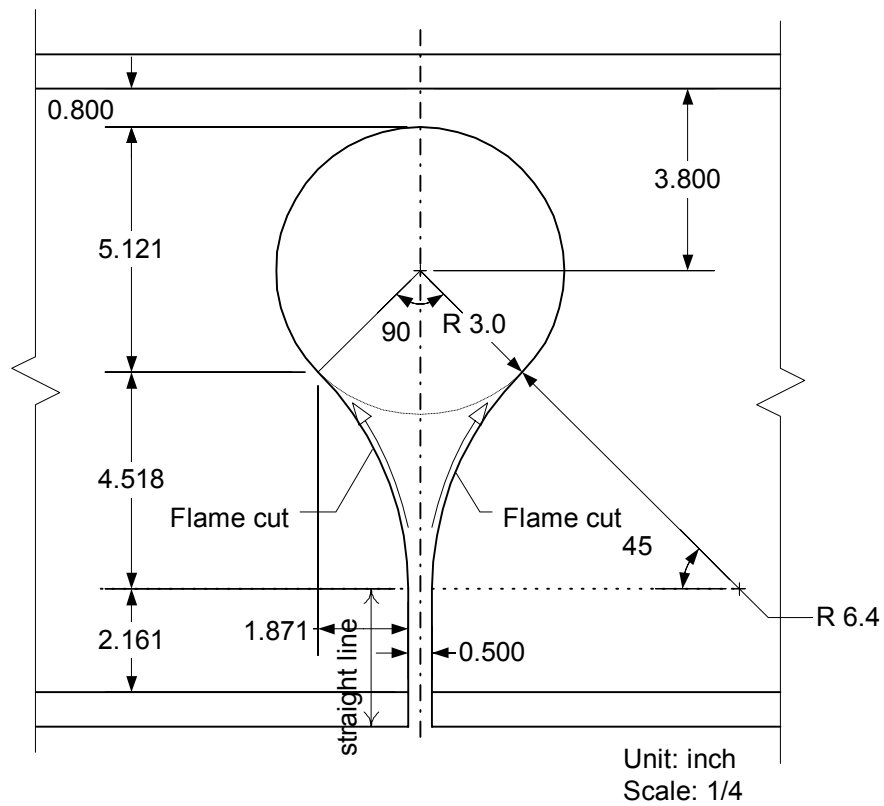
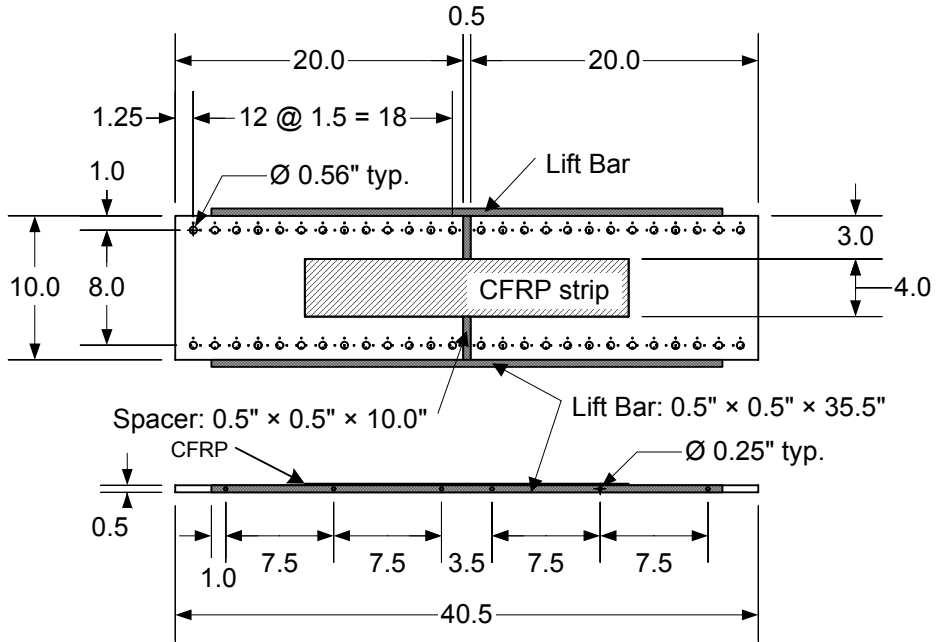
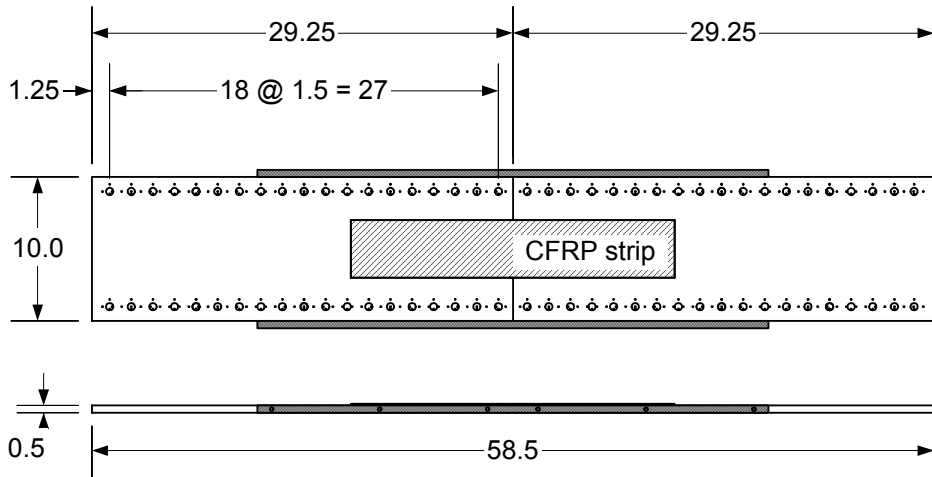


Figure 3.2 Detail of Hole



Specimen Type A



Specimen Type B

Unit: inch
Scale: 3/40

Figure 3.3 Dimensions of Specimens and Holding Devices



Figure 3.4 Typical Specimen before being Bolted to W14x68 Girder - Specimen 1-2



Figure 3.5 Detail of Bolted Connection between Base Girder and Specimen

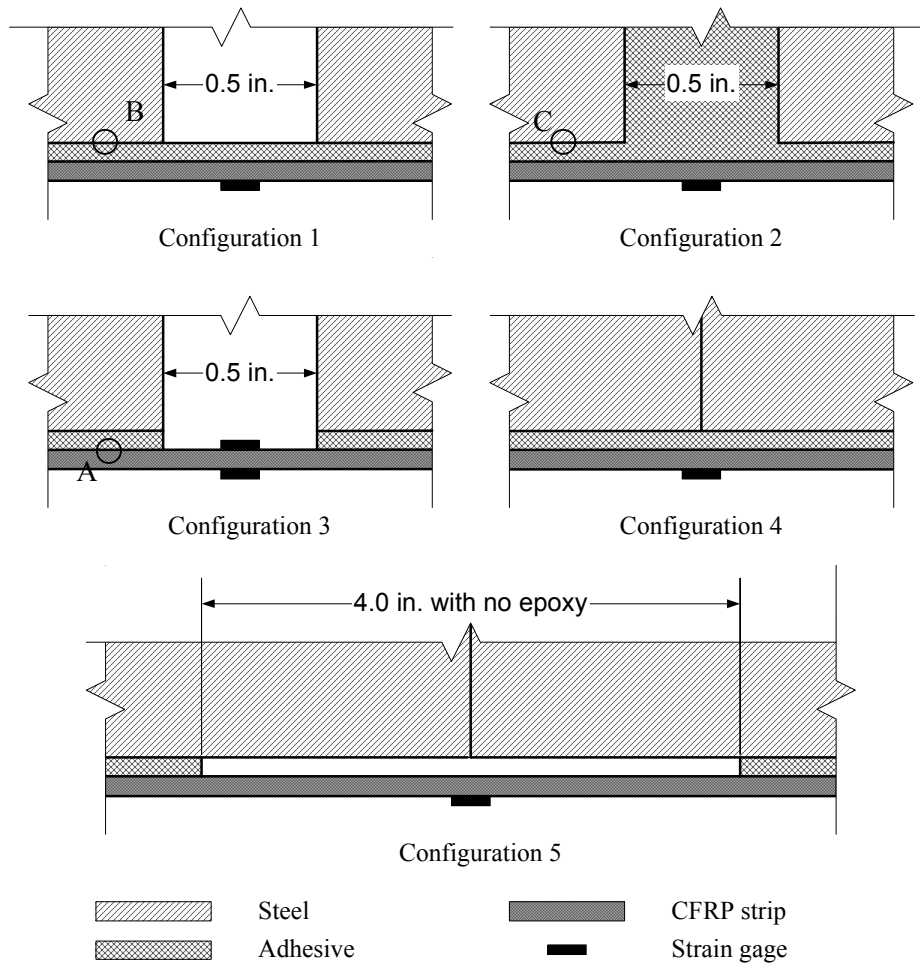


Figure 3.6 Configurations of Specimen around Slit

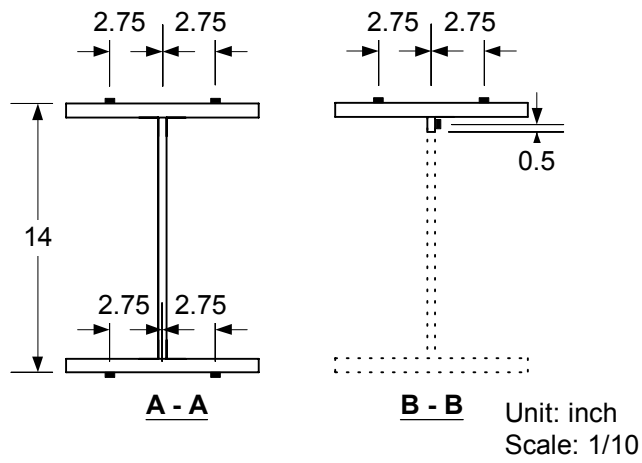
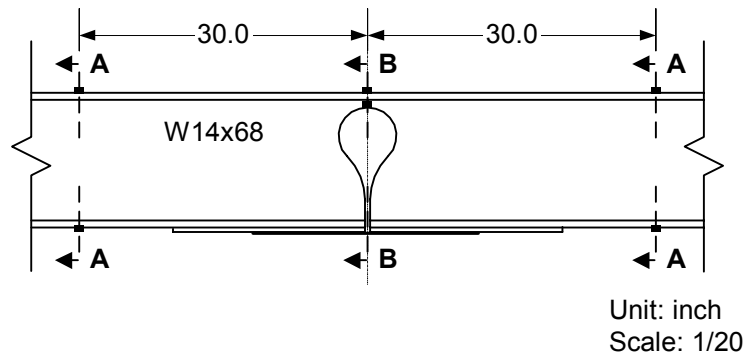
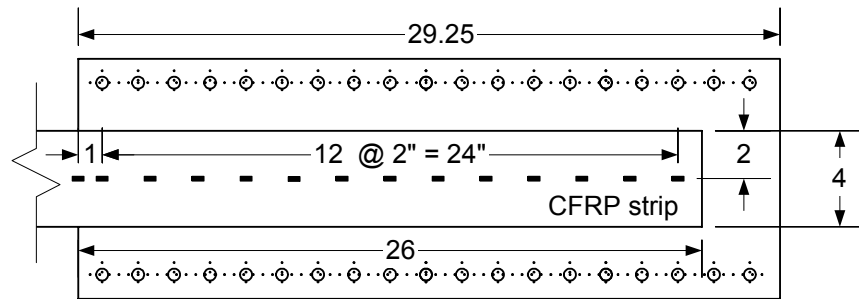
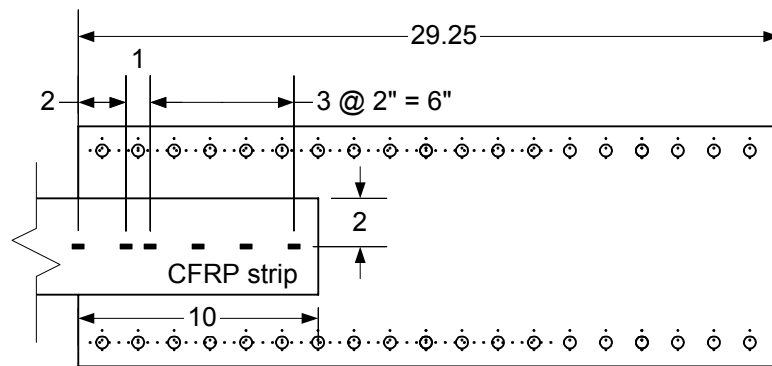


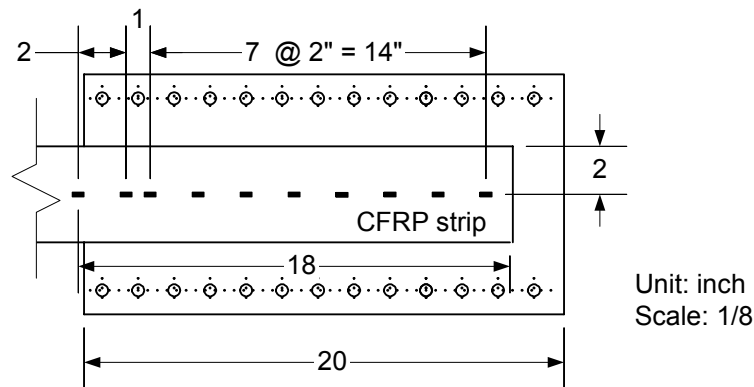
Figure 3.7 Strain Gauge Instrumentation of Base Girder



a) Gauge Scheme for Specimen 1-4



b) Gauge Scheme for Specimen 1-8



c) Gauge Scheme for Specimen 1-14 and 2-3

Unit: inch
Scale: 1/8

Figure 3.8 Strain Gauge Instrumentation of CFRP Strips

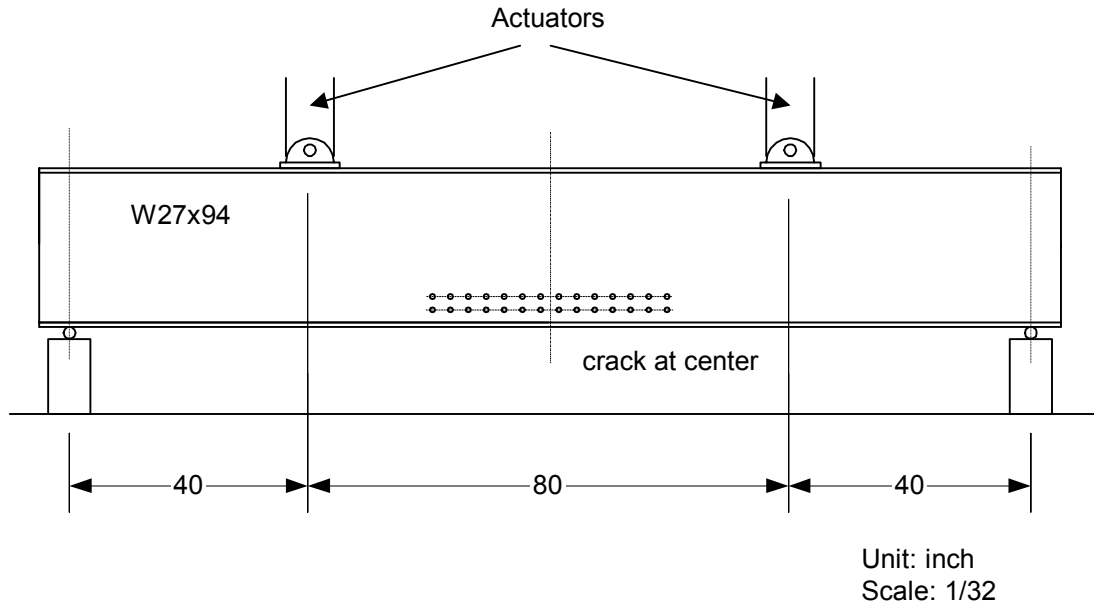


Figure 3.9 Sketch of Test setup for W27x94 Girder



Figure 3.10 Test Setup for Static Test on W27x94

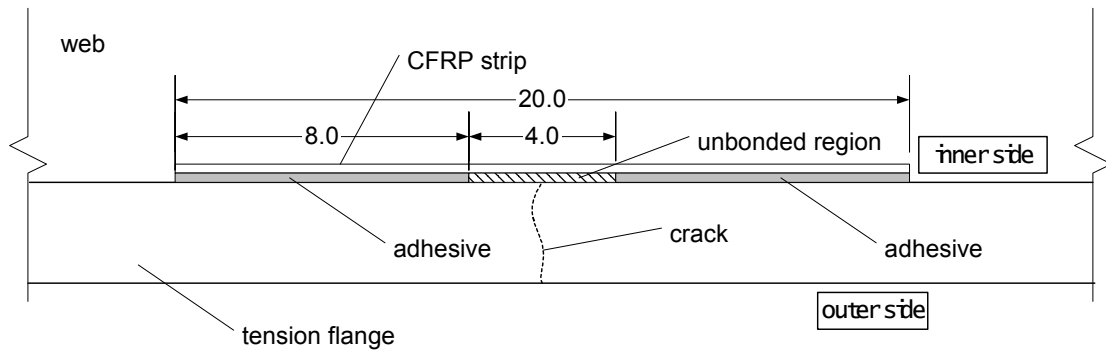


Figure 3.11 Sketch of Rehabilitated Fatigued Tension Flange

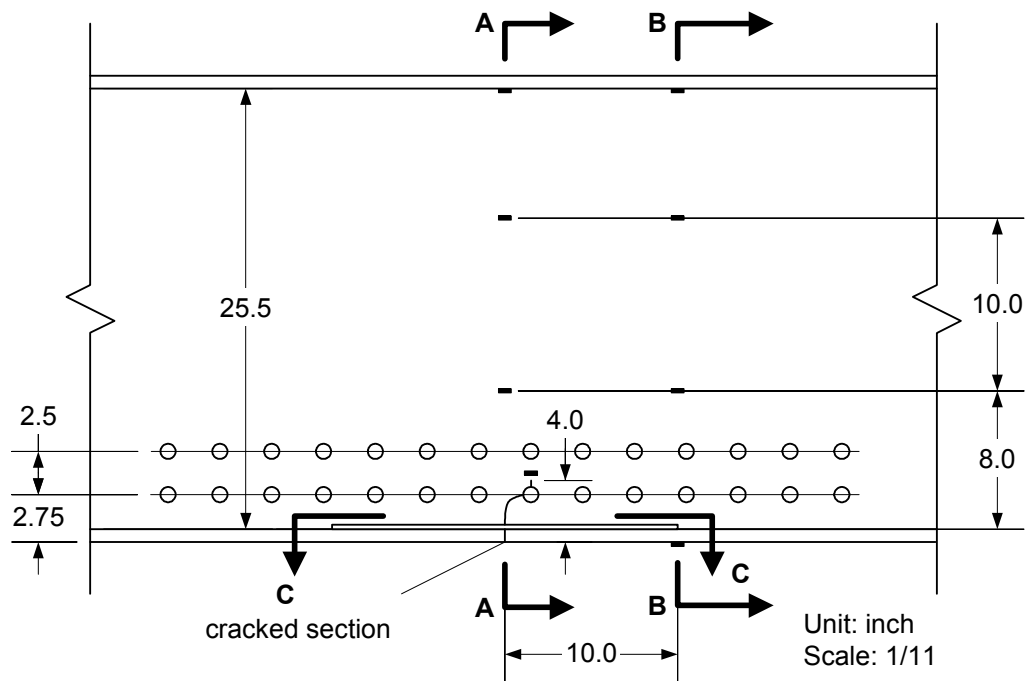


Figure 3.12 Gauge Instrumentation on W27x94 -1

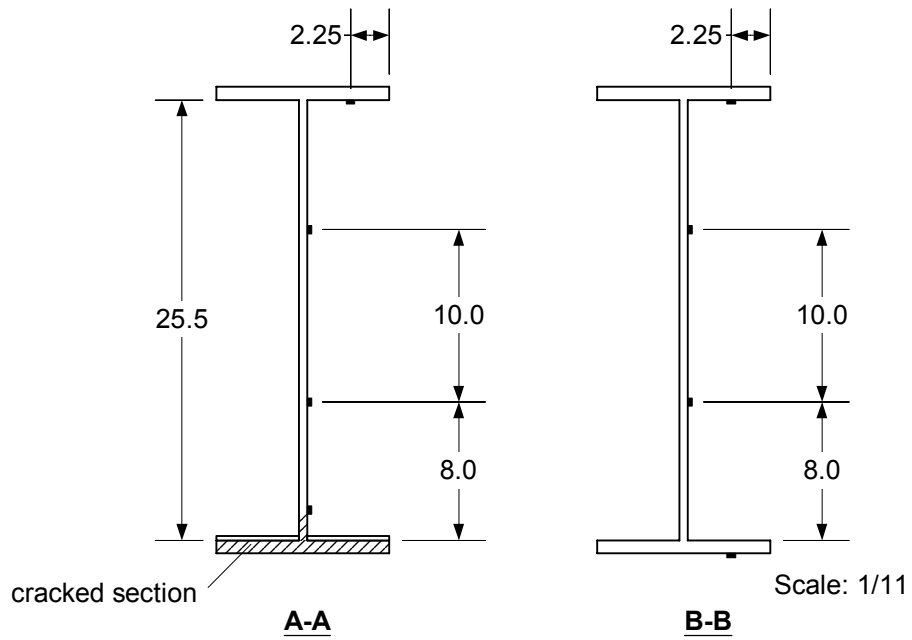


Figure 3.13 Gauge Instrumentation on W27x94 -2

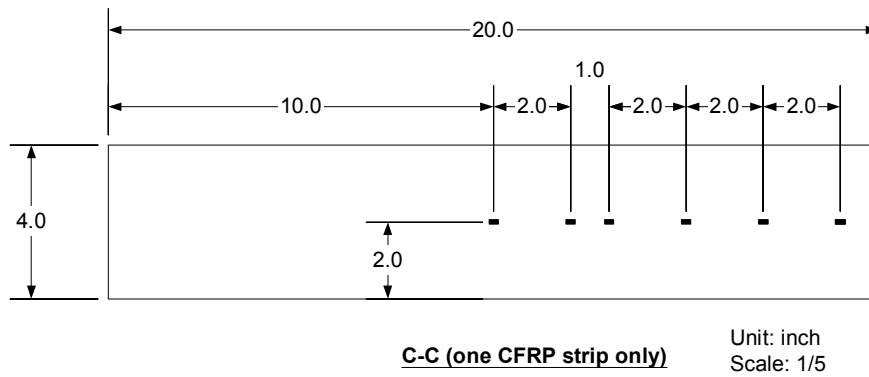


Figure 3.14 Gauge Instrumentation on CFRP Strip

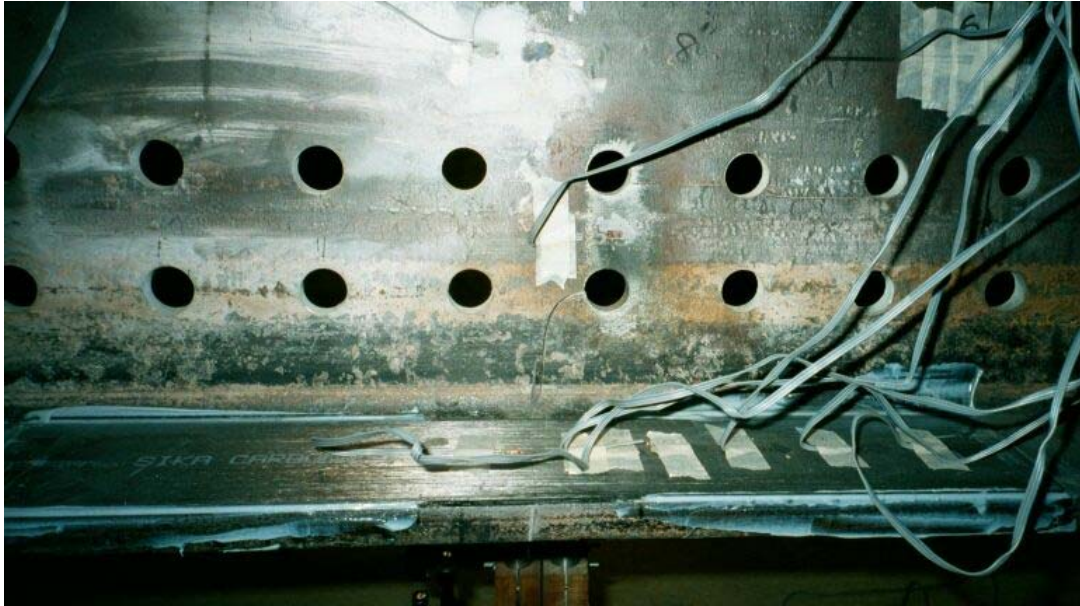


Figure 3.15 Rehabilitated Girder and Instrumented Gauges

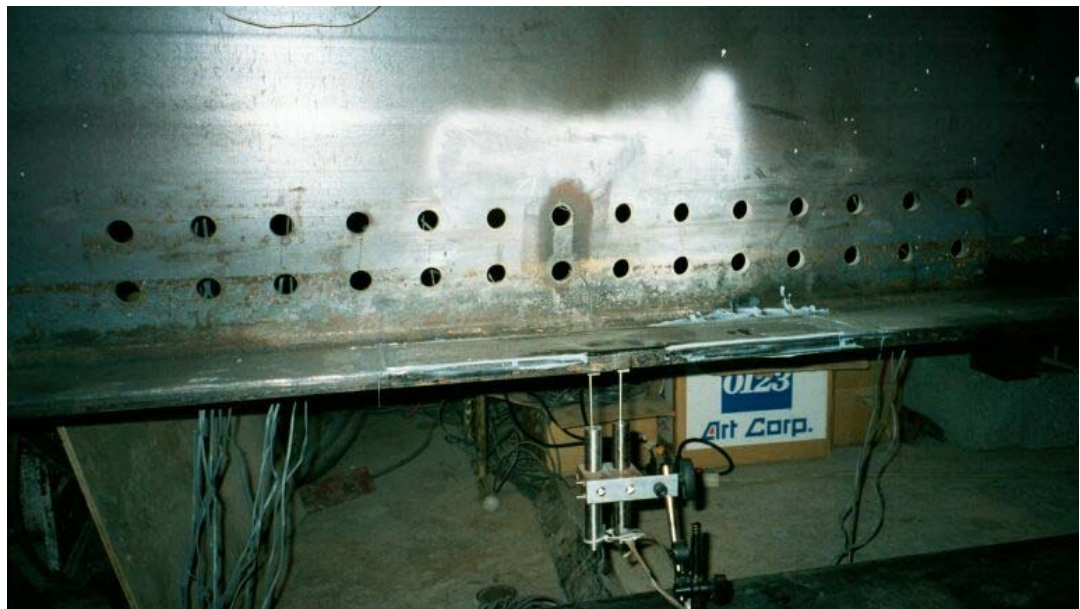


Figure 3.16 LVDTs for Deflection Measurement

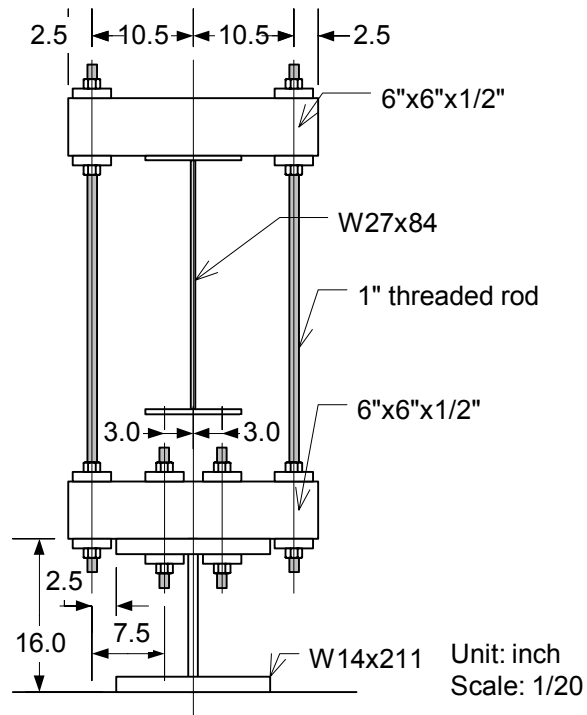


Figure 3.18 Detail of Dead Load Application Device (Section A-A)

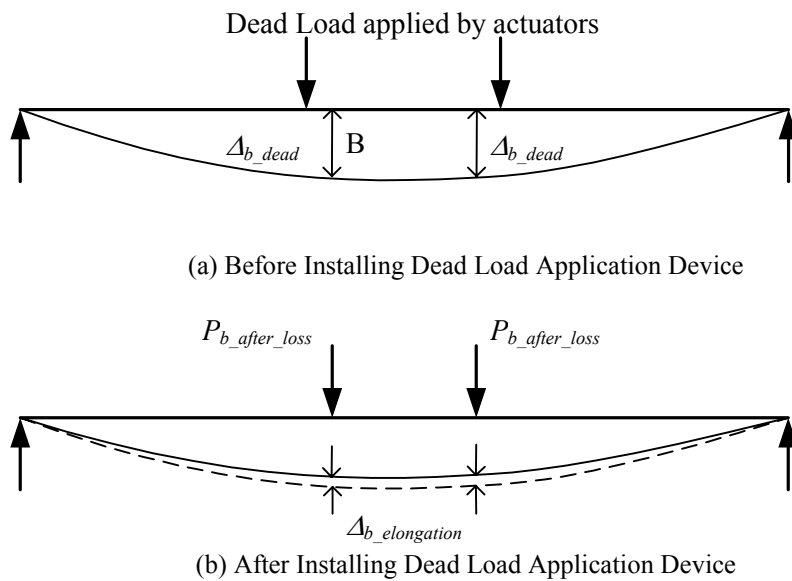


Figure 3.19 Sketch for Calculation of Loss of Dead Load

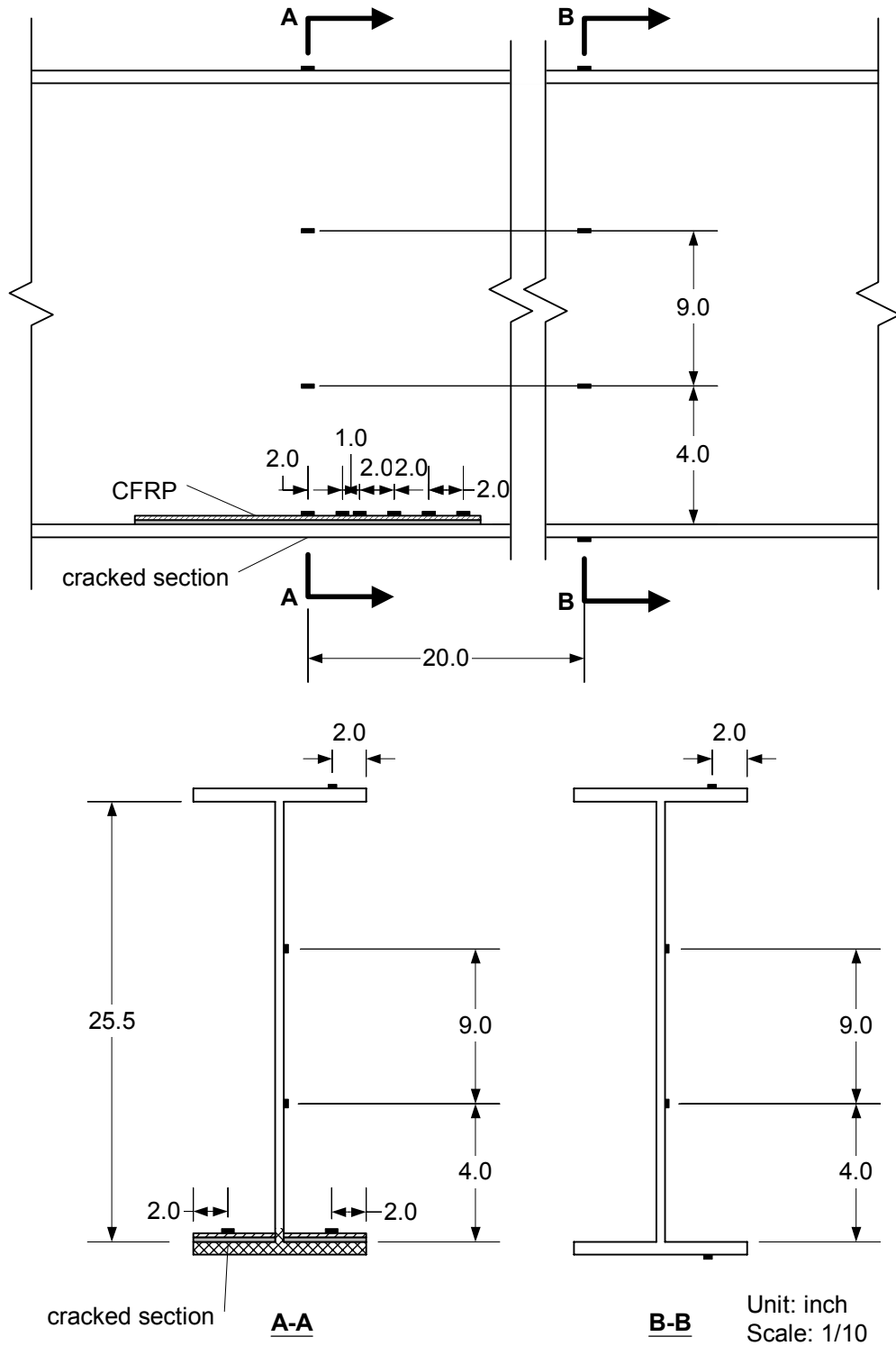


Figure 3.20 Instrumentation for W27x84 (all gauges are shown)



Figure 4.1 Post Failure Photograph - Specimen 1-3



Figure 4.2 Post Failure Photograph - Specimen 1-5



Figure 4.3 Post Failure Photograph - Specimen 1-8



Figure 4.4 Post Failure Photograph – Specimen 1-14

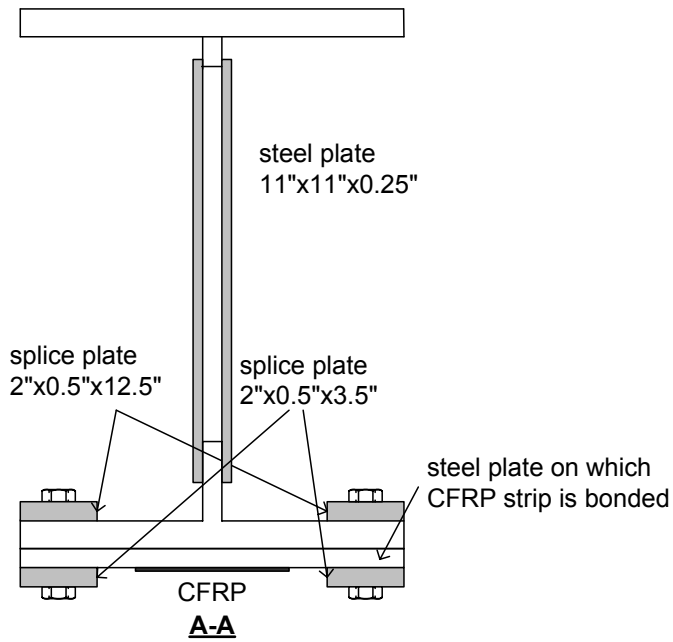
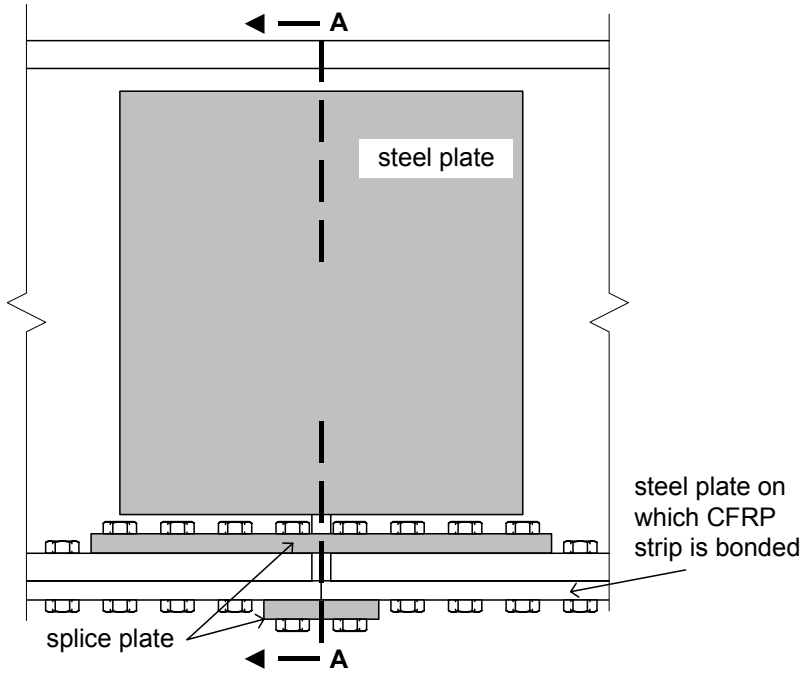


Figure 4.5 Detail of Splice Plates and Web Plates for Application of Cyclic Loading during Adhesive Curing

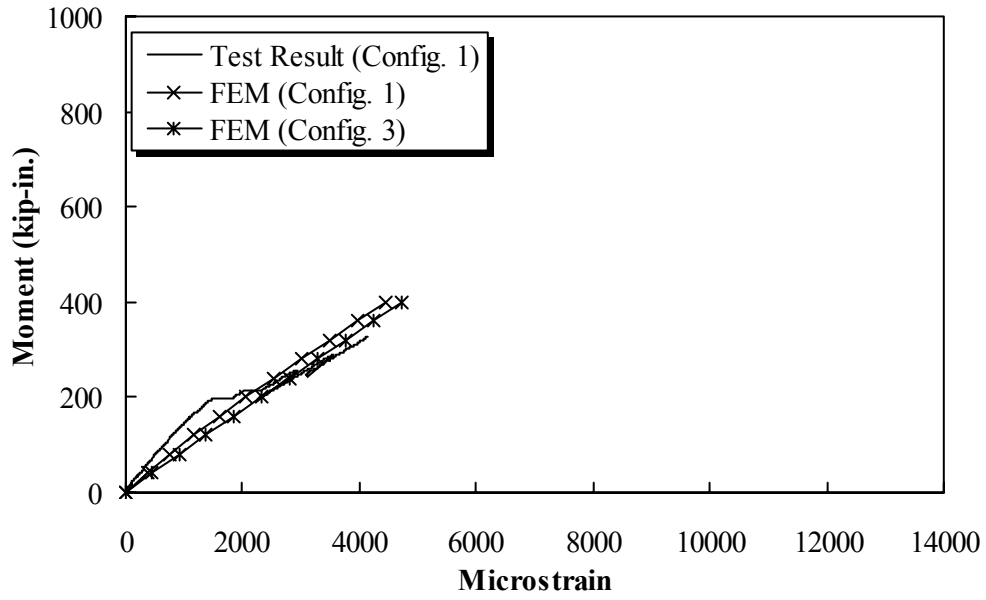


Figure 4.6 Applied Moment vs. CFRP Strain - Specimen 1-1

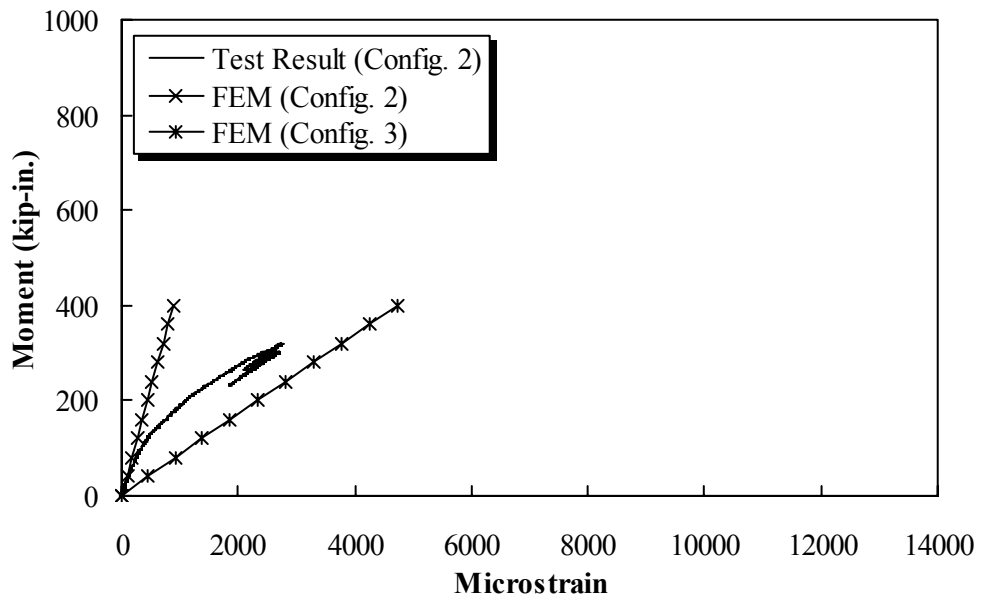


Figure 4.7 Applied Moment vs. CFRP Strain - Specimen 1-2

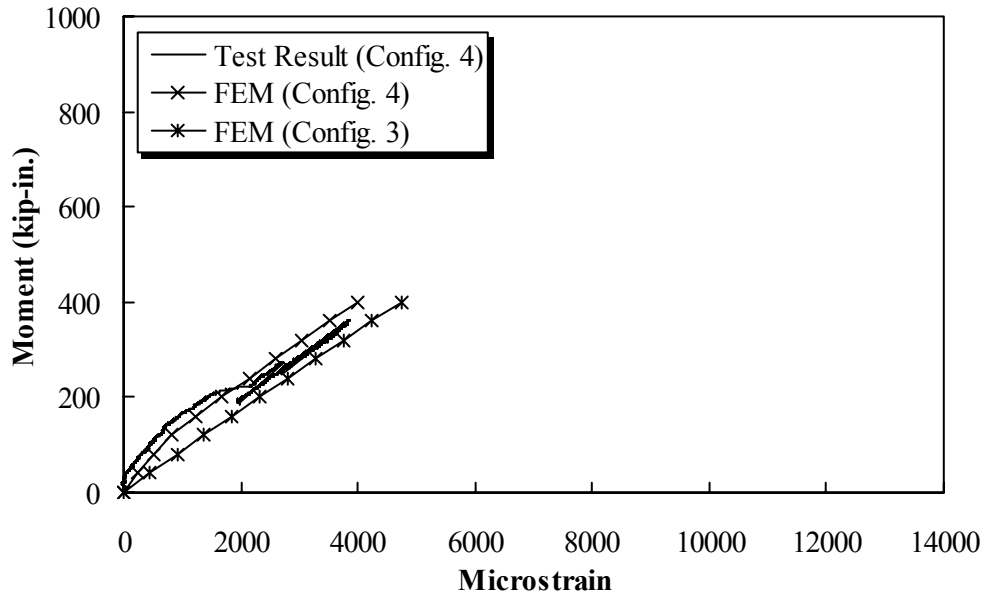


Figure 4.8 Applied Moment vs. CFRP Strain - Specimen 1-3

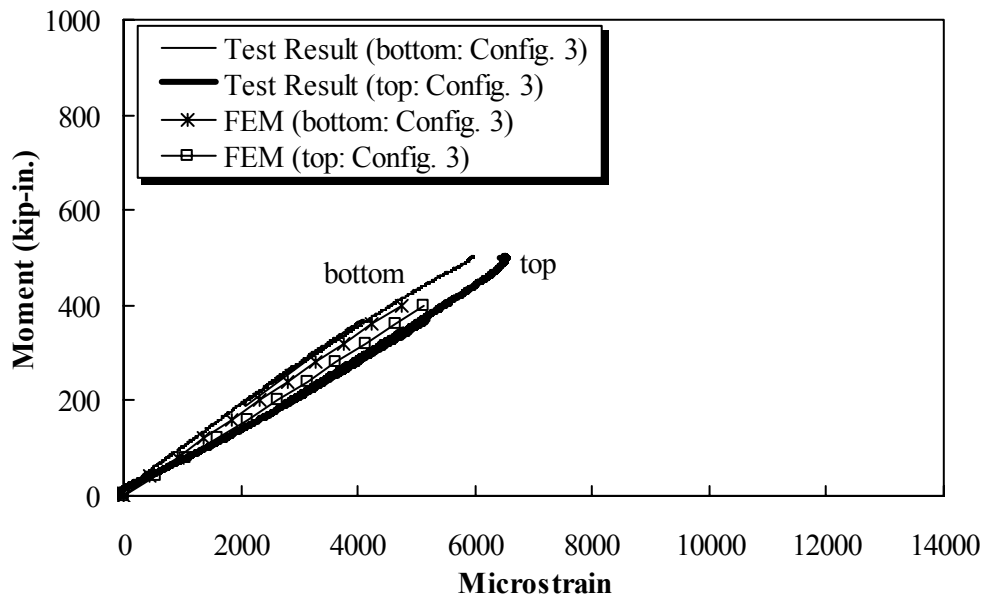


Figure 4.9 Applied Moment vs. CFRP Strain - Specimen 1-5

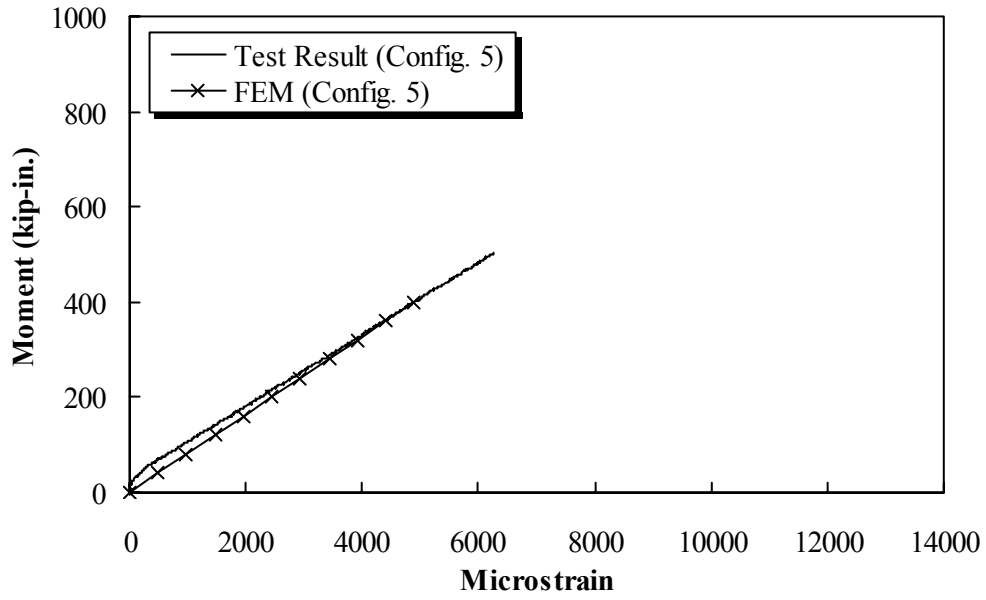


Figure 4.10 Applied Moment vs. CFRP Strain - Specimen 1-8

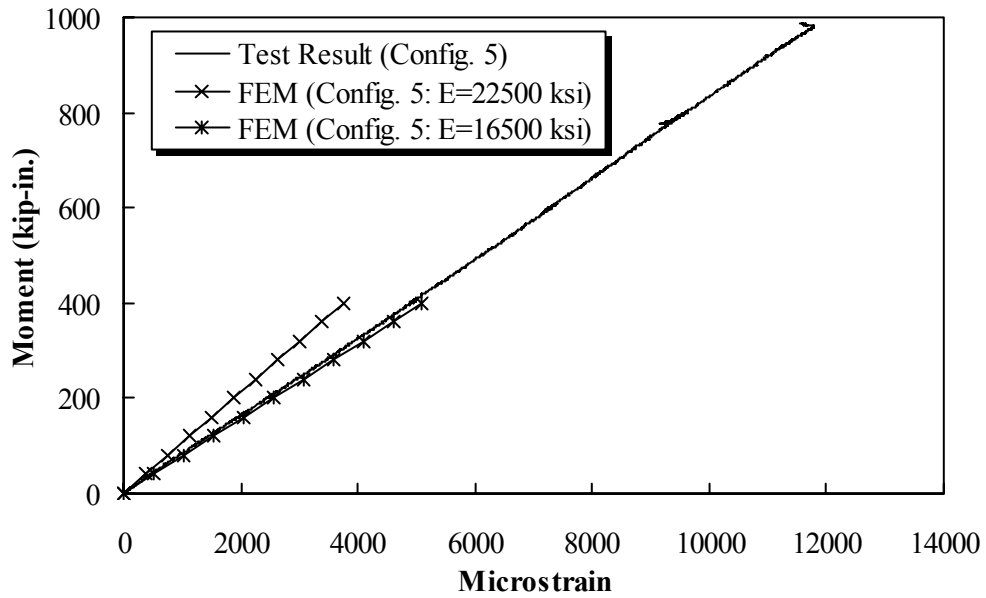


Figure 4.11 Applied Moment vs. CFRP Strain - Specimen 1-14

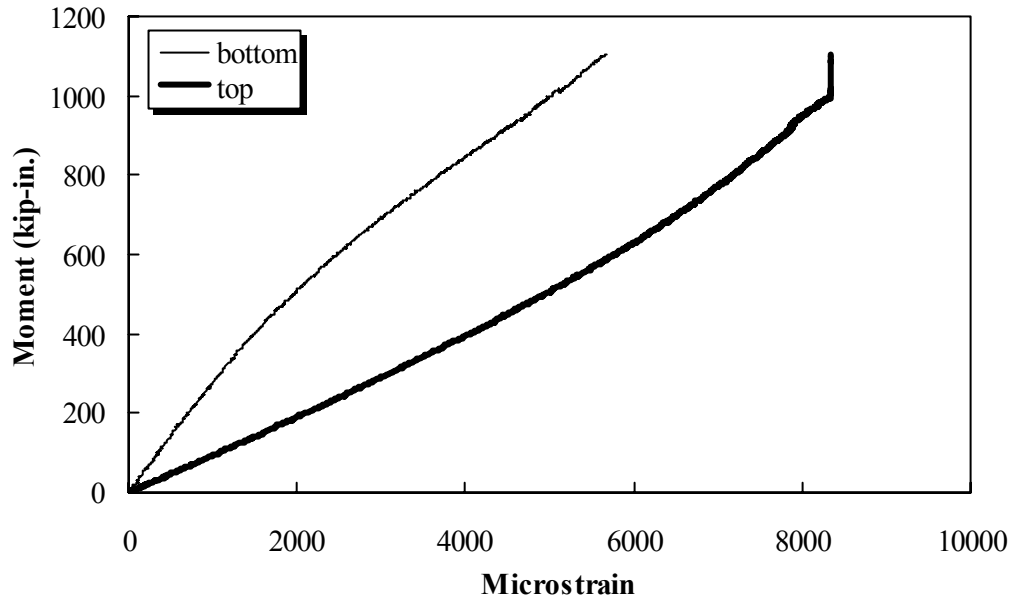


Figure 4.12 Applied Moment vs. CFRP Strain - Specimen 2-2

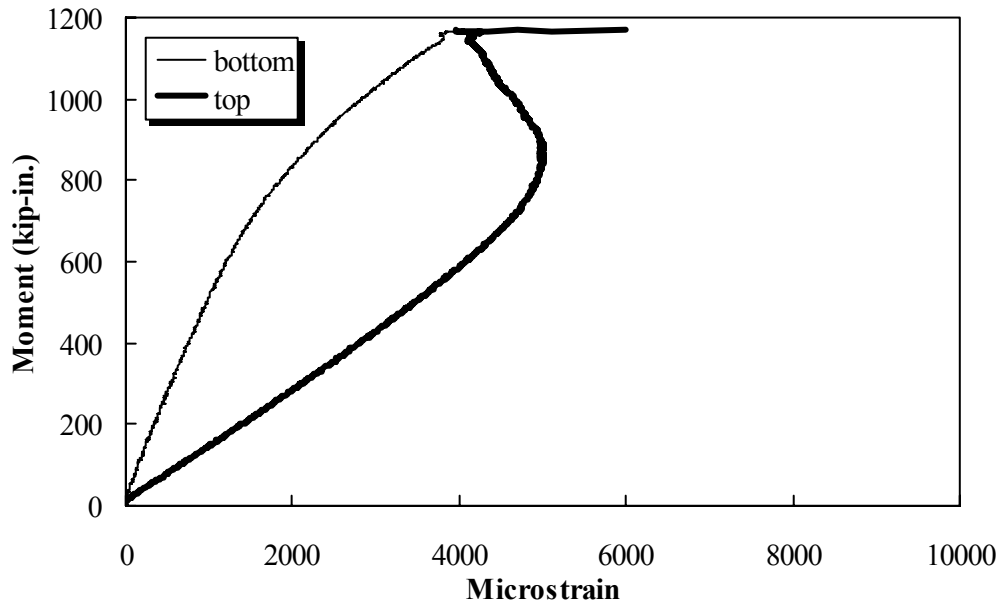


Figure 4.13 Applied Moment vs. CFRP Strain - Specimen 3-1

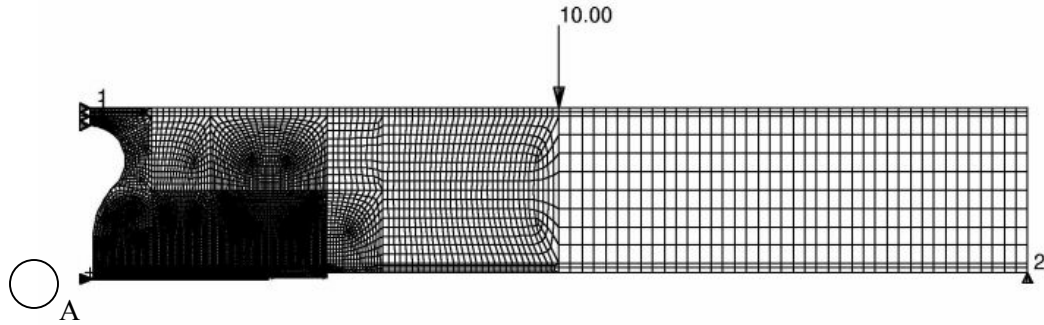


Figure 4.14 Computational Model of Specimen for Effective Bond Length Test

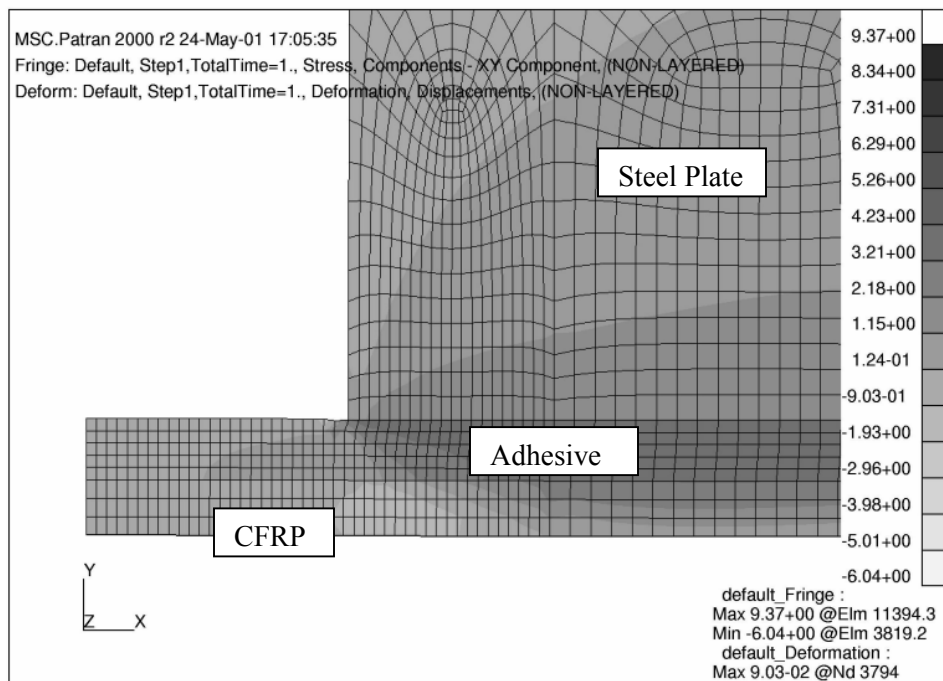


Figure 4.15 Detail of Circle A (Configuration 1)

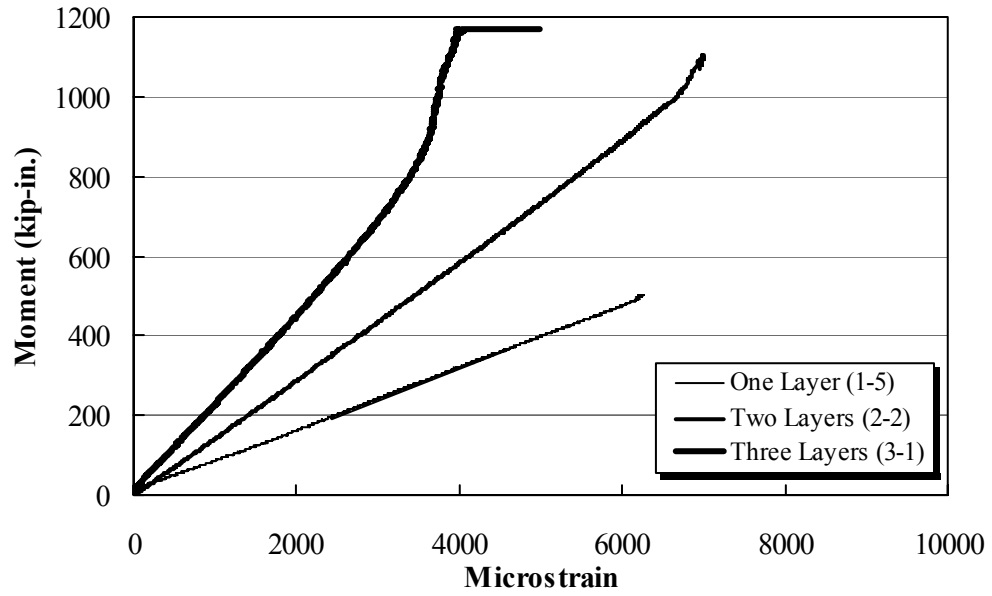
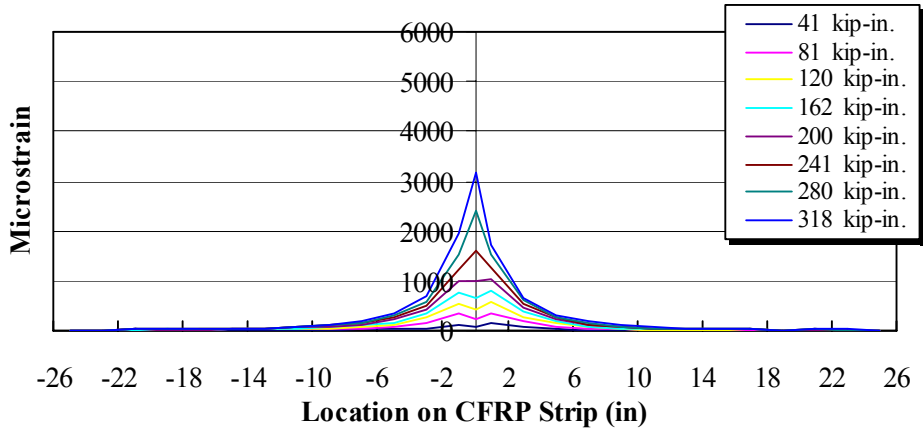
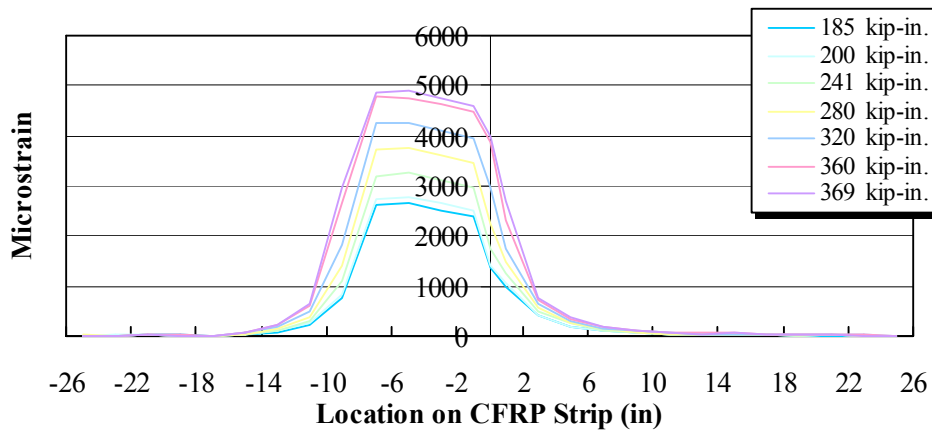


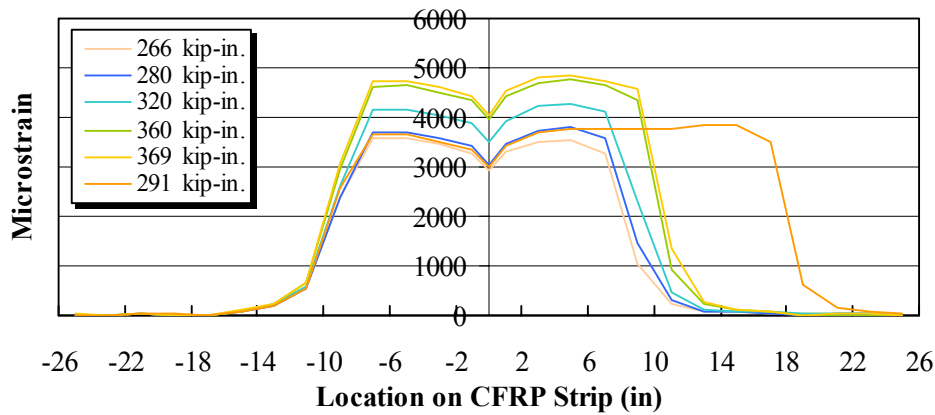
Figure 4.16 Comparison of Strain Gradient (same Strain at Bottom Surface)



a) Strain Distribution up to First Debonding



b) Strain Distribution up to Second Debonding



c) Strain Distribution up to the End of Experiment

Figure 4.17 Tensile Strain Distribution in Specimen 1-4

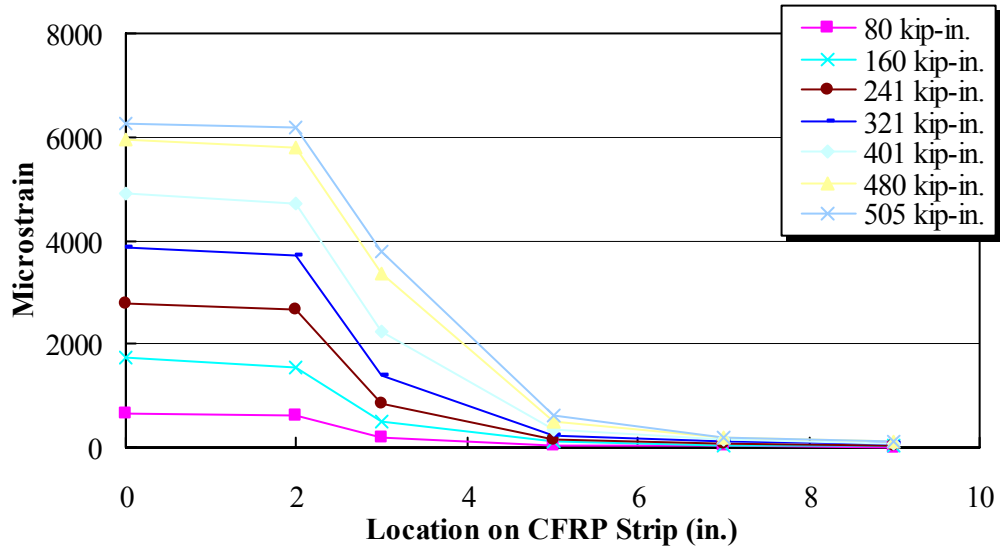


Figure 4.18 Tensile Strain Distribution in Specimen 1-8

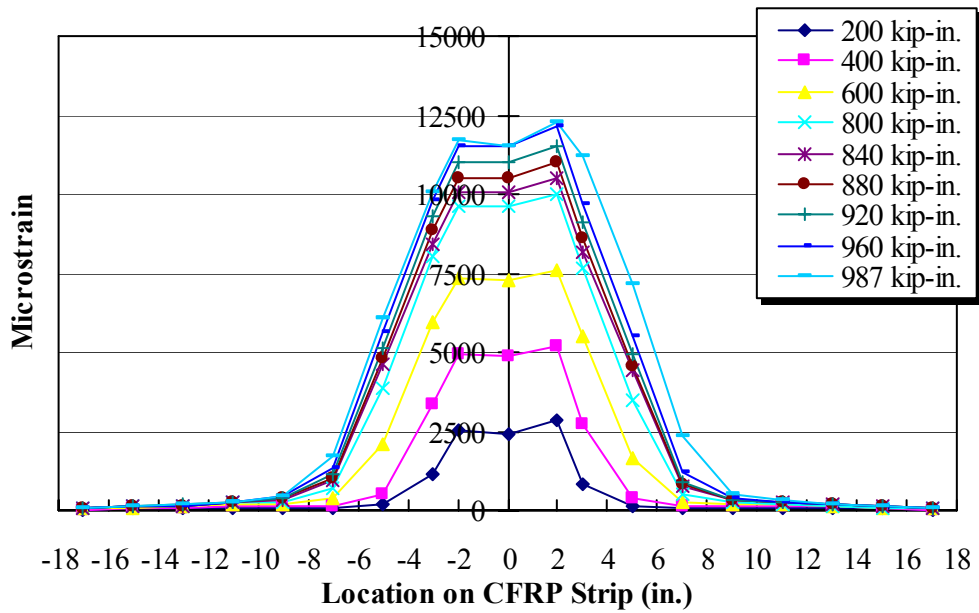


Figure 4.19 Tensile Strain Distribution in Specimen 1-14

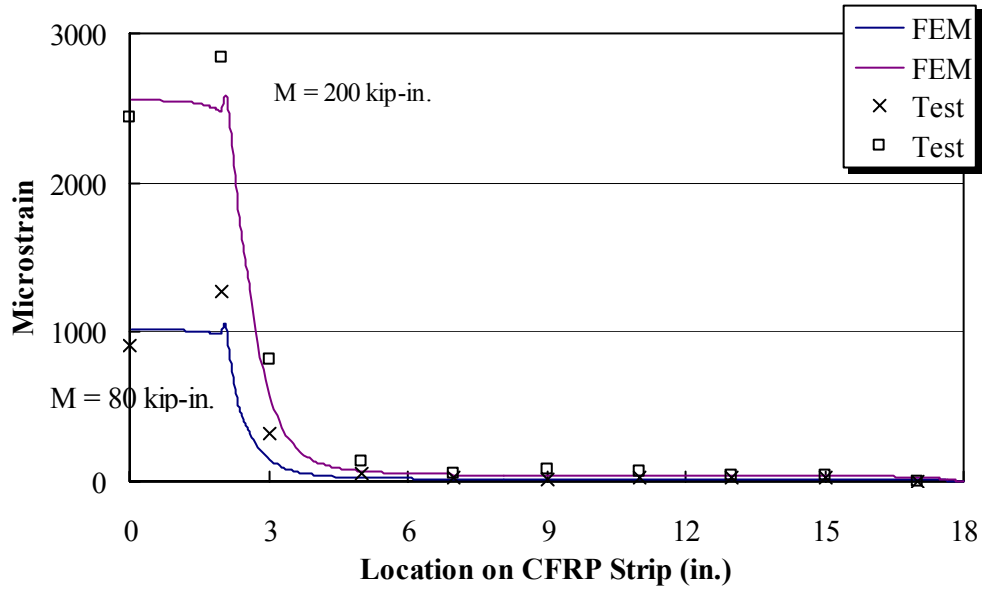


Figure 4.20 Comparison between FEM and Test Results for Specimen 1-14

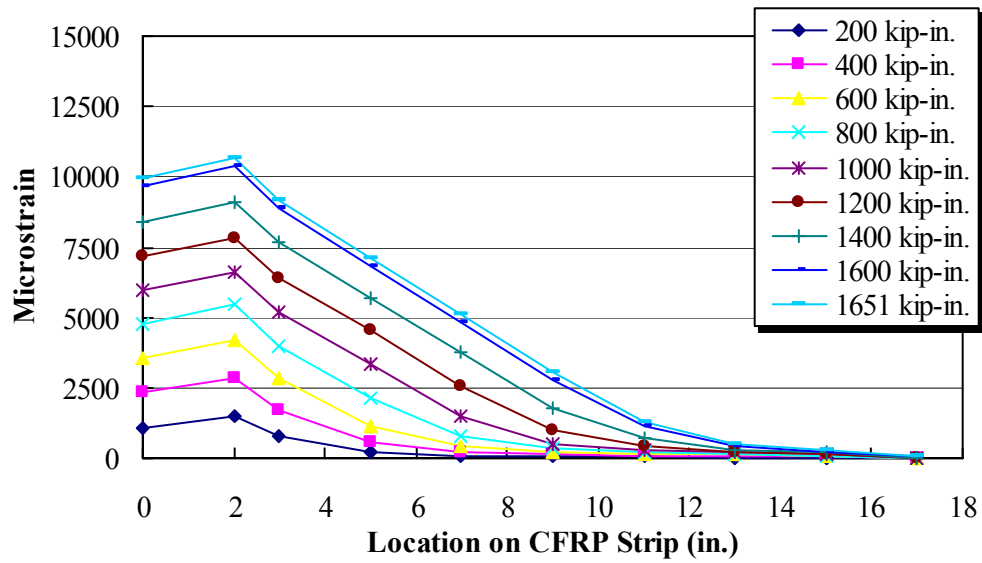


Figure 4.21 Tensile Strain Distribution in Specimen 2-3

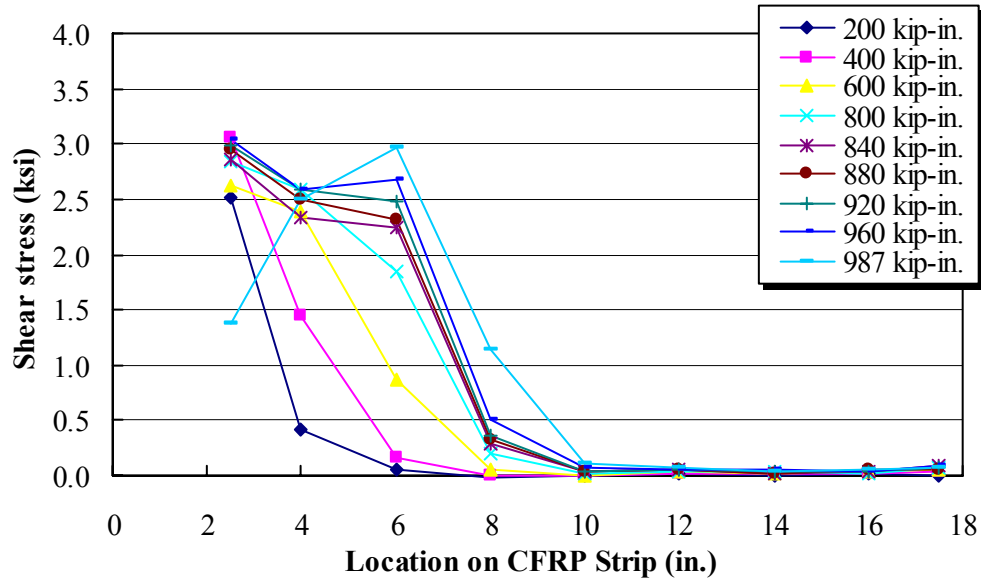


Figure 4.22 Shear Stress Distribution Based on Measured Strain in Specimen 1-14

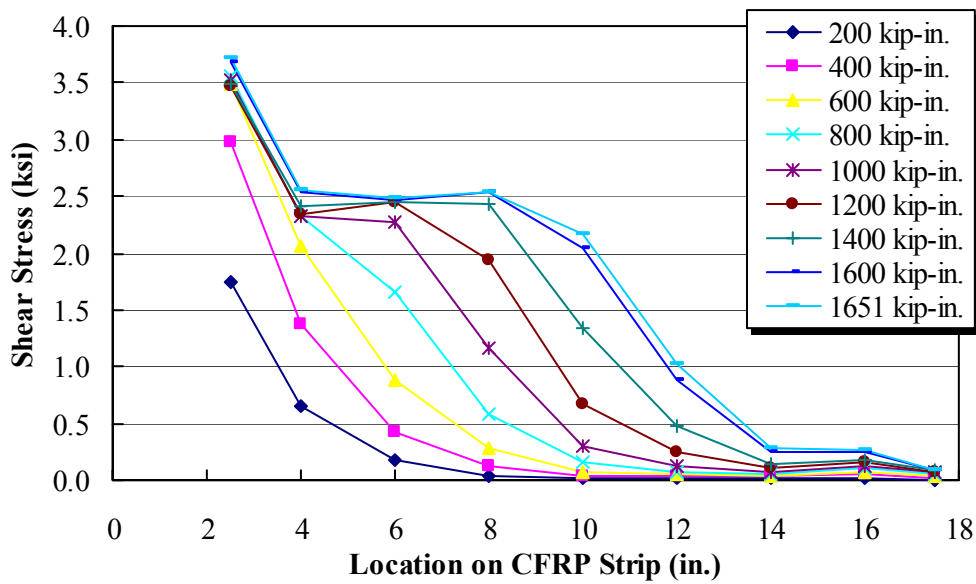


Figure 4.23 Shear Stress Distribution Based on Measured Strain in Specimen 2-3

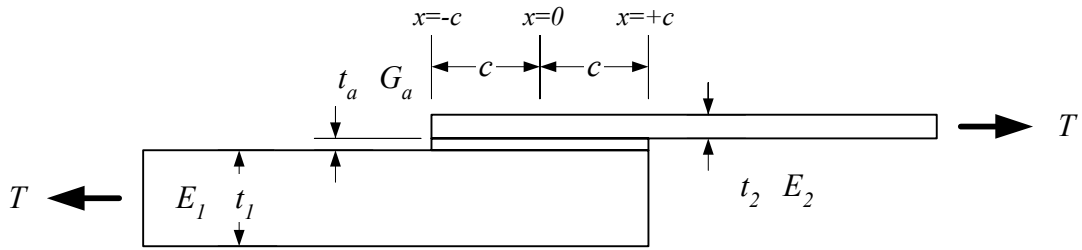


Figure 4.24 Dimension of Single-Lap Joint: Elastic Adhesive

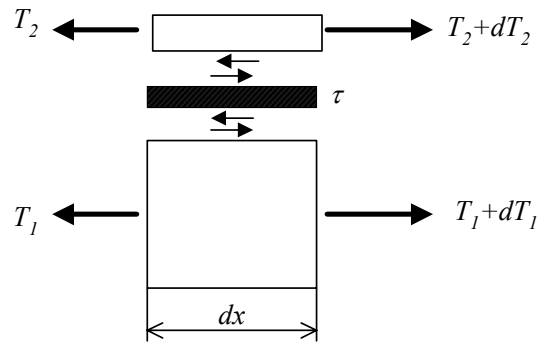


Figure 4.25 Simplified Free Body Diagram for Analytical Model

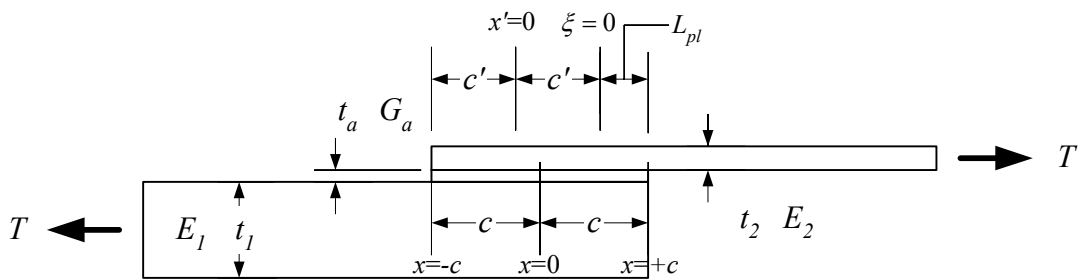


Figure 4.26 Dimension of Single-Lap Joint: Elastic-Plastic Adhesive

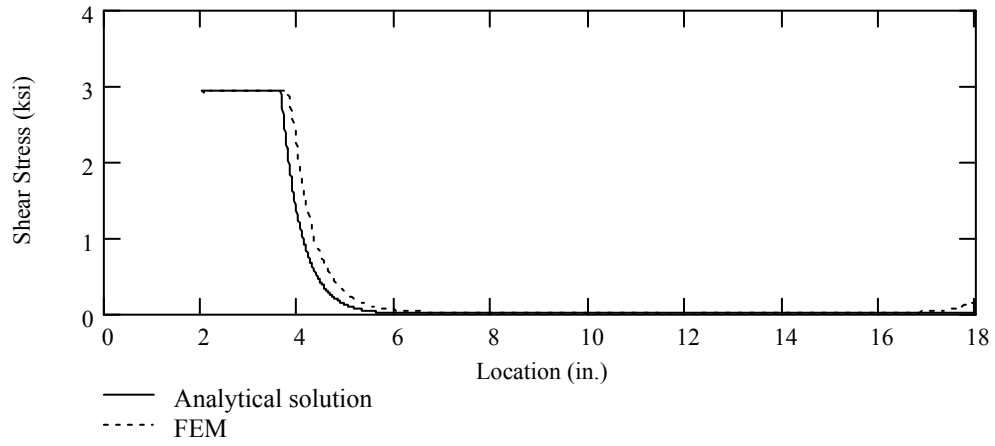


Figure 4.27 Shear Stress Distributions for Example Lap Joint

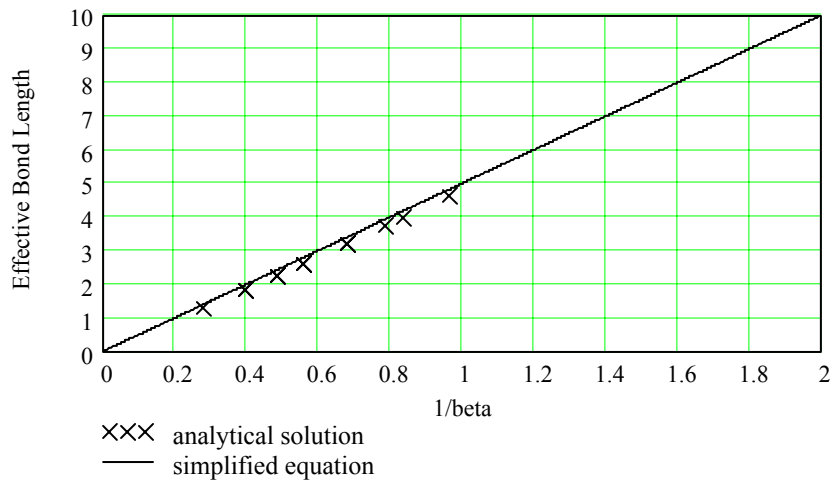


Figure 4.28 Effective Bond Length for Adhesive Elastic Region

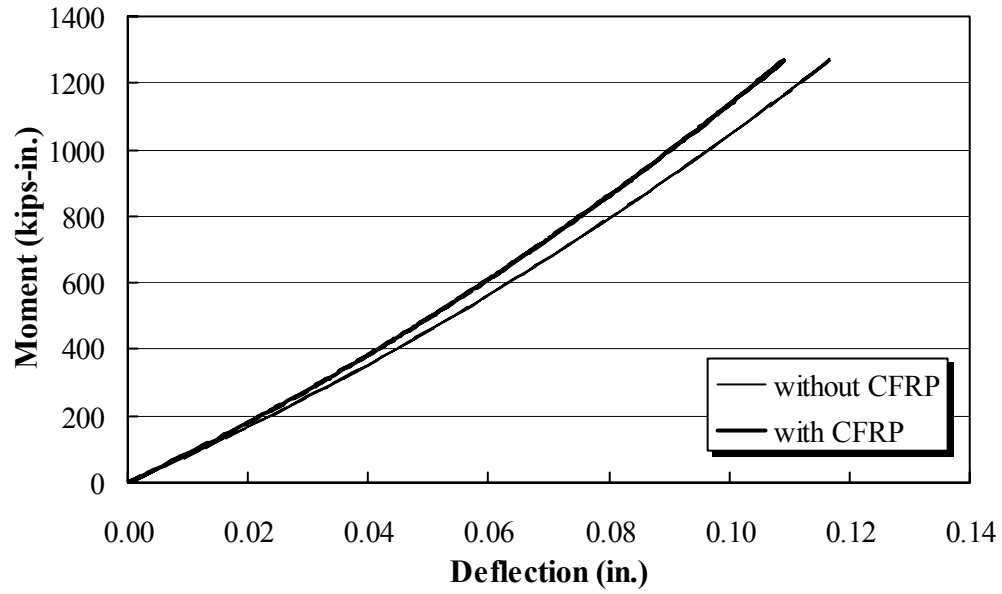


Figure 4.29 Moment-Deflection Curves with and without CFRP

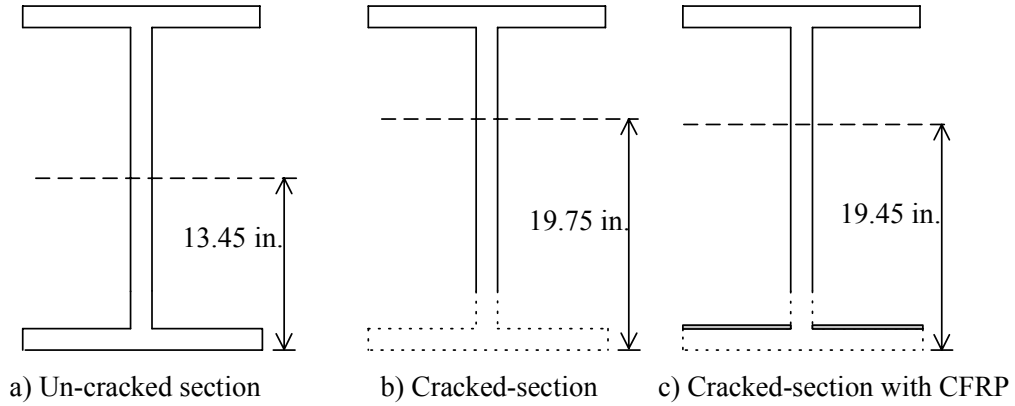


Figure 4.30 Sections and Locations of Neutral Axis

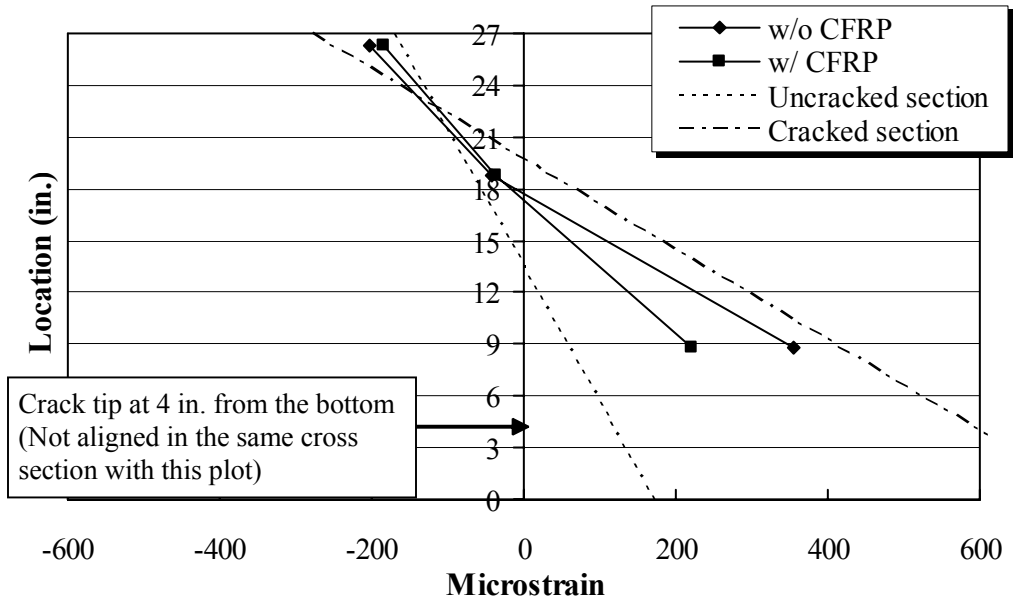


Figure 4.31 Strain Distributions in Cross Section at Center

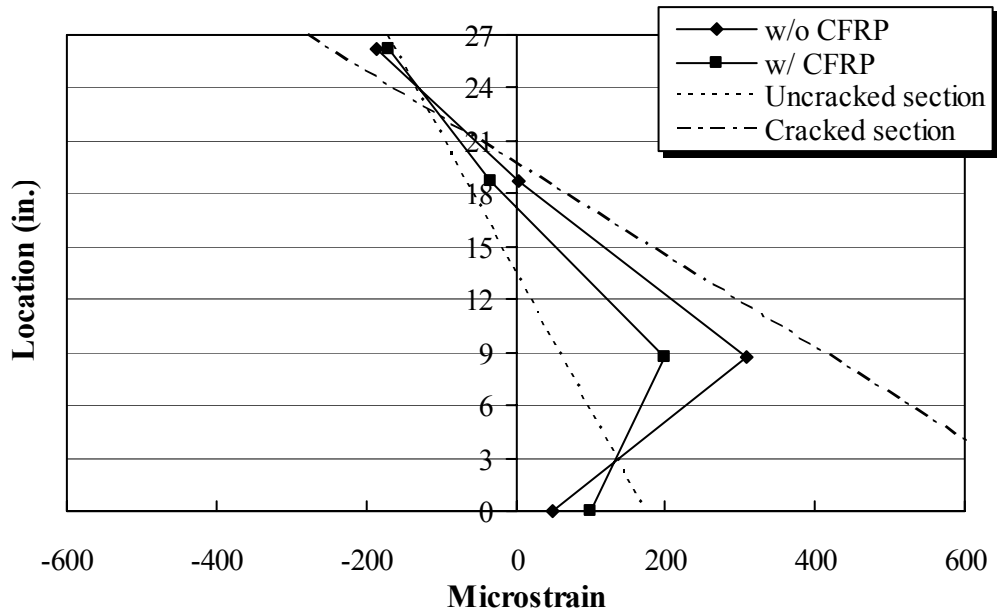


Figure 4.32 Strain Distributions in Cross Section at 10 in. from Center

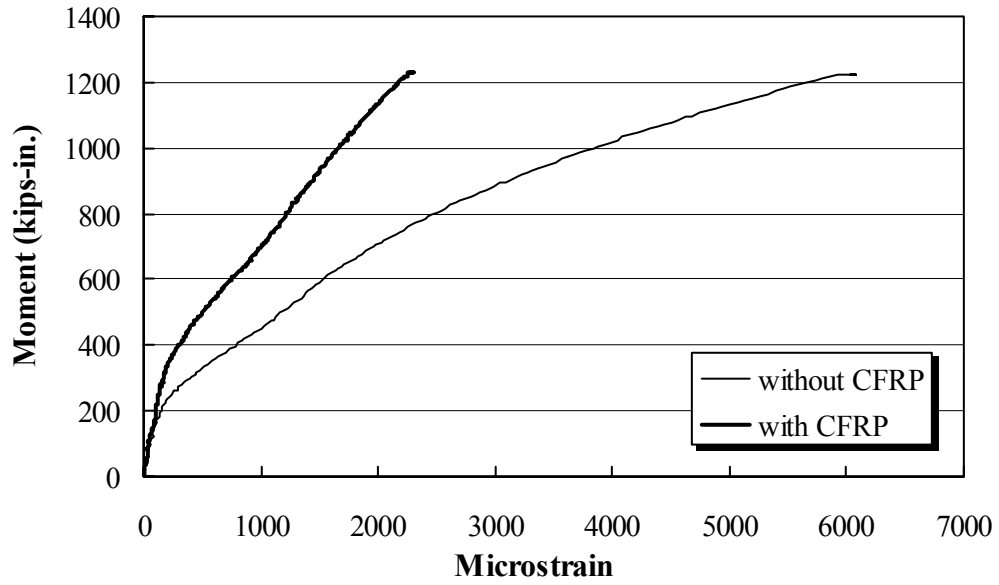


Figure 4.33 Strain Near Crack Tip with and without CFRP

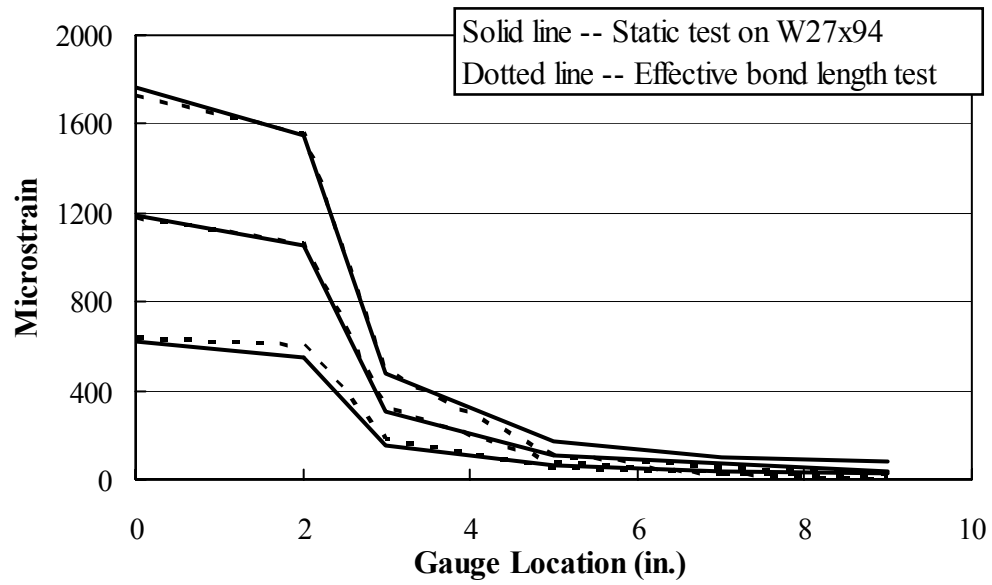


Figure 4.34 Tensile Strain Distribution in CFRP



Figure 4.35 Test Setup for Cyclic Loading Tests on W27x84



Figure 4.36 Welded Steel Plates for Initiating Crack



Figure 4.37 Specimen with Crack and Holes (NR-3)

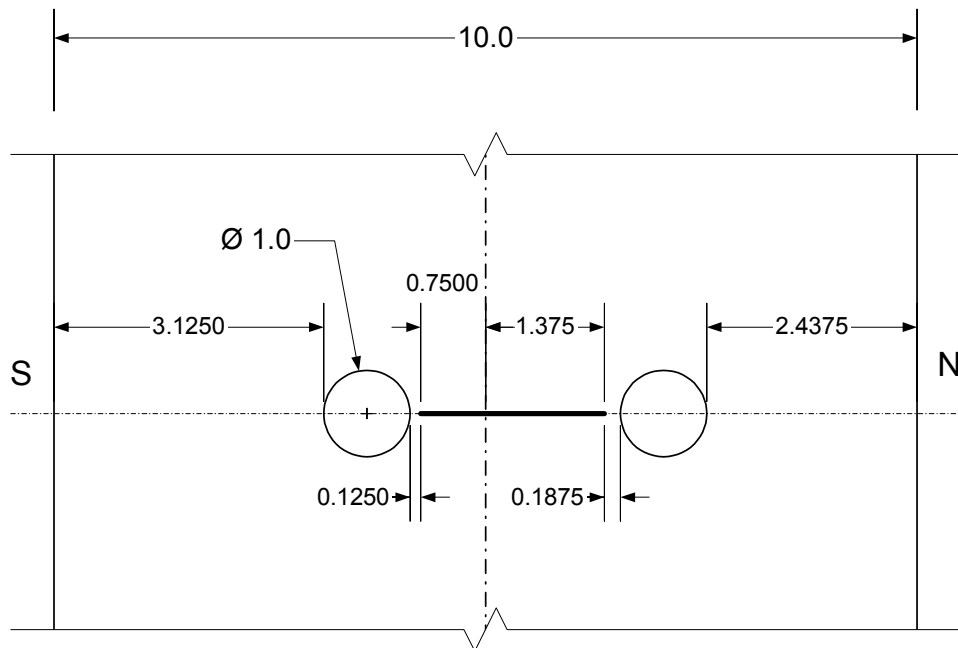


Figure 4.38 Sketch of Crack Length and Hole Locations (NR-3)



Figure 4.39 Crack Reached Inner Surface of Tension Flange

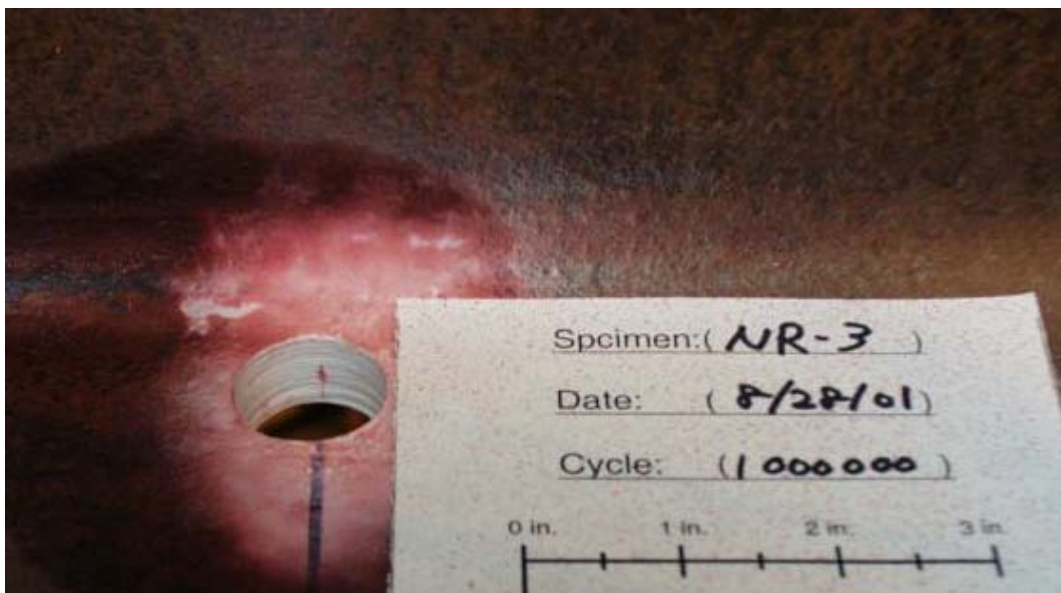


Figure 4.40 Crack Tip Growing through Thickness of Flange (NR-3)

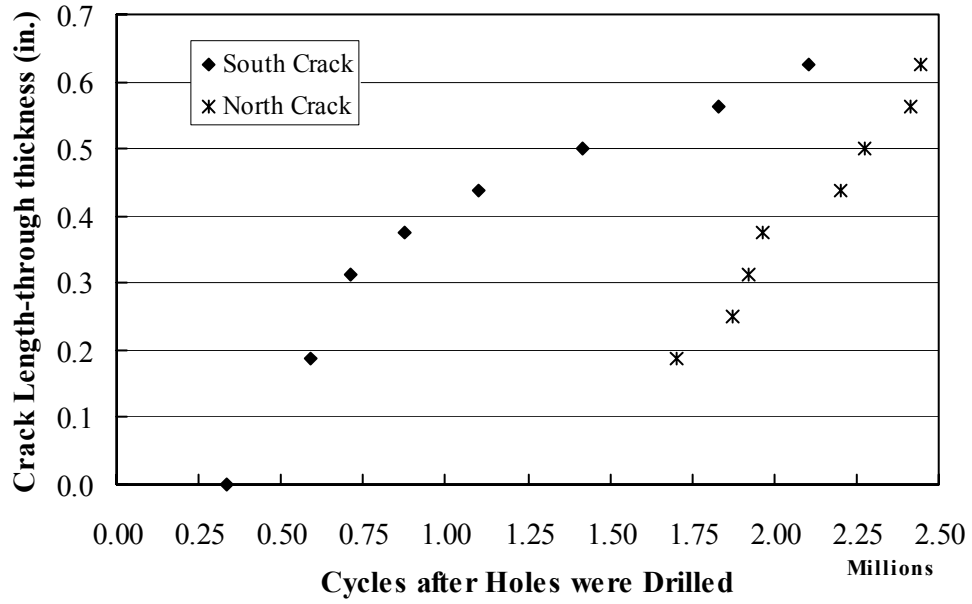


Figure 4.41 Crack Growth vs. Number of Cycles (NR-3)

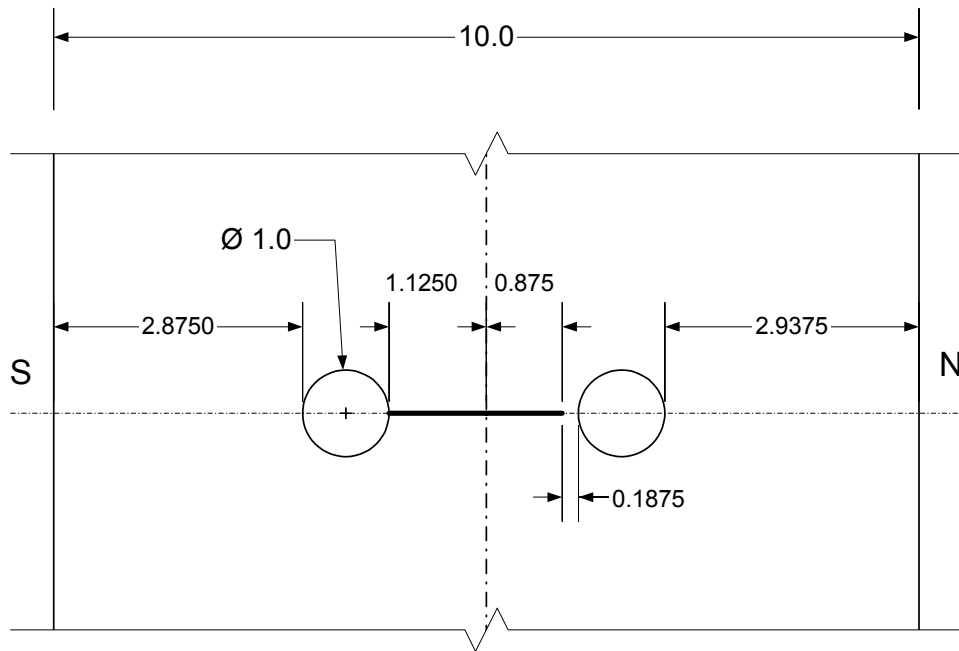


Figure 4.42 Sketch of Crack Length and Hole Locations (R-3-1)



Figure 4.43 Specimen with Crack and Holes (R-3-1)

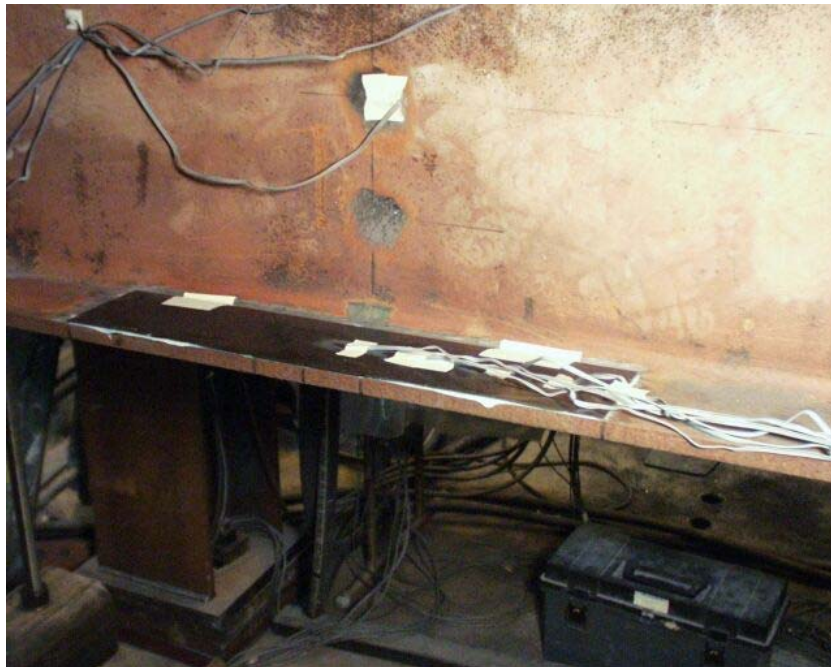


Figure 4.44 Rehabilitated Specimen with Bonded CFRP Strip

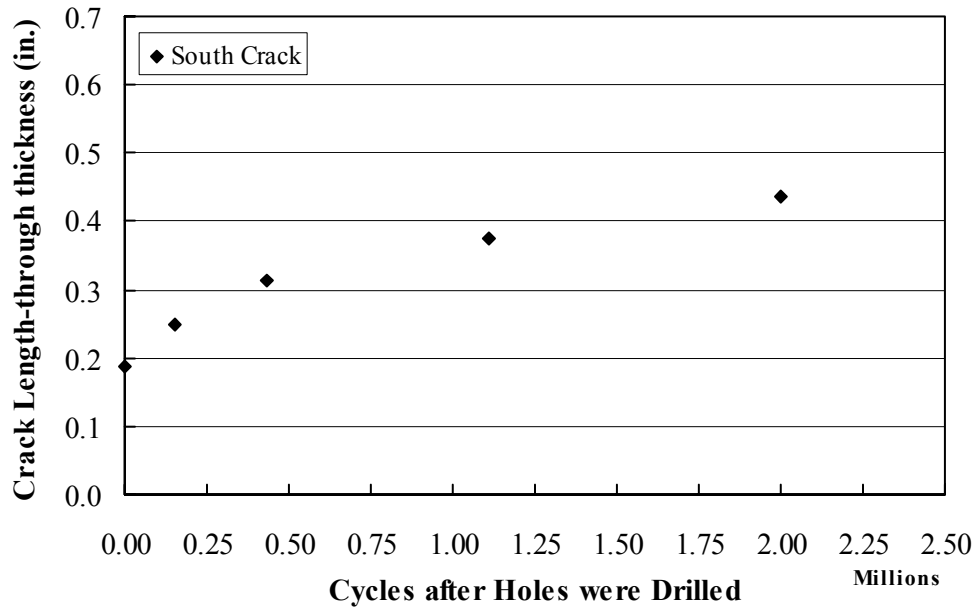


Figure 4.45 Crack Growth vs. Number of Cycles (R-3-1)

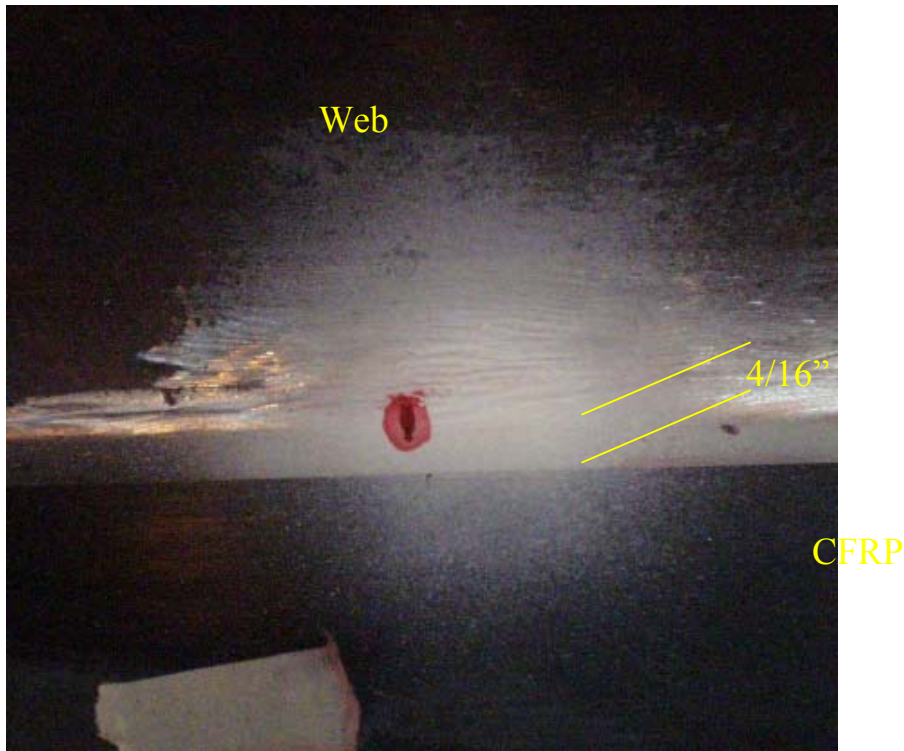


Figure 4.46 South Crack Reached Inner Surface of Tension Flange

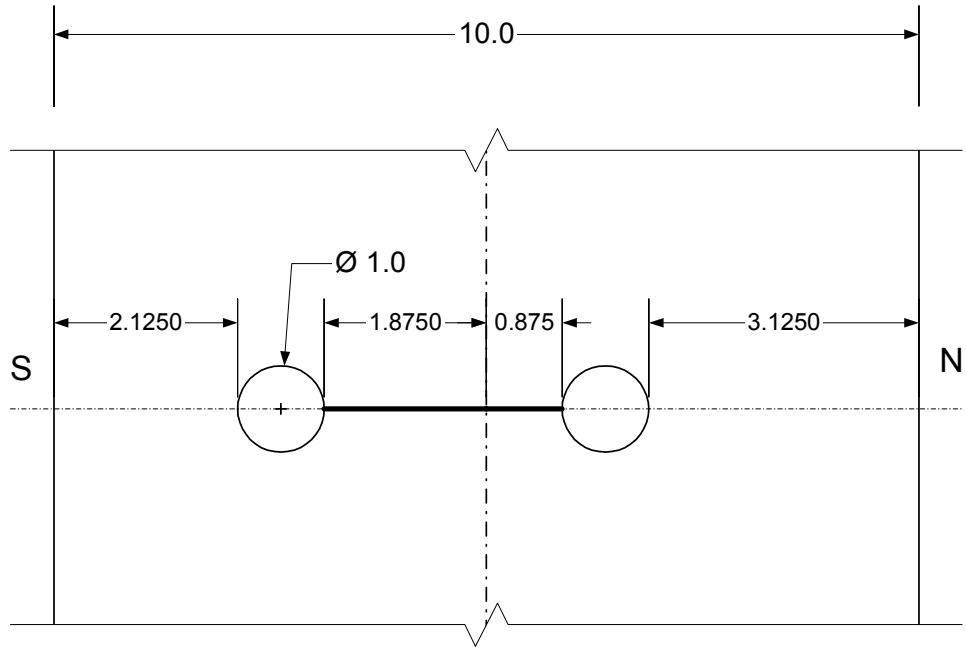


Figure 4.47 Sketch of Crack Length and Hole Locations (R-3-2)



Figure 4.48 Specimen with Crack and Holes (R-3-2)



Figure 4.49 Crack Tip in Web (R-3-2)

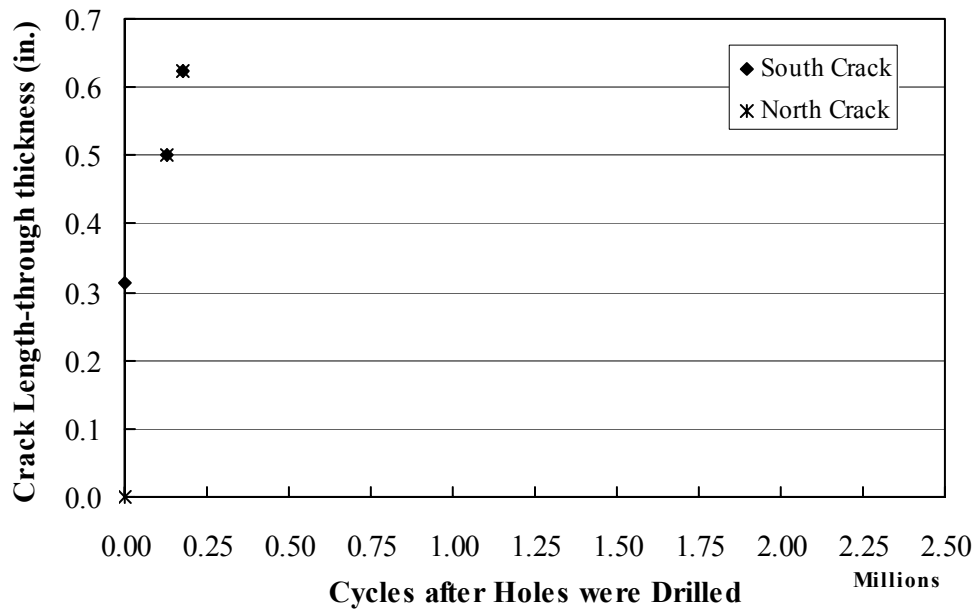


Figure 4.50 Crack Growth vs. Number of Cycles (R-3-2)

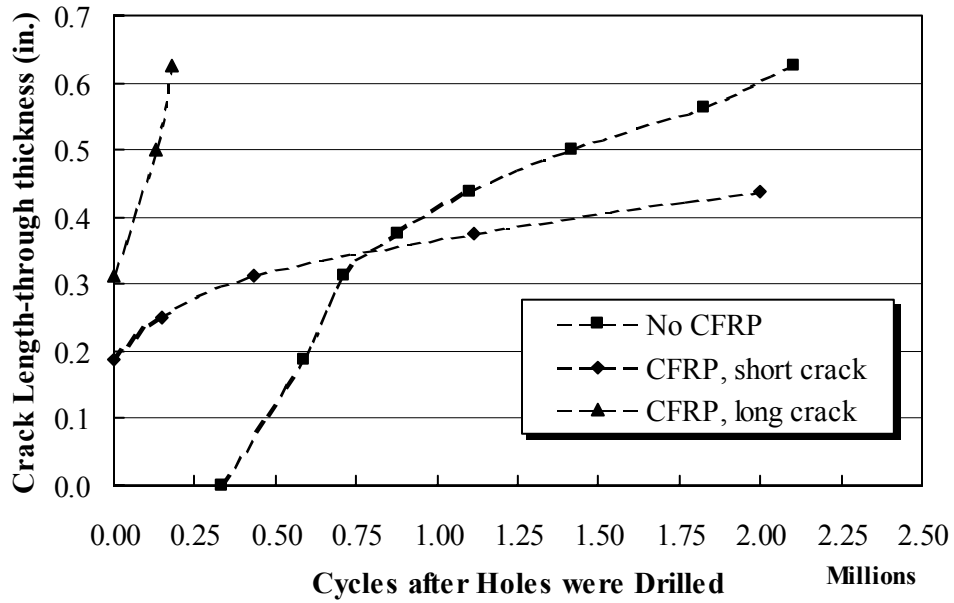


Figure 4.51 Comparison of Crack Growth vs. Number of Cycles

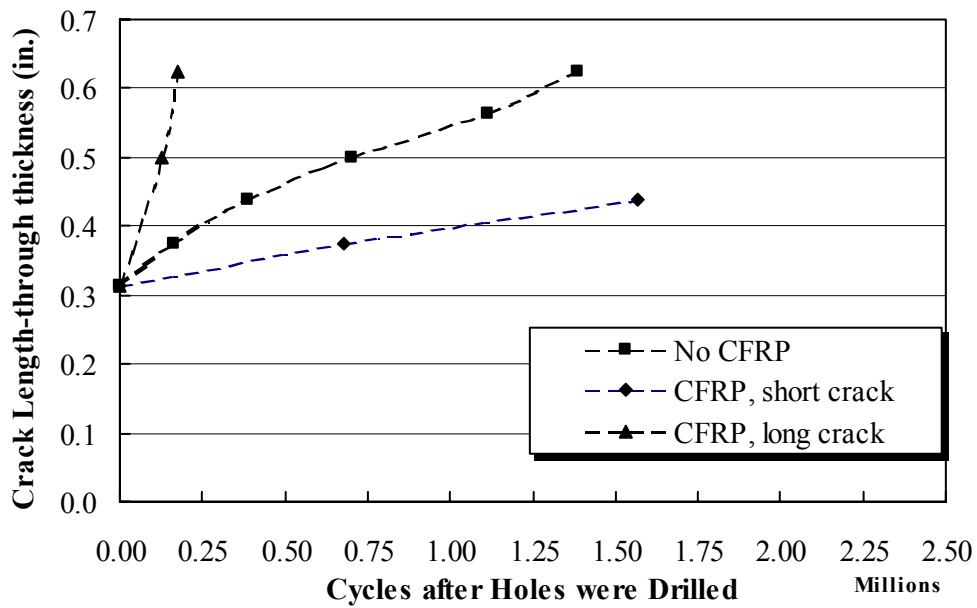


Figure 4.52 Comparison of Crack Growth vs. Number of Cycles - Modified

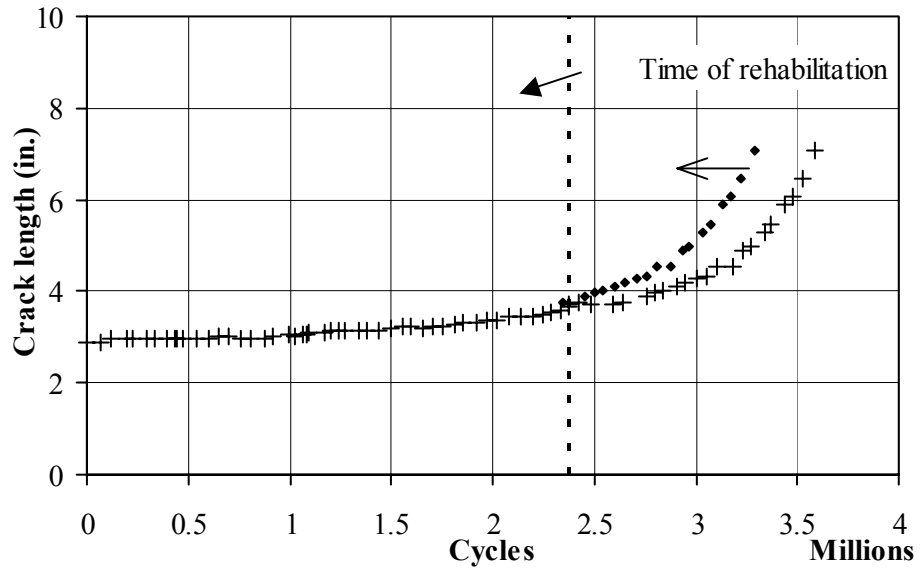


Figure 4. 53 Crack Growth vs. Number of Cycles (R-3-3)

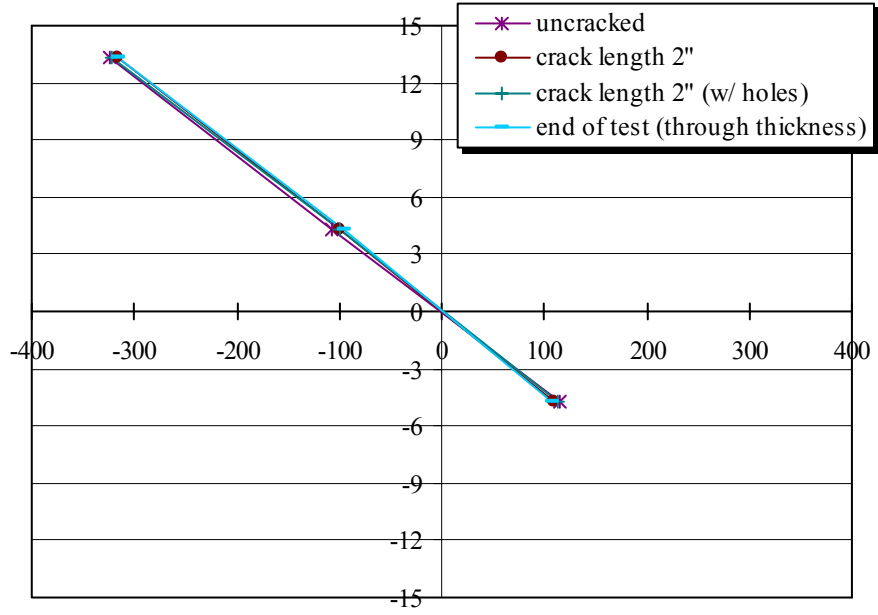


Figure 4.54 Strain Distribution in Section at Center (NR-3)

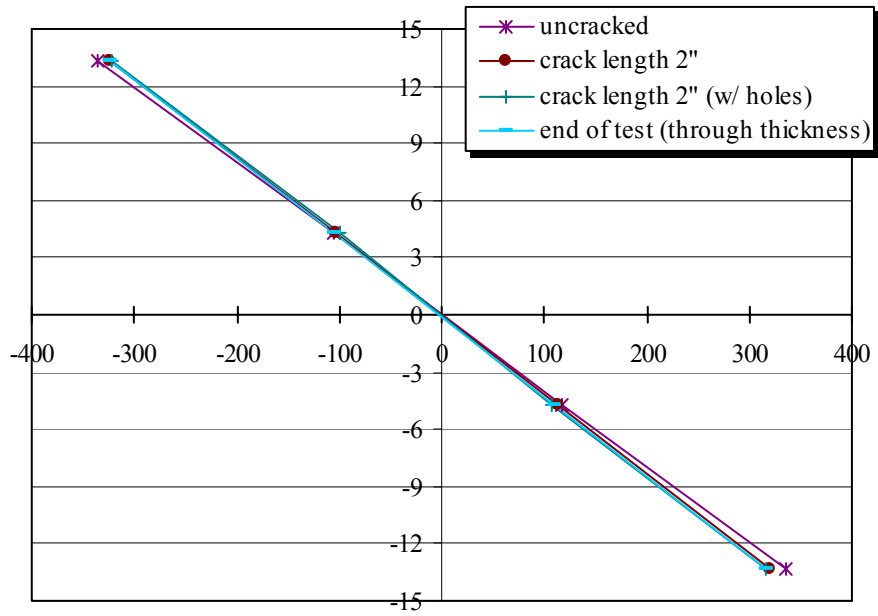


Figure 4.55 Strain Distribution in Section 20 in. from Center (NR-3)

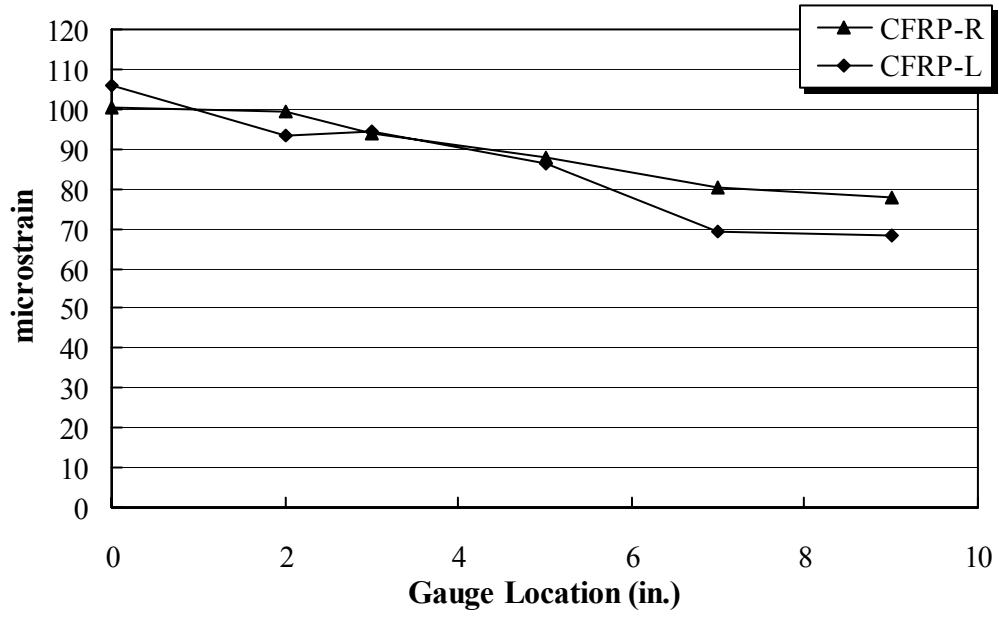


Figure 4.56 Strain Distribution in CFRP Strips (R-3-1) – 0 Cycles

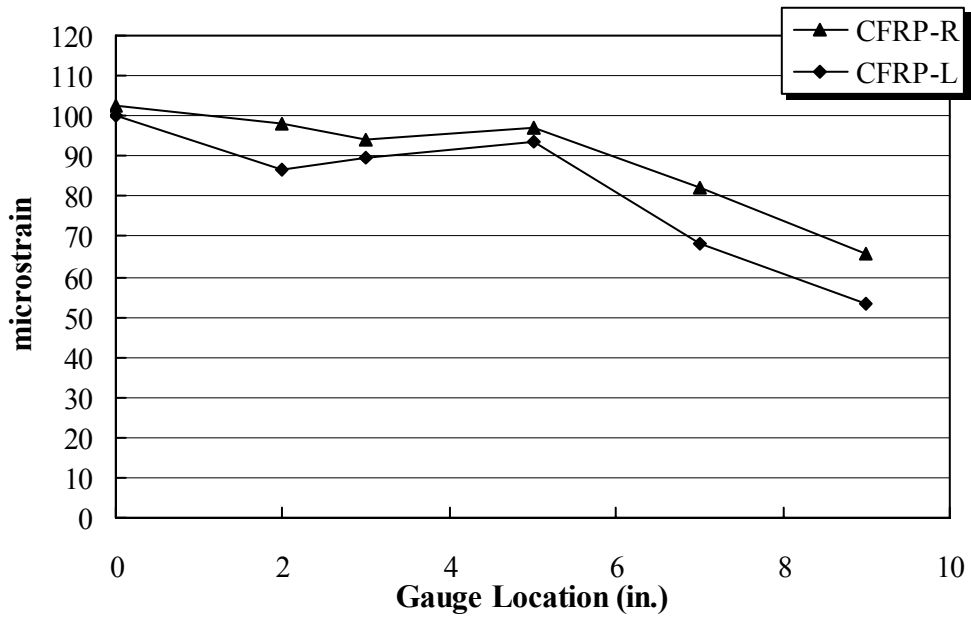


Figure 4.57 Strain Distribution in CFRP Strips (R-3-1) – After 2 Million Cycles

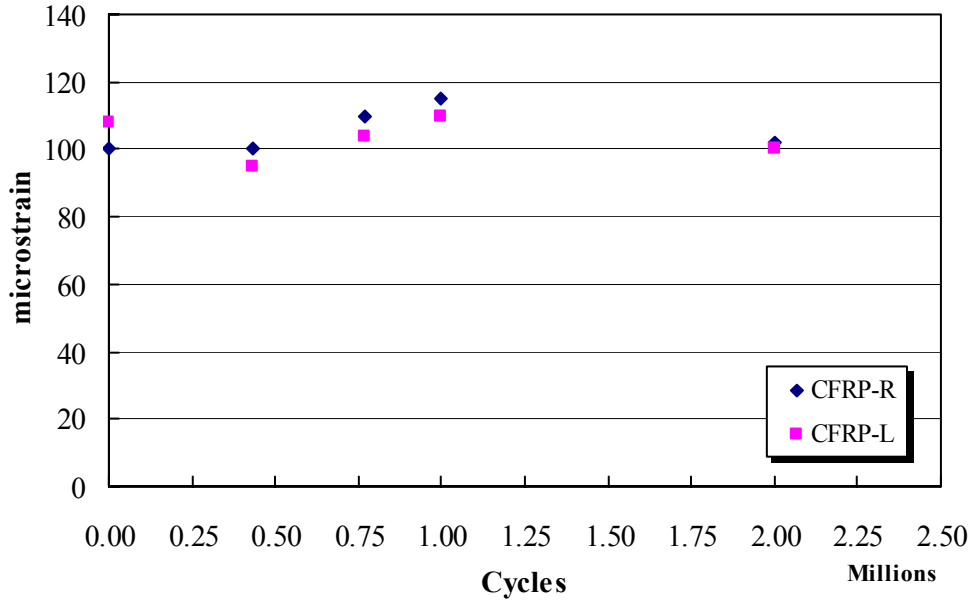


Figure 4.58 Change in Tensile Strain at Center of CFRP Strip (R-3-1)

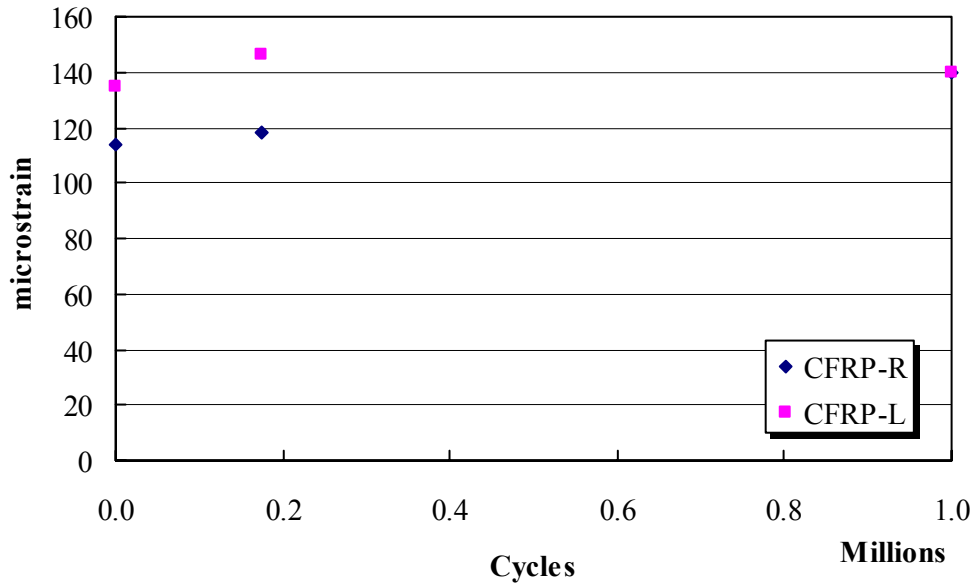


Figure 4.59 Change in Tensile Strain at Center of CFRP Strip (R-3-2)

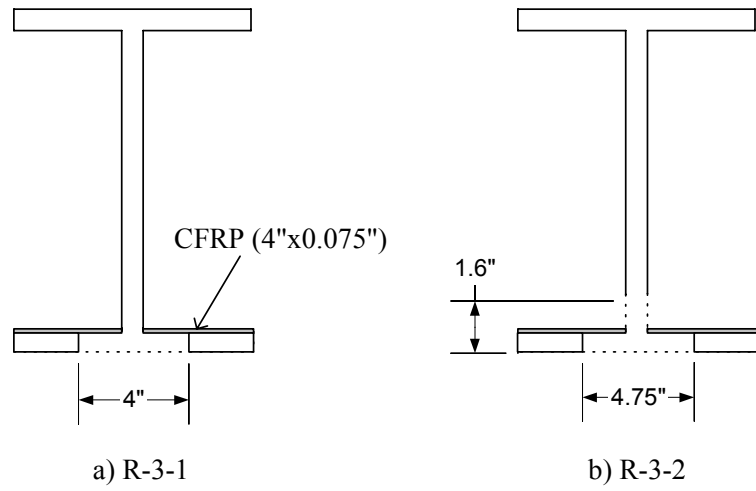


Figure 4.60 Idealized Composite Sections

Appendix A

Design of Specimen and Test Setup for Effective Bond Tests

Appendix A Design of Specimen and Test Setup for Effective Bond Length Tests

In order to investigate the strength of the bond between the steel and the CFRP, an appropriate test setup for this purpose needed to be developed. This appendix will present the design of the test setup and the specimen. Because the failure of the adhesive depends on the stress state in the adhesive, it was necessary to understand the stress distribution in the adhesive used for the rehabilitation of fatigued girders before designing the specimen for the experimental tests. In the first section, a prototype girder is analyzed using the finite element method in order to investigate the stress distributions in the adhesive layer used to bond CFRP strips on the tension flange. Then, the second section examines possible specimen configurations so that the specimen can reproduce the stress distributions that are close to that in the prototype girder.

A.1 Stress Analysis of the Prototype Girder

A.1.1 Prototype Girder

To investigate stresses acting on a rehabilitated fatigued steel girder, a prototype girder was selected and analyzed. By analyzing the stresses in the steel flange and the adhesive layer, it would be possible to design a test specimen that is able to reproduce similar stress distributions with those in the prototype girder. As shown in Figure A-1, the prototype girder was a W36×150 ($d = 35.85$ in., $t_w = 0.625$ in., $b_f = 11.975$ in., and $t_f = 0.94$ in. where, d , t_w , b_f , and t_f are the depth and thickness of the web, width of the flange, and thickness of the flange, respectively). The prototype girder represented a part of a two-span, composite continuous girder around an intermediate pier; the length of the girder ($L = 480$ in.) was taken as the length between two inflection points under a uniform load. This length was longer than the length of the cover plate (assumed as 240 in.); i.e., the location of the crack was within its span. For simplicity, however, a concentrated load was considered at the point of the pier instead of a uniform load, and the cover plate was ignored throughout the analyses. The effect of the cover plate at this location was insignificant due to the shear lag. Thus, it was reasonable to assume no cover plates in the prototype girder. The prototype girder had a crack in the tension flange at a distance of 120 in. from the intermediate pier. At the crack location, two CFRP strips, with a width of 4 in. and a

length of 10 in., were bonded onto the inner surface of the tension flange in symmetry with the web.

A.1.2 3D Model for the Prototype Girder

The stress distributions in the adhesive were analyzed using ABAQUS, a commercial finite element analysis program. Due to the complexity of the stress distributions around the crack, the prototype girder with a crack through the tension flange was modeled in three-dimensions as illustrated in Figure A-2. The figure for the computational model is shown upside down with respect to Figure A-1. Figure A-3 shows a magnified view of a part of the tension flange around the crack with the bonded CFRP strip. In this analysis, a quarter of the prototype girder was modeled due to the symmetry, and the concentrated load was applied to the point of the pier, i.e., the left edge of the model. The boundary condition representing the simple support was introduced at the right bottom edge of the model, and the boundary conditions for symmetry were introduced at the left end and the web (the back surface in the figure). Isoparametric 8-node brick elements were used for all elements; the adhesive layer, 0.06 in. thick, was divided into three layers of elements, while the CFRP layer, 0.054 in. thick, was divided into two layers. Because of the stress concentrations at the edges of the adhesive, the elements in the regions of the high stress concentration were refined to be small compared to the other elements. The number of elements was 240,704 and the element size was on the order of a hundredth of inch in the area of high refinement. The analyses were both materially and geometrically nonlinear; an elastic-perfectly plastic relationship was implemented for the stress-strain curve for the steel and adhesive. Material properties used in the analysis were: $E_s = 29,000$ ksi, $E_c = 23,900$ ksi, and $E_a = 650$ ksi (where, E_s , E_c , E_a are Young's modulus for the steel, CFRP strip, and adhesive, respectively), and $\nu_s = 0.3$, $\nu_c = 0.3$, $\nu_a = 0.4$ (where, ν_s , ν_c , and ν_a are Poisson's ratios for steel, CFRP strip, and adhesive, respectively). The yield strength of steel and adhesive, and the ultimate strength of CFRP strip were 50 ksi, 6 ksi, and 406 ksi, respectively. It should be noted that because Poisson's ratios of the CFRP strip and adhesive used in this research were not specified by the manufacturer, these values were estimated based on values that had been used in the analyses by other researchers. An 80 kip concentrated load was applied at the center of the prototype girder; this caused approximately 10 ksi nominal stress at the bottom and top flanges. In the analysis model, the load was distributed to 3 nodes through the web thickness with the

ratio of 1:2:1 by considering the area around each node; thus, 10 kips per each node in the quarter size model was specified.

A.1.3 Results from 3D analysis

Before analyzing the 3D model with the bonded CFRP strip, the bare steel girder with a crack through the flange was analyzed. The peeling stress, σ_z and the shear stress, τ_{zx} distribution near the crack are shown in Figure A-4 and Figure A-5. In addition, Figure A-6 shows a plot of the shear and peeling stresses along the web-flange intersection. The location in the x direction was measured from the location of the crack, increasing toward the support. It can be seen from the plot that the shear stress decays slowly while the peeling stress is concentrated at the location of the crack and decays rapidly. Similar figures were obtained for the prototype girder with the crack and the bonded CFRP strip as shown in Figure A-7 through Figure A-9. As can be seen from these figures, the shear stress was reduced because of the bonded CFRP strip. The peeling stress far from the crack increased in compression while the peeling stress increased in tension near the crack. This stress distribution indicates the bending effect on the flange caused by the change of the neutral axis from the tension flange to the CFRP strip. The moment in the tension flange makes the tension flange bend so that the tension flange at the crack is separated from the web; however, the web prevents the flange from bending, causing the peeling stress in tension near the crack and in compression slightly away from the crack at the intersection between the flange and the web.

To design a specimen model, it was necessary to compare the results between the prototype and possible specimen models. For this purpose, the shear stress and the peeling stress distributions were chosen because these stresses were thought to be critical for the failure of the adhesive. Figure A-10 shows the shear stress distribution in the adhesive layer; data are taken from elements that were nearest to the CFRP strip. The peeling stress distribution is shown in Figure A-11. It should be noted that these plots are corresponding to 30%, i.e., about 3 kips at each node, of the total load that is a 80 kip for the prototype girder (10 kips per node). At 10 kips per node, a part of the adhesive layer had already yielded. However, for comparison with the specimen model, the stress distribution before the yielding of the adhesive was selected due to the unknown behavior of the adhesive after yielding at this time. The vertical axis indicates the magnitude of the stresses in ksi; the x -axis indicates a distance from the location of the crack,

increasing toward the support. The y -axis is a distance from the center of the adhesive layer along the width direction. As expected, both stresses are at their maximums at the crack, and decrease toward the center between the crack and the end of the CFRP strip; then, both stresses again slightly increase at the ends of the adhesive. Both the shear and the peeling stresses slightly increased toward the both side edges of strip, indicating that the edge effect.

A.2 Stress Analysis on Specimen Models

A.2.1 Modification of the Single-Lap Type Specimen

In the last section, it was discovered that the web plate prevents the fatigued tension flange with the bonded CFRP strips from bending. However, this restraint on deformation of the adherends cannot be simulated by the single-lap specimen. Therefore, the single-lap specimen needed to be modified in order to reduce the deformation of the specimen; and three ways of the modification were considered as illustrated in Figure A-12. In the first model (model 1), the thickness of the steel plate was increased at the end where the load was applied in order to align the applied load, P , with the center of the CFRP strip. In the second (model 2) and the third (model 3) models, additional restraints were applied to prevent the large rotation of the specimen; i.e., the vertical displacement was fixed along the bottom surface of the steel plate in the second model and at the lower right corner for the third model. The same magnitude of a tensile load, $P = 5$ kips, was applied to all three models. Each steel plate was 9 in. in length and 0.5 in. in thickness. The overlap length was 5 in., which was the same as in the prototype girder. The thicknesses of the adhesive layer and the CFRP strip were 0.06 in. and 0.054 in., respectively. The number of elements through the thickness is three for both the adhesive and the CFRP strip, and 156 elements in length (5 in.). The width of the analytical model was 1 in. for all materials, and plane-strain condition was assumed. Material properties used in the analysis were the same as those indicated in the analysis of the prototype girder; four-node isoparametric elements were used for all elements in this analysis. Analyses were geometrically nonlinear and materially nonlinear; an elastic-perfectly plastic stress-strain curve was used for the adhesive.

The shear and peeling stress distributions in the adhesive for these three models are shown in Figure A-13 and Figure A-14, respectively. Both figures also show the stress

distributions in the adhesive obtained from the prototype at the center of the strip width. In order to draw these results on one figure, the results from the analysis models (model 1 to model 3) were modified so that the tensile load (in x -axis) at the center of the CFRP strips in both width and length was the same for all results. The magnitude of the stresses near the crack is almost the same for all three models, while there are significant differences at the far-end of the strip. This is because the magnitude of the shear stress mainly depends on the difference in the longitudinal strains in the adherends. At the crack ($x = 0$ in.), there is no longitudinal strain in the steel plate while strain exists in the CFRP strip, and its magnitude is directly related to the total load in the CFRP strip. Because the applied loads for all models are the same, the tensile stresses in the CFRP strips are expected to be close to each other, resulting in similar magnitude in the shear stresses at the crack. At the other end of the CFRP strip ($x = 5.0$ in.), the tensile stress exists in the steel plate, while no tensile stress exists in the CFRP strip. The tensile stress in the steel plate will vary with its shape and boundary conditions because the bending moment in the steel plate affects the tension stress at the top fiber of the steel plate. Considering the boundary condition of the model 2, there is no bending deformation; thus, no increase in the tensile stress is expected, resulting in the minimum shear stress among these three models as shown in the figure. As can be seen in the figures, the stress distributions of these three models are very comparable to the stress distribution of the prototype girder near the crack.

A.2.2 Effect of Steel Plate Thickness on Stress Distributions

Although the results from all three models were similar, model 1 was chosen for further study because the boundary conditions for the other two models were deemed difficult to achieve in the laboratory. Because the thickness of the CFRP strip and the adhesive layer were already defined by the manufacturer, only the thickness of the steel plate was varied, and the effect on stress distribution was investigated. Two additional thicknesses were analyzed, and the results are illustrated in Figure A-15. The results with $t = 0.5$ in. are the same results shown in Figure A-13. The results from the prototype girder are also shown in these figures. Similar to the case with the different models, all three results show almost the same magnitude near the location of the crack while there are differences at the far end of the CFRP strip. This indicates that making the steel plate thicker does not change the stress distribution around the crack significantly, but it does reduce the shear and peeling stress at the other end.

Figure A-16 shows the normal stress distribution in model 1 with the steel plate thickness of 1.0 in. It should be noted that these stress distributions are not modified as was done for Figure A-13 to Figure A-15; thus, the stress distributions in Figure A-16 corresponds to an applied load of 5 kips. The maximum tensile stress in the adherend is 25 ksi as can be seen in the figure. Stresses at the same location in Figure A-16 corresponding to the steel plate thicknesses of 0.75 in. and 0.5 in. are 35 and 50 ksi, respectively; the tension stress in the steel plate decreases as the thickness increases. Comparing the applied load, 5 kips per unit width, and the strength of the CFRP strip, 22 kips per unit width, the tensile stress at this location in the steel adherend would be beyond the yield strength of the steel, which is assumed to be 50 ksi, before the failure of the CFRP strip. Because the yielding of the adherends alters the stress distribution in the adhesive significantly, and because it is desirable to have failure in the adhesive but not in the adherends, this type of specimen could not be used for the experimental tests.

A.2.3 Final Specimen Model and Stress Distributions in the Adhesive Layer

The problem with single-lap joint specimens was related to the bending effect of the adherents, resulting in the large tensile stress. In order to prevent this problem, it was required to increase the bending stiffness of the adherends; this could be done either by increasing the thickness of the steel plate further, or by modifying the specimen configuration. Although altering the thickness of the steel plate would be simple, this would have resulted in a heavy, expensive specimens. Thus, the lap-shear joint specimen was further modified by bolting the specimen to the flange of a steel girder as shown in Figure 4.14. By connecting the specimen to the girder flange, the bending stiffness of the specimen was increased while maintaining the thickness of the steel plates. In addition to eliminating the problem in the adherend, the proposed specimen and test setup enable the reuse of the steel plates of the specimen by allowing the removal of the CFRP strip and adhesive after each test. The details of a typical computational model is discussed in Section 4.1.2.1.

The shear stress distribution of the specimen model was taken from the elements near the CFRP strip and compared to that of the prototype girder in Figure A-17. Two models were compared at the load that gave similar average tensile stresses in the CFRP strip; average tensile stresses in the CFRP strip were 33.2 ksi and 31.8 ksi for 3D model and specimen model,

respectively, as shown in the figure. Although the shear stress at the crack in the specimen model is larger near the crack, indicating that the specimen model gives conservative results, the specimen model seemed to be able to represent the stress distributions in the prototype girder with sufficient accuracy. In particular, the effective bond length, a distance between the location of the crack and the point of near zero stress, is almost identical in both results. Thus, this specimen configuration and test setup seemed possible to be used for the bond strength test for the application considered in this report, the rehabilitation of the fatigued steel girder.

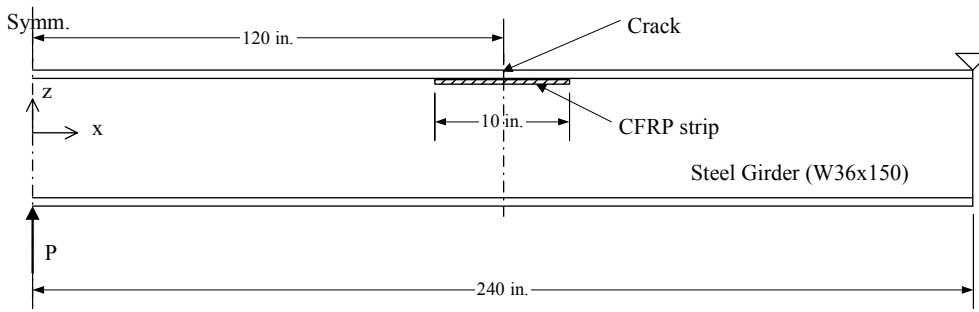


Figure A-1 Prototype Girder

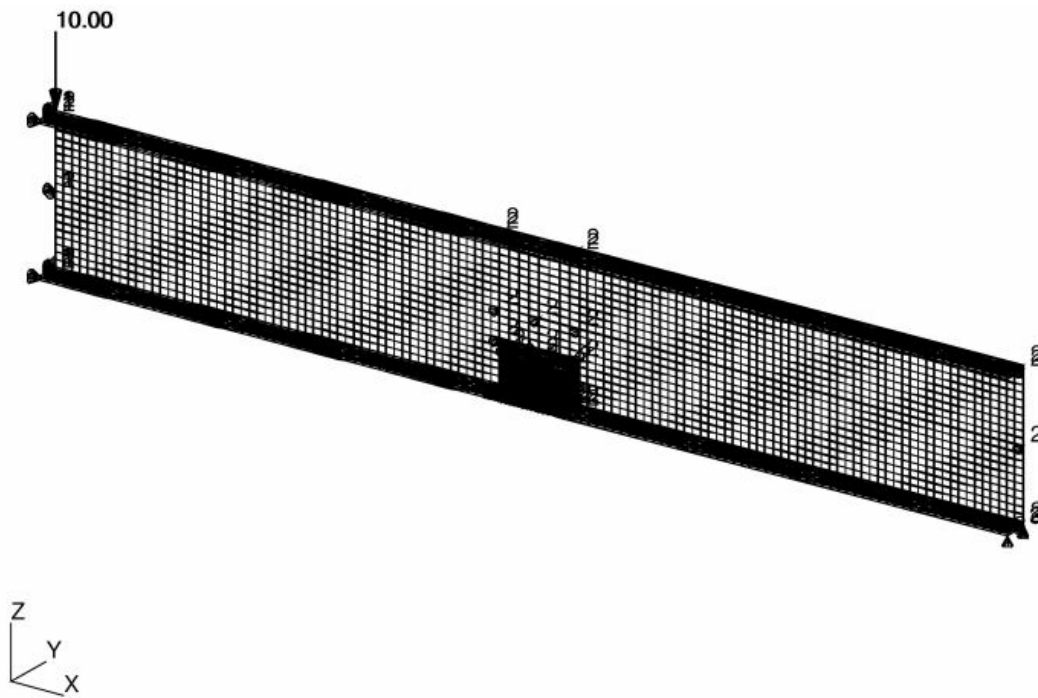
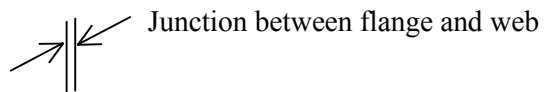


Figure A-2 Analysis Model for Prototype Girder



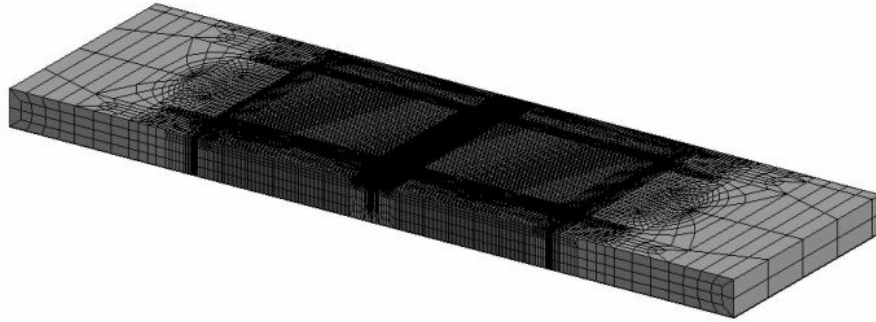


Figure A-3 Analysis Model for Prototype Girder: Detail of Flange with Bonded CFRP

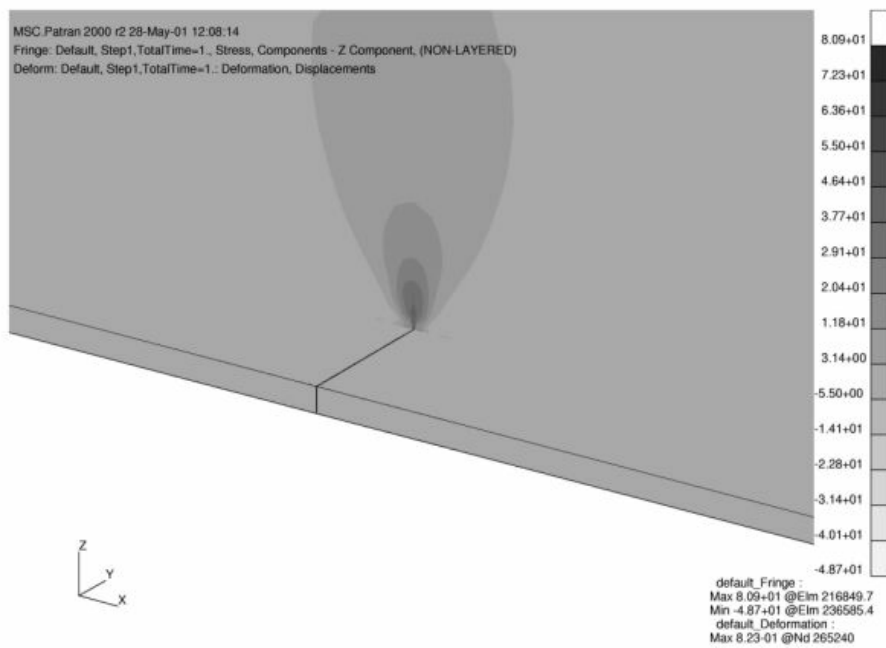


Figure A-4 Peeling Stress (σ_z) Distribution

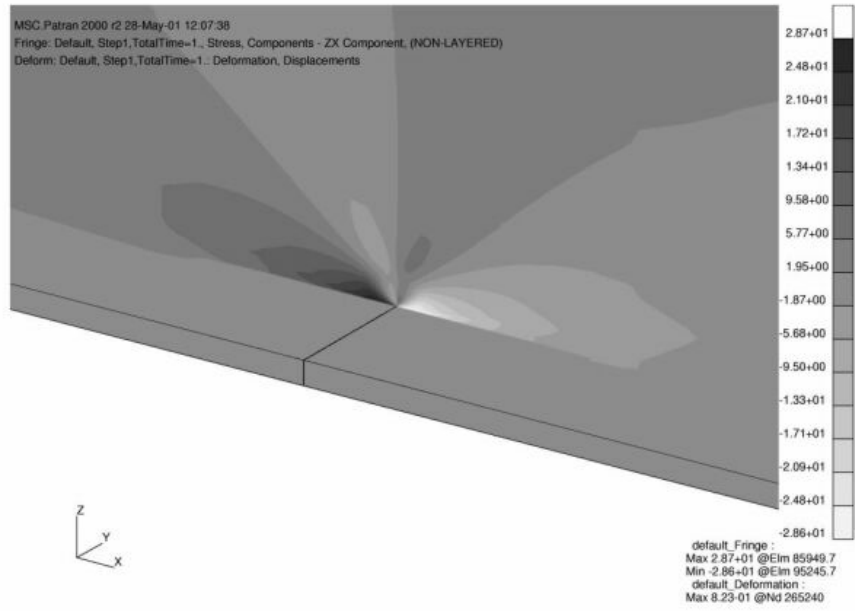


Figure A-5 Shear Stress (τ_{zx}) Distribution

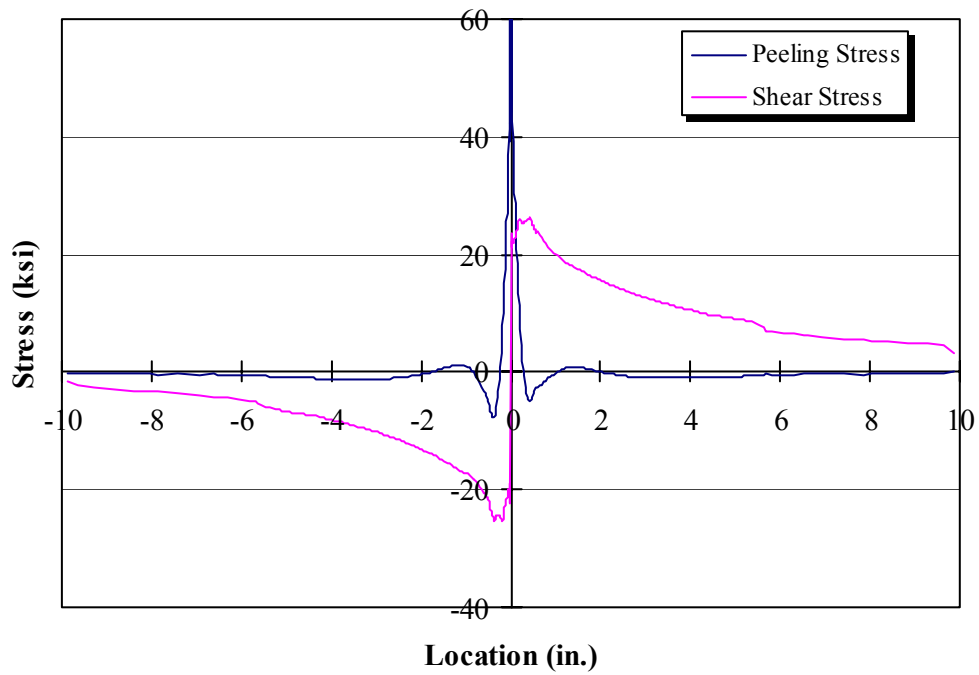


Figure A-6 Plot of Shear (σ_z) and Peeling (τ_{zx}) Stresses along Flange-Web Intersection

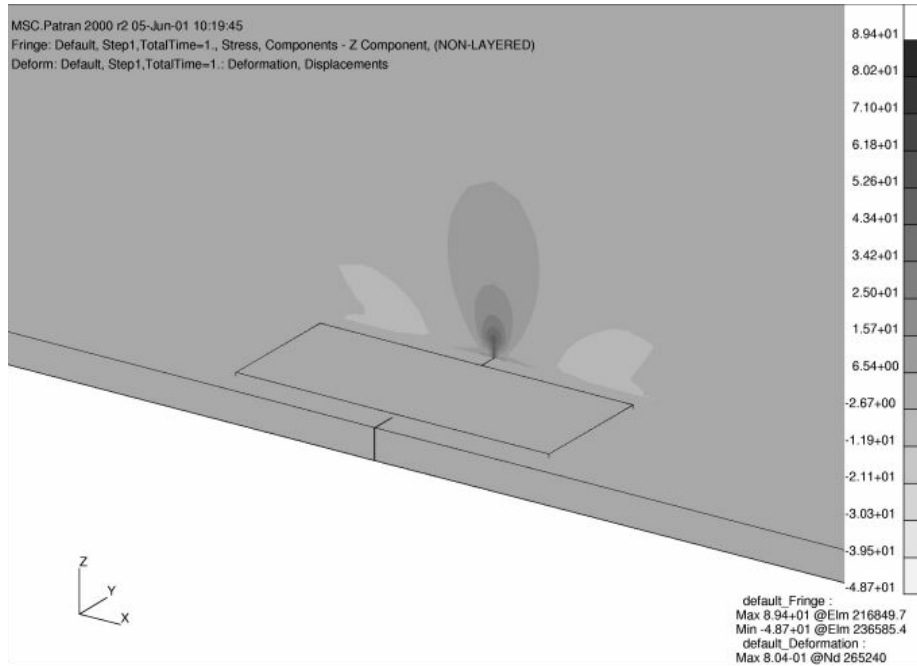


Figure A-7 Peeling Stress (σ_z) Distribution

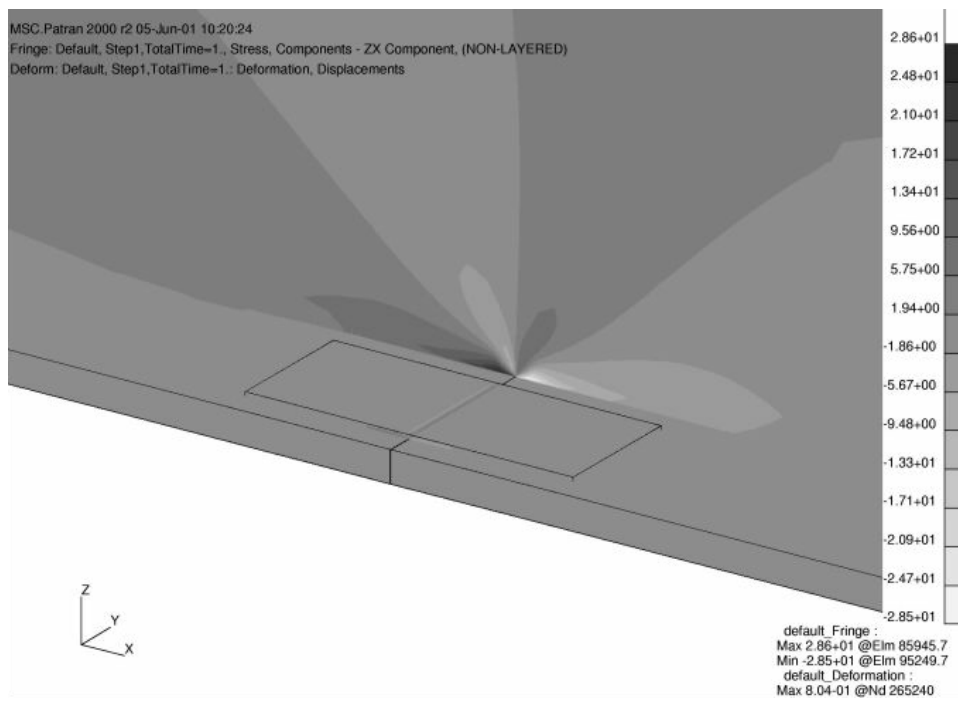


Figure A-8 Shear Stress (τ_{zx}) Distribution

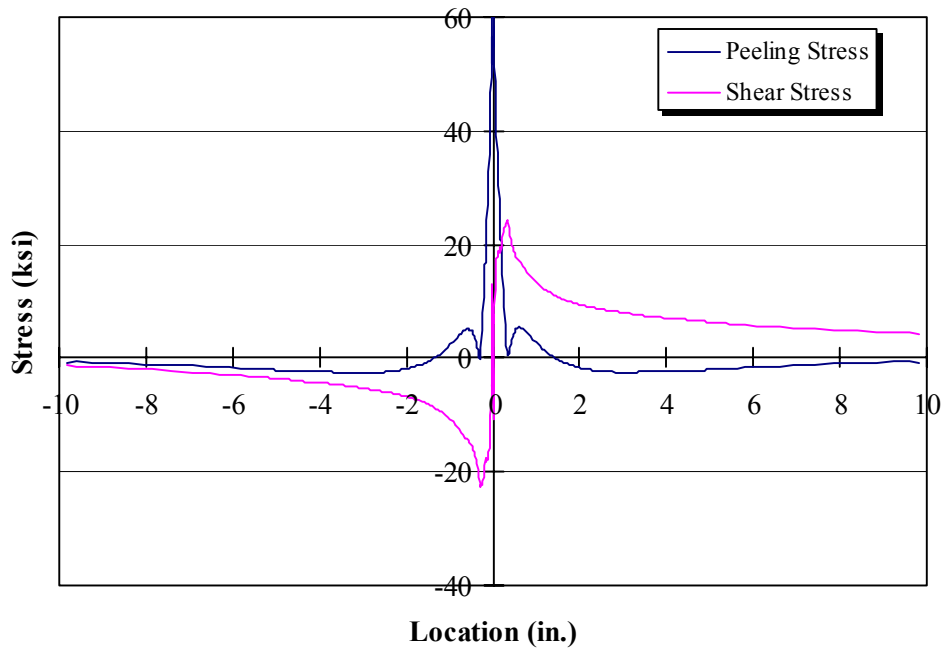


Figure A-9 Plot of Shear (σ_z) and Peeling (τ_{zx}) Stresses along Flange-Web Intersection

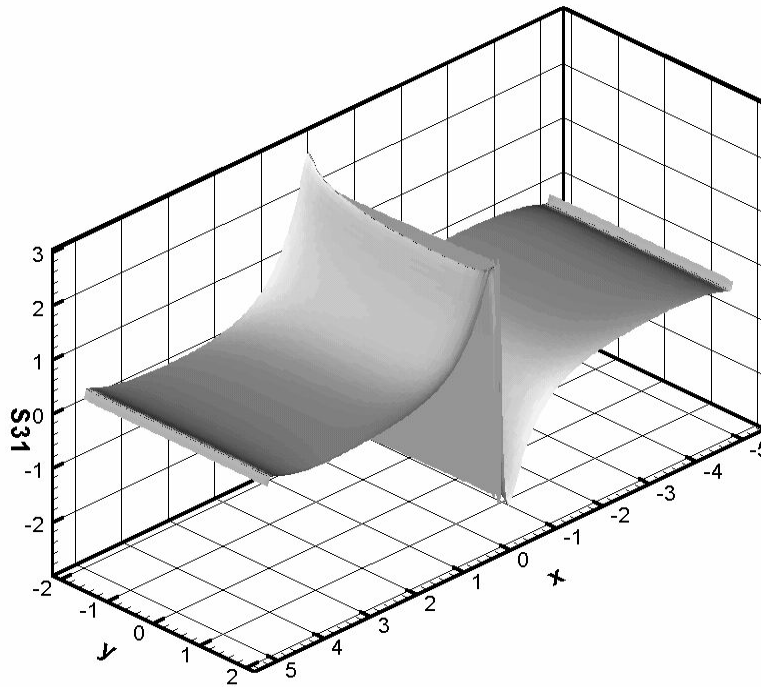


Figure A-10 Shear Stress Distribution in the Adhesive

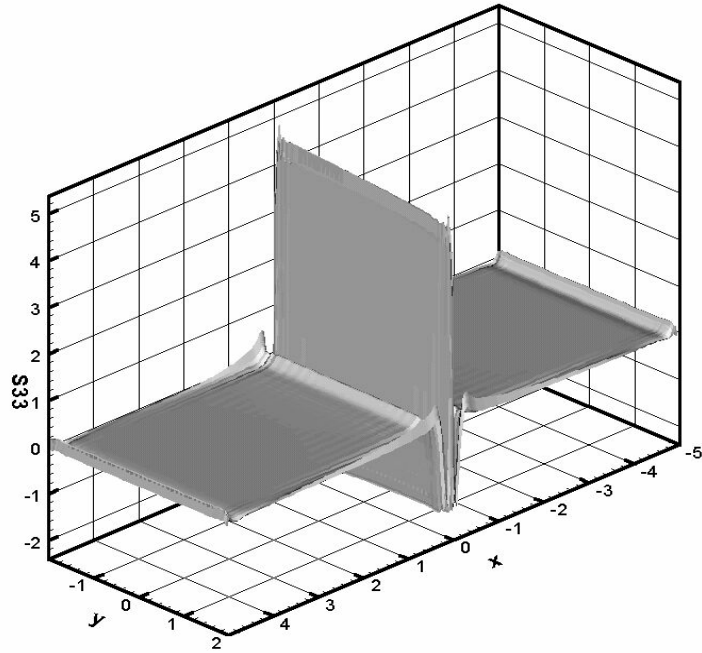
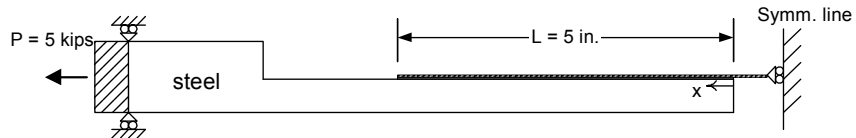
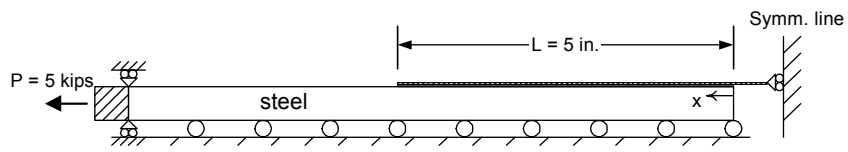


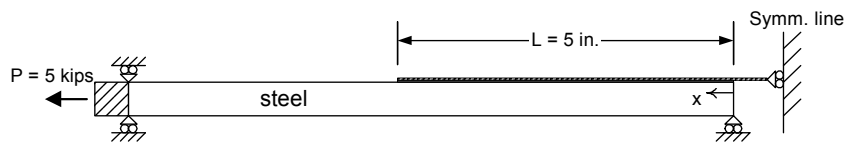
Figure A-11 Peeling Stress Distribution in the Adhesive



a. model1



b. model2



c. model3

Figure A-12 Modified Specimen Models

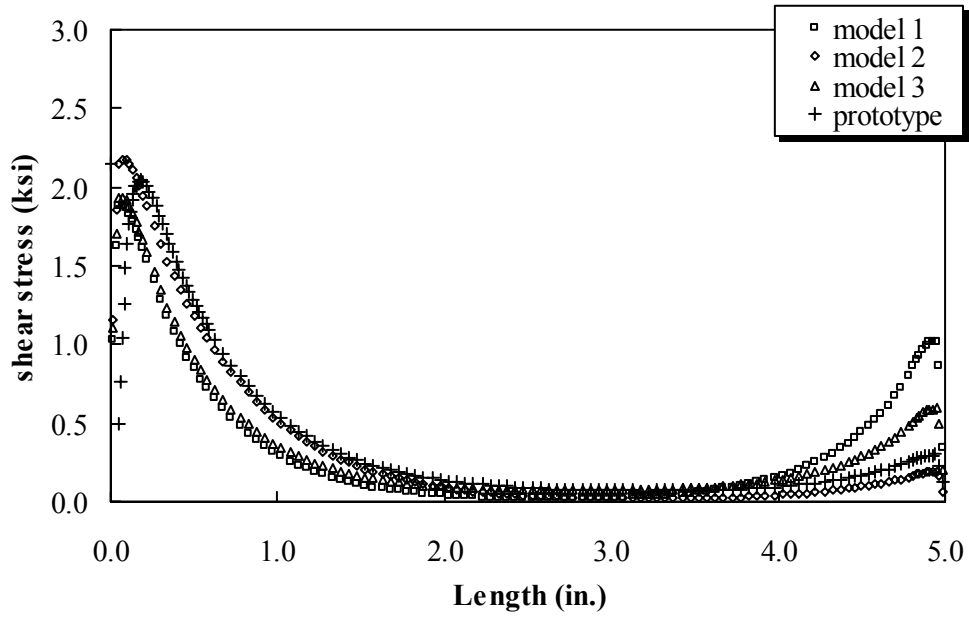


Figure A-13 Shear Stress Distribution in Adhesive

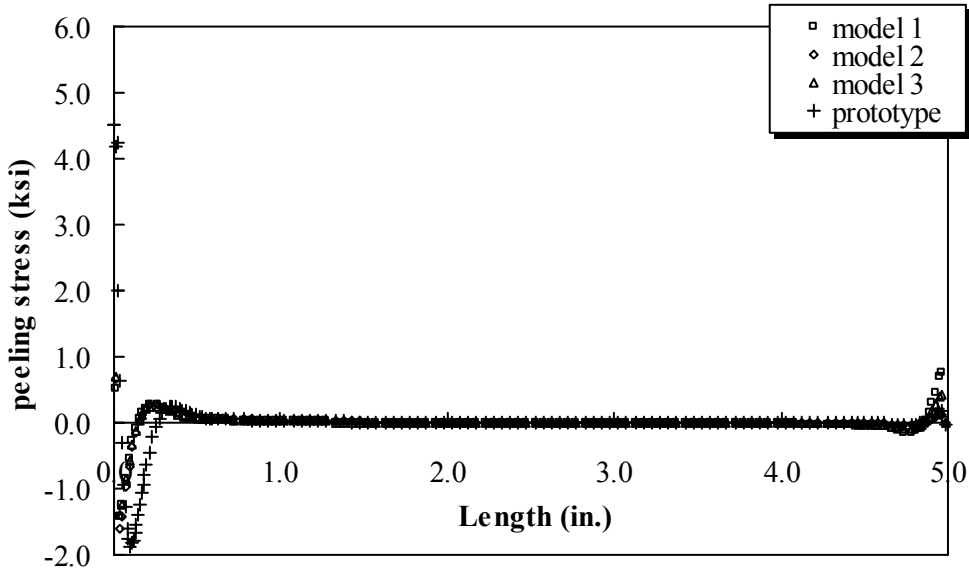


Figure A-14 Peeling Stress Distribution in Adhesive

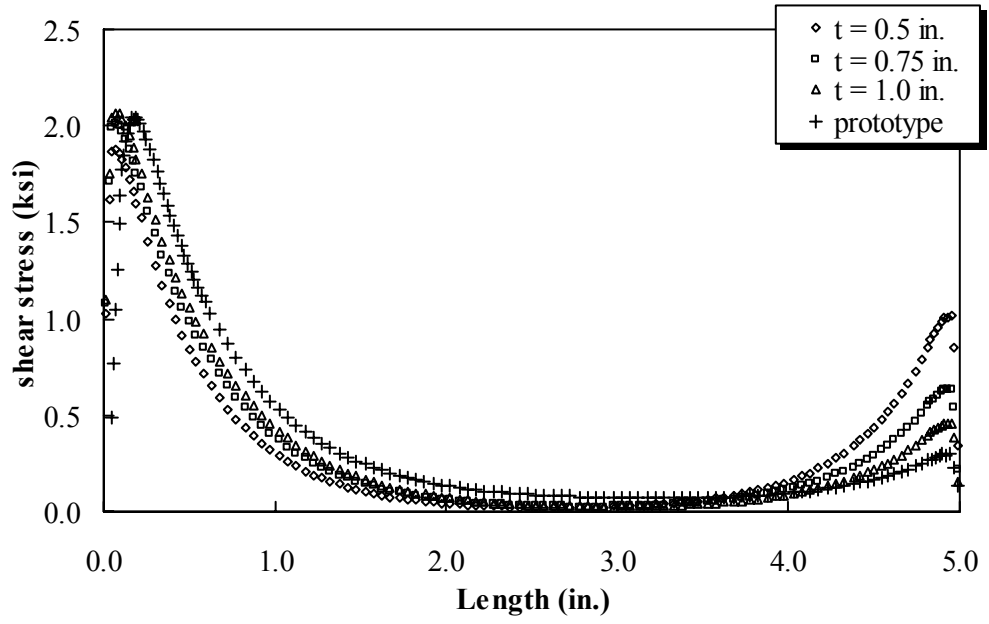


Figure A-15 Comparison of Shear Stress Distributions in Adhesive

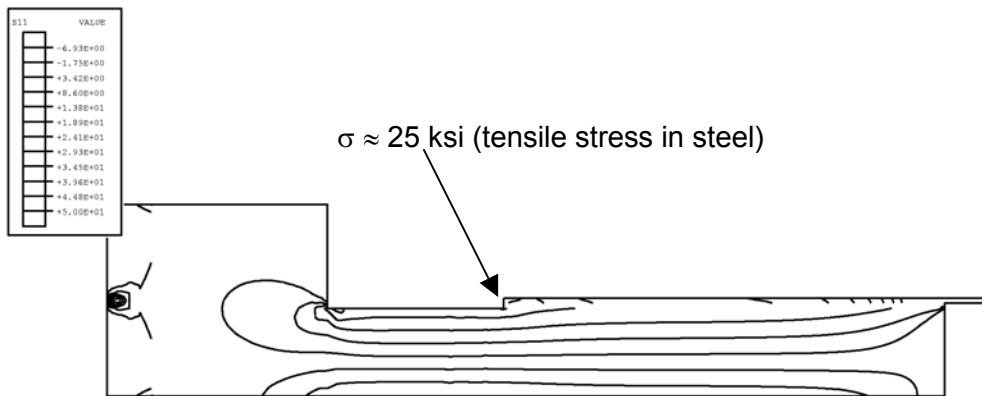


Figure A-16 Normal Stress Distribution (t = 1.0 in.)

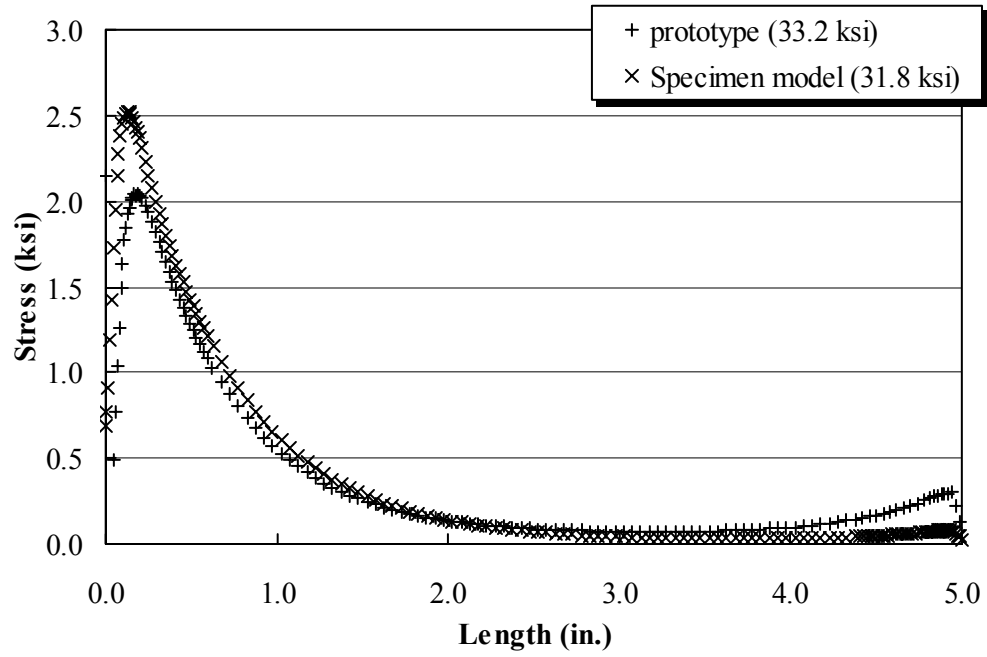


Figure A-17 Comparison Shear Stress Distribution in Adhesive

Appendix B

Cyclic Loading Test Using Test Setup for Effective Bond Length Tests

Appendix B Cyclic Loading Test using Test Setup for Effective Bond Length Tests

In addition to the static test, cyclic loading tests were conducted using the test setup for the effective bond length tests in order to investigate the effect of cyclic loading on the debonding failure of the strip. These tests were done only with Sikadur 330 adhesive and CarboDur CFRP strip before any other materials were considered. The results presented here will support necessity of selecting a more ductile adhesive compared to Sikadur 330.

B.1 Test Setup and Instrumentation

The test setup and instrumentation were identical with those for the effective bond length tests (see Chapter 3 for details). One strain gauge was placed at the center of the CFRP strip to determine the load range corresponding to the desired strain level in the CFRP strip.

B.2 Test Matrix

Two specimens were tested under different loading levels as shown in Table B-1. Specimen C-L was loaded so that the minimum and maximum tensile strain in the CFRP strip were 500 and 2,000 microstrain, respectively; and C-H was loaded with a tensile strain range of 500 to 3,500 microstrain. The frequency of loading was 0.5 Hz for both tests. The adhesive and CFRP strips were Sikadur 330 and Carbodur, respectively, and the bond length was 8 in. with Configuration 5 for both tests.

B.3 Results

A summary of the results is listed in the Table B-2. As can be seen in the table, the CFRP strip debonded from the adhesive partially or completely, and specimen C-H lasted only 20,000 cycles. Examining the failure surfaces of the adhesive and CFRP strips, the failure surface was actually in the adhesive layer just beneath the interface between the CFRP strip and adhesive as shown in Figure B-1 and Figure B-2. The amount of adhesive layer left on the CFRP strip was larger for specimen C-H compared with specimen C-L as can be seen in the

figure. Note that the CFRP strip of specimen C-L was peeled off from the steel plates after the test to confirm the debonded length.

The location of the failure surface indicates that the weakest material in the system was the adhesive, and changing the adhesive to one with more ductility could have prevented this premature debonding failure.

Table B-1 Specimen Matrix for Cyclic Tests

Specimen	CFRP	Adhesive	Config.	Bond Length	Bond Thickness	Type	Strain range ($\mu\epsilon$)
C-L	CarboDur	Sikadur 330	5	8 in.	0.05 in.	B	500 - 2000
C-H						A	500 - 3500

Table B-2 Summary of Cyclic Tests

Specimen	CFRP	Adhesive	Config.	Failure	# of Cycles
C-L	CarboDur	Sikadur 330	5	No failure, partially debond	1,000,000+
C-H				Debond	20,000

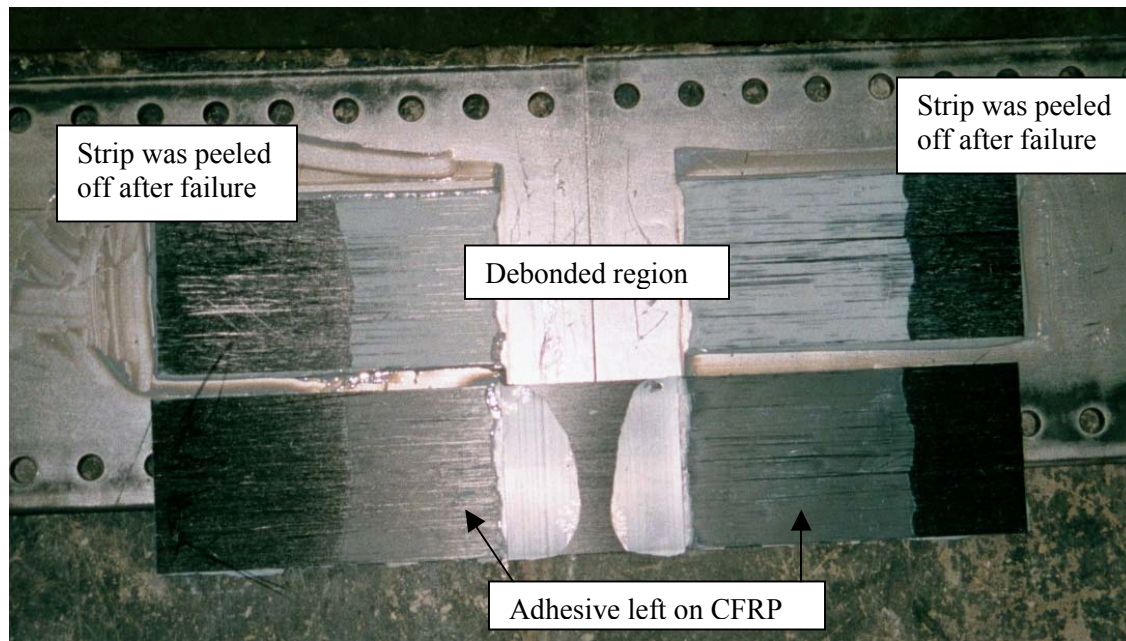


Figure B-1 Debonded Surface after Experiment (C-L)

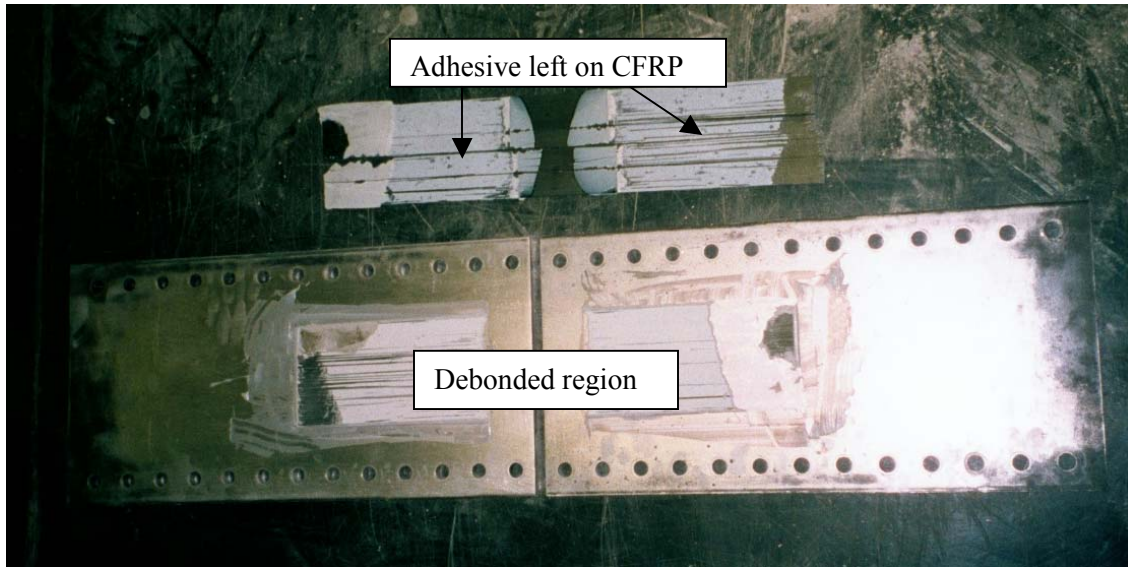


Figure B-2 Debonded surface (C-H)

Appendix C

Cyclic Tests on Rehabilitated W27x94 Girder

Appendix C Cyclic Tests on Rehabilitated W27x94 Girder

In this appendix, cyclic loading tests on the W27x94 girder, for which the static loading tests were conducted as discussed in Sections 3.3 and 4.2, will be presented. This test was conducted after the static tests were finished in order to see if crack growth could be stopped by the rehabilitation of bonded CFRP strips.

C.1 Test Specimen instrumentation

The test specimen was a W27x94 girder that was used for the static tests discussed in Sections 3.3 and 4.2. After the static tests, CFRP strips bonded onto the tension flange were removed and new CFRP strips were bonded for the cyclic tests. A 1 Hz cyclic load was applied to create a 5 ksi nominal stress range at the top and bottom flanges. One strain gauge was placed on at the center of one of the CFRP strips to record the tensile strain in the strip; gauges on the girder were the same as those for the static test except for the one at the crack tip, which was removed after the static test. During the cyclic loading, strain data were periodically recorded to investigate the effect of crack growth and debonding of the strips.

C.2 Test Results

C.2.1 Crack Growth

Crack growth measured during the experiment is shown in Figure C-1. Because there are bolt holes in the web (see Section 3.3), the crack was arrested by one of holes just above the crack; the crack reached the hole after 104,875 cycles when the crack had grown about 0.85 in, to a total length of 4.85 in. It should be noted that the crack growth in vertical axis in the figure was measured from the location of the crack tip at the beginning of the cyclic test; see Sections 3.3 and 4.2 for pictures of the crack at the time of the static tests. Although the strain reduction near the crack tip was about 60% as discussed in Section 4.2, crack growth was not arrested by the rehabilitation with the bonded CFRP strips due to the high stress concentration. Because this experiment was not able to tell how much the rehabilitation reduced the crack growth, another set of experiments was thought to be required as discussed in Section 3.4.

C.2.2 Strain in Girder and Strip

Strain distributions in the cross section of the girder are shown in Figure C-2; data were taken at the center of the girder, and strain measured on the CFRP strip is shown in Figure C-3. Strain distributions were recorded several times through the experiment, and legends in the figure indicate the number of cycles when data were recorded. The data can be divided into four groups: 1) before the crack reached the hole (0-104,875 cycles), 2) after the crack reached the hole and before one of the strip completely debonded, 3) after one of the strip completely debonded (at 535,047 cycles), and 4) after the other strip was removed from the girder (w/o strip). The strain 9 in. from the bottom of the girder increased about 150 microstrain after the crack reached the hole and stayed almost constant until one of the CFRP strips completely debonded. This indicates that the crack length had a significant effect on the strain distribution even though the rehabilitation was applied. Another finding was that the bond length did not have much influence on the reduction of strain in the girder at the stress range tested, and the strain in the CFRP strip decreased only 20% after 424,931 cycles with more than 50% loss of bond length. It should be noted, however, that only one of the strips finally debonded and the other one remained intact (Figure C-4 and Figure C-5). Thus, it would be possible that the other strip started to pick additional loads as one strips debonded.

Although one specimen tested cyclically in the effective bond length test setup did not debond through 1 million cycles (Appendix B), one of strips in this test debonded after 0.5 million cycles. The reason for this discrepancy in the results was not clear. Again, however, the debonded surface was in the adhesive layer as it was observed in the cyclic test presented in Appendix B. Thus, using more ductile adhesive would be the solution for avoiding the debonding failure.

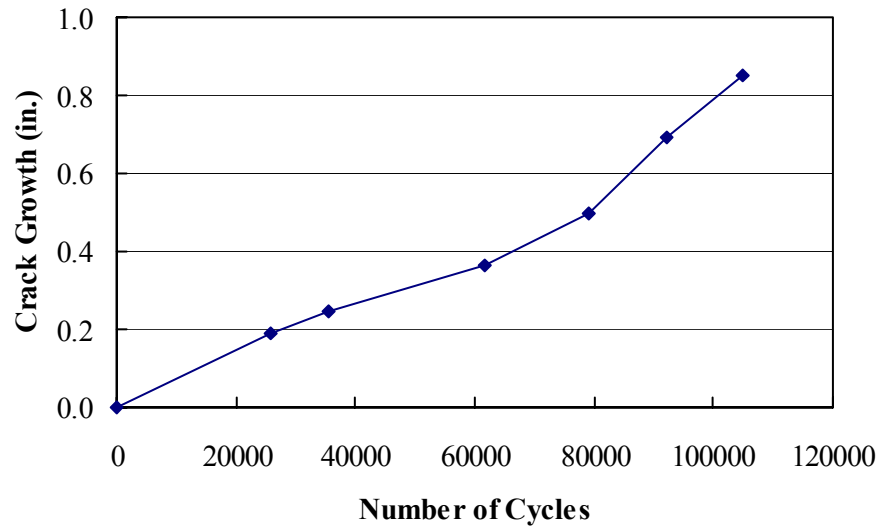


Figure C-1 Crack Growth (measured from the beginning of the cyclic test)

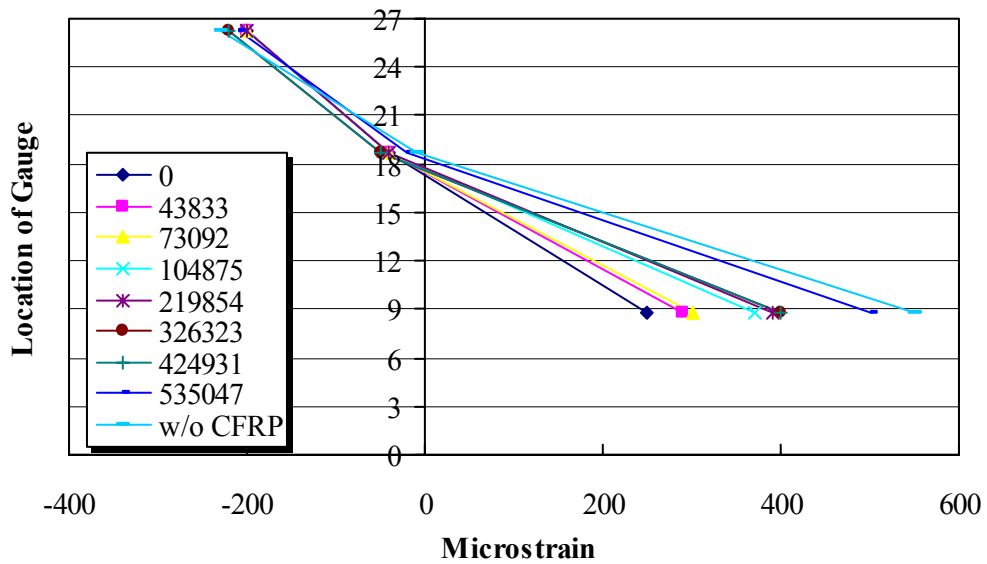


Figure C-2 Strain Distribution in W27x94 Girder

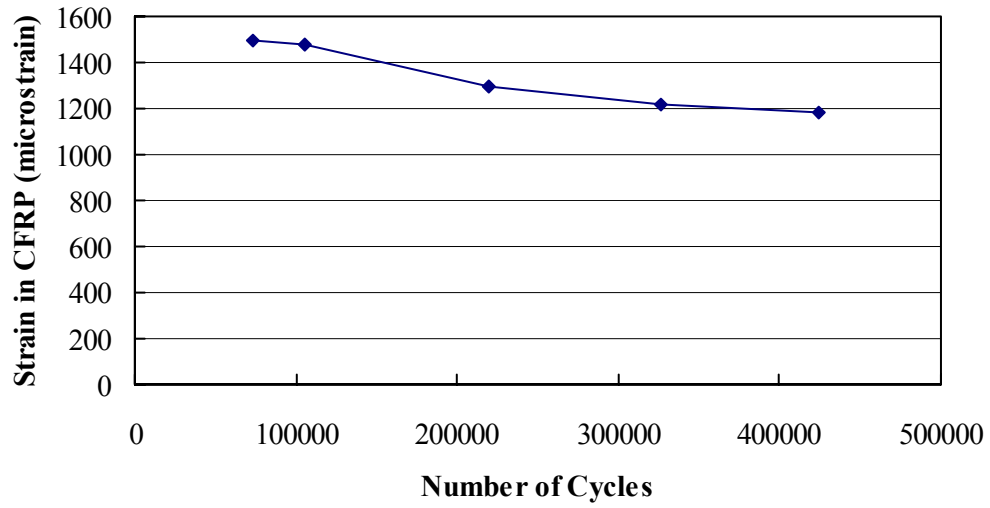


Figure C-3 Change of Strain in CFRP strip as Crack Grows

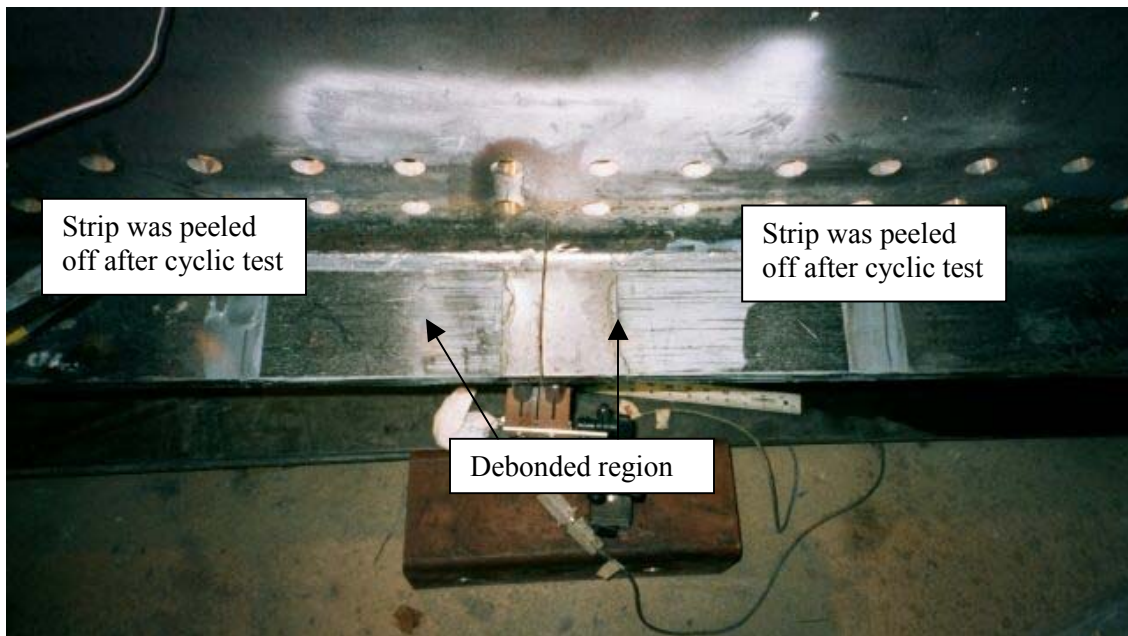


Figure C-4 Surface of Adhesive Layer after Experiment (one partially debonded)

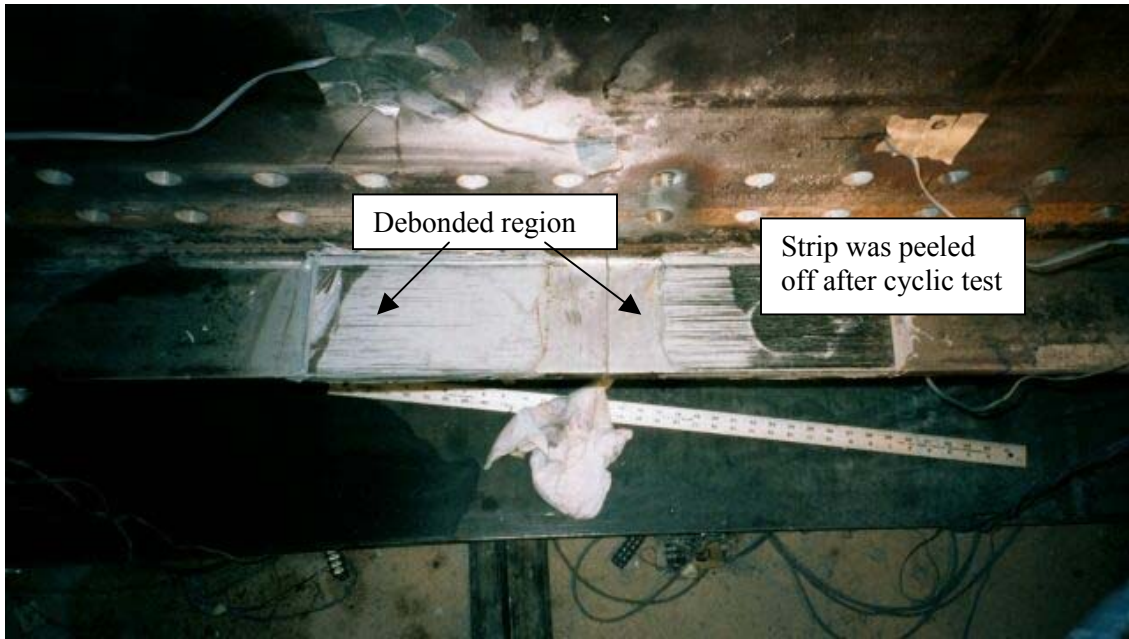


Figure C-5 Surface of Adhesive Layer after Experiment (one that completely debonded)

Appendix D

Recommended Application Procedure

Appendix D Recommended Application Procedure

In this section, a recommended application procedure of the bonded CFRP strip will be presented. Based on the experimental results, it was concluded that two layers of CFRP with a minimum 16 in. of bond length plus a 2 in. unbonded region near the crack should be used. The recommended bonded length is increased 1.25 times, i.e., 20 in. plus the 2 in. unbonded region, in order to avoid a loss of bond length due to an application error; this increase corresponds to the sum of the effective bond length (16") and twice the elastic part of the effective bond length for one layer of the strip. This ensures enough bond length so that stress transfer can take place at both ends of the CFRP strips. Surface preparation of the CFRP strip and steel flange is based on the recommended procedure by the manufacturer of those materials, and is the most important factor to affect the bond strength.

D.1 Preparation of One Two-Layered Strip

- Cut the CFRP strip into two pieces 44" in length.
- Lightly abrade the dark surfaces on both strips using fine sandpaper (#150).
- For one of the two strips, abrade the shiny surface until the surface turns into a dark color using coarse (#50~#100) sand paper first, then finish the surface with fine sandpaper (#150).
- Clean all surfaces with cotton cloth soaked in acetone; wait for 5-10 min. for the acetone to evaporate.
- Cut fishing line with about 0.02 in. diameter into several pieces (1/16" in length).
- Apply adhesive on the CFRP surface which was shiny before abrasion, and spread the adhesive over the surface using a spatula – the thickness of adhesive layer needs to be more than the diameter of fishing line.
- Sprinkle the fishing lines on the adhesive layer.

- Apply the CFRP strip which does not have adhesive onto the one with adhesive so that the abraded surface faces the adhesive, i.e., the shiny surface will be the top of the two layers (see Figure D-1 for a sketch of the stacking sequence).
- Gently apply pressure on the strip so that the excess of the adhesive is squeezed out from the edges of the strip. Because the fishing lines will keep the necessary bond thickness, do not hesitate to apply the pressure.
- Leave the strips undisturbed at least 6 hours for handling, it will take 24 hours for the adhesive to fully cure.

Repeat the above procedure to make the desired number of two-layered strips; two two-layered strips will be required for the rehabilitation of one location. The preparation listed above needs to be done before going out to the rehabilitation site, and it will take about 0.5 hours for preparation of one two-layered strip. When handling the cured two-layered strip, avoid contact with abraded surface as much as possible. It will be good idea to store the two-layered strip in a plastic bag to avoid surface contamination during transportation of the CFRP strips to the rehabilitation site.

D.2 Application of CFRP Strips on Steel Flange

- DO NOT PROCEED IF THE TEMPERATURE IS LOWER THAN 50°F.
- See Figure D-2 for a sketch of an application sequence.
- Locate the steel flange where the CFRP strip will be bonded.
- Mark the location where the center of CFRP strip will be aligned and 2” from the center towards each side to indicate the unbonded region.
- Locate the crack tips and drill a hole at each crack tip.
- Grind the surface of steel flange to remove rust until the metal surface is exposed over the area where CFRP strips will be bonded, 44” in length being centered at the crack and 4” in width.

- Abrade the steel surface with coarse (#50~#100) sandpaper then wipe the surface with cotton cloth soaked in acetone.
- Abrade the steel surface with fine (#150) sandpaper, and then wipe the surface with cotton cloth soaked in acetone.
- Wipe the surface to be bonded (dark surface, abraded in the last subsection) of the two-layered CFRP strip again with cotton cloth soaked in acetone at least 10 min. before application.
- Mark the center of the CFRP strip and 2" from the center toward the ends for unbonded region.
- Cut fishing line with about 0.02 in. diameter into several pieces (1/16" in length)
- Apply adhesive on the CFRP surface except for the unbonded region, and spread adhesive over the surface – check the adhesive thickness is more than the diameter of fishing line.
- Apply a thin layer of adhesive on the steel flange over the area to be bonded. The thickness is not important here.
- Sprinkle fishing lines on the adhesive layer on the CFRP strip.
- Apply the two-layered CFRP strip on the steel flange, gently applying pressure so that the excess of the adhesive comes out from the edges. Because the fishing lines will keep the necessary bond thickness, do not hesitate to apply the pressure.
- Tape the CFRP strips to the steel flange so that the CFRP strips will not be moved by accident.
- It will take 24 hours for the adhesive to fully cure.

Repeat the above procedure for each CFRP strip. Note that if temperature is below 50°F, the adhesive will become too viscous to be mixed and to be spread over the area. The

application process listed above will take approximately 3 hours including drilling a hole at the crack tip, and approximately 1.5 hours without drilling a hole. As indicated in Section 5.1, vibration from traffic will not affect the bond strength. Therefore, the bridge can be open for traffic during the rehabilitation.

D.3 Comments on Application of CFRP Strip

In this section, the recommended application procedure has been presented. The listed procedure was based on the assumption that a half of the steel flange width is about 4.5" so that one CFRP strip with 4" width can be placed. If a half of the flange width is less than 4", a CFRP strip with less width, 2", should be available from the manufacturer. If a half of the flange width is more than 7", it is possible to combine 4" and 2" width strips to cover entire width of the flange.

Because of the lightweight of CFRP strips, one person can handle the two-layered strip and finish the application of the CFRP strips. If one person can drill a hole in the flange, it is possible to finish the necessary work with one person (not including gaining access to the girder). Therefore, this approach offers a great savings for rehabilitation costs compared with the rehabilitation method with bolted angle members.

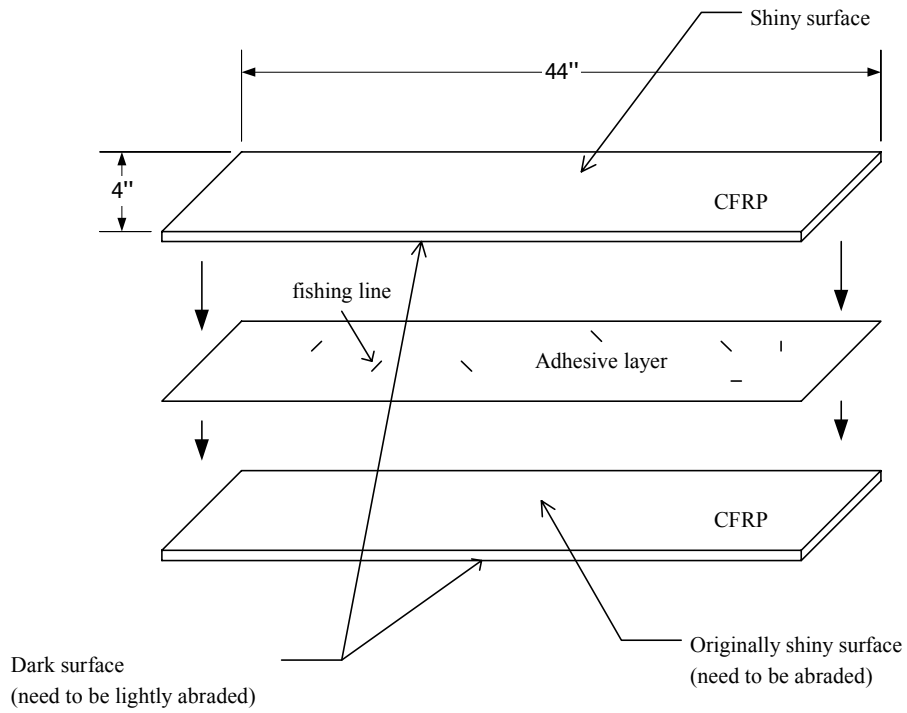


Figure D-1 Stacking Sequence for Fabrication of Two-layered CFRP Strip

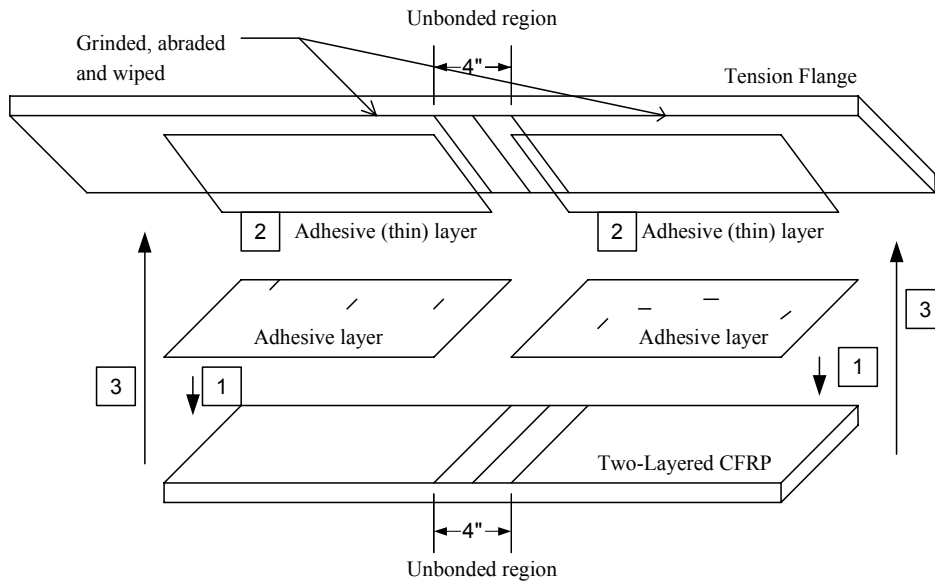


Figure D-2 Application of CFRP Strip onto Steel Flange